TECHNICAL REPORT STANDARD TITLE PAGE

1. Report No.	2. Government Accession No.	3. Recipient's Catalog No.
FHWA/TX-86/ +324-3		

4. Title and Subtitle	5. Report Date
Repetitive Load Test on Composite Precast Concrete Decked Bridges	April 1986
	6. Performing Organization Code
7. Author(s)	8. Performing Organization Report No.
R. A. Osegueda, and J. S. Noel	Research Report 324-3
9. Performing Organization Name and Address	10. Work Unit No.
Texas Transportation Institute Texas A&M University College Station, Texas	11. Contract or Grant No. Study No. 2-5-82-324
	13. Type of Report and Period Covered
12. Sponsoring Agency Name and Address	Interim- September 1981 April 1986
Texas State Department of Highways and Public Transportation, Transportation Planning Division P.O. Box 5051 Austin, Texas 78763	14. Sponsoring Agency Code

15. Supplementary Notes
Research performed in cooperation with DOT, FHWA.
Research Study Title: Rapid Bridge Deck Replacement.

16. Abstract

Bridge deck replacement using precast concrete panels minimizes replacement time as well as traffic interference. An experimental study consisting of a repetitive load test on a 1/3 scale model of a 60-ft I-beam composite bridge with precast concrete panels connected with epoxy mortar and shear stud connectors is described here.

Two million load cycles of an equivalent HS20-44 AASHTO design truck were applied to the model while deflections, flexural strains and slip displacements were continuously instrumented to determine changes in the flexural properties of the bridge or deteriorations at the interface connections.

The reults were analyzed and revealed no significant changes in the flexural properties after the two million cycles were applied. There was also no evidence of any epoxy mortar bond failure at the interface even though the amount of bond area was minimized. The epoxy mortar bond, although it is not considered for design, prolongs the fatigue life of the mechanical shear stud connectors. It is concluded that this type of construction yields a fatigue-resistant interface connection.

17. Key Words	18. Distribution Statement
Bridge Decks, Precast Concrete, Epoxy Mortar, Composite Bridges, Fatigue, Shear Connectors, Dynamic Test, and Dynamic Analysis	No restrictions, This document is available to the public through the National Technical Information Service 5285 Port Royal Road Springfield, Virginia 22161

19. Security Classif. (of this report)	20. Security Classif. (of this page)	21. No. of Pages	22. Price
Unclassified	Unclassified	103	

Form DOT F 1700.7 (8-69)

REPETITIVE LOAD TEST ON COMPOSITE PRECAST CONCRETE DECKED BRIDGES

by

Roberto Alejandro Osegueda
Research Assistant

and

James S. Noel
Associate Research Engineer

Research Report Number 324-3

Rapid Bridge Deck Replacement
Research Study Number 2-5-82-324

Sponsored by
Texas State Department of Highways and Public Transportation
in cooperation with
The United States Department of Transportation
Federal Highway Administration

April 1986
Texas Transportation Institute
Texas A&M University
College Station

METRIC CONVERSION FACTORS

Approximate Conversions to Metric Measures

Symbol	When You Know	Multiply by	To Find	Symbol
		LENGTH		
in	inches	*2.5	centimeters	cm
ft	feet	30	centimeters	cm
yd	yards	0.9	meters	m
mi	miles	1.6	kilometers	km
		AREA		
in^2	square inches	6.5	square centimeters	cm^2
ft^2	square feet	0.09	square meters	m^2
yd^2	square yards	0.8	square meters	m^2
mi^2	square miles	2.6	square kilometers	km^2
	acres	0.4	hectares	ha
		MASS (weight)		
oz	ounces	28	grams	g
lb	pounds	0.45	kilograms	kg
	short tons (2000 lb)	0.9	tonnes	t
		VOLUME		
tsp	teaspoons	5	milliliters	ml
Tbsp	tablespoons	15	milliliters	ml
fl oz	fluid ounces	30	milliliters	ml
c	cups	0.24	liters	l
pt	pints	0.47	liters	l
qt	quarts	0.95	liters	l
gal	gallons	3.8	liters	l
ft^3	cubic feet	0.03	cubic meters	m^3
yd^3	cubic yards	0.76	cubic meters	m^3
		TEMPERATURE (exact)		
°F	Fahrenheit temperature	5/9 (after subtracting 32)	Celsius temperature	°C

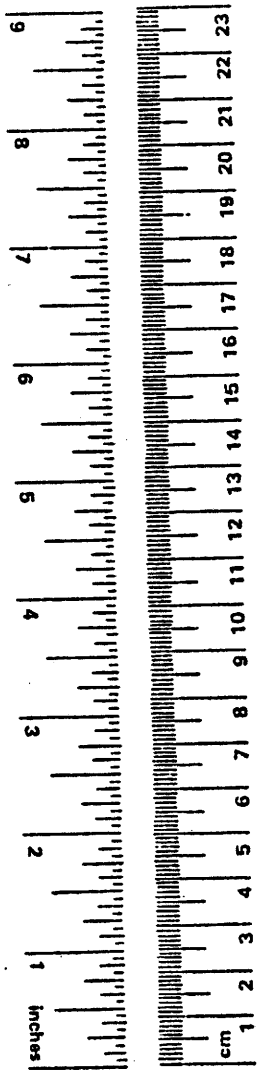

Approximate Conversions from Metric Measures

Symbol	When You Know	Multiply by	To Find	Symbol
		LENGTH		
mm	millimeters	0.04	inches	in
cm	centimeters	0.4	inches	in
m	meters	3.3	feet	ft
m	meters	1.1	yards	yd
km	kilometers	0.6	miles	mi
		AREA		
cm^2	square centimeters	0.16	square inches	in^2
m^2	square meters	1.2	square yards	yd^2
km^2	square kilometers	0.4	square miles	mi^2
ha	hectares (10,000 m^2)	2.5	acres	
		MASS (weight)		
g	grams	0.035	ounces	oz
kg	kilograms	2.2	pounds	lb
t	tonnes (1000 kg)	1.1	short tons	
		VOLUME		
ml	milliliters	0.03	fluid ounces	fl oz
l	liters	2.1	pints	pt
l	liters	1.06	quarts	qt
l	liters	0.26	gallons	gal
m^3	cubic meters	35	cubic feet	ft^3
m^3	cubic meters	1.3	cubic yards	yd^3
		TEMPERATURE (exact)		
°C	Celsius temperature	9/5 (then add 32)	Fahrenheit temperature	°F

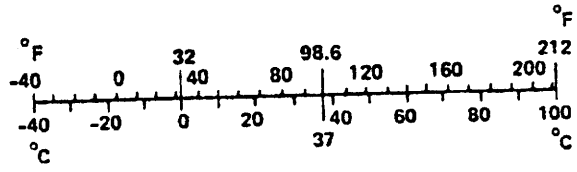

*1 in = 2.54 (exactly). For other exact conversions and more detailed tables, see NBS Misc. Publ. 286, Units of Weights and Measures, Price $2.25, SD Catalog No. C13.10:286.

DISCLAIMER

The contents of this report reflect the views of the authors, who are responsible for the opinions, findings, conclusions and recommendations presented herein. The contents do not reflect the official views or policies of the Federal Highway Administration. This report does not constitute a standard, specification, or regulation.

KEY WORDS

Bridge Decks, Precast Concrete, Composite Bridges, Epoxy Mortar, Shear Connectors, Fatigue, Dynamic Test, Dynamic Analysis.

ACKNOWLEDGEMENTS

The authors are grateful to the Texas State Department of Highways and Public Transportation and the Federal Highway Administration for sponsoring this study, to Mr. John Panak, whose professional advice was most helpful, and to Dr. Mrinmay Biswas, who was instrumental in the early phases of this project.

ABSTRACT

Bridge deck replacement using precast concrete panels minimizes replacement time as well as traffic interference. An experimental study consisting of a repetitive load test on a 1/3 scale model of a 60-ft I-beam composite bridge with precast concrete panels connected with epoxy mortar and shear stud connectors is described here.

Two million load cycles of an equivalent HS20-44 AASHTO design truck were applied to the model while deflections, flexural strains and slip displacements were continuously instrumented to determine changes in the flexural properties of the bridge or deteriorations at the interface connections.

The results were analyzed and revealed no significant changes in the flexural properties after the two million cycles were applied. There was also no evidence of any epoxy mortar bond failure at the interface even though the amount of bond area was minimized. The epoxy mortar bond, although it is not considered for design, prolongs the fatigue life of the mechanical shear stud connectors. It is concluded that this type of construction yields a very fatigue-resistant interface connection.

TABLE OF CONTENTS

CHAPTER | Page

LIST OF TABLES

LIST OF FIGURES

CHAPTER I

INTRODUCTION

Nature of the Problem

The installation of full-depth precast concrete panels has become a popular method for replacement of deteriorated bridge decks. The modular precast panels are connected to steel I-beams using epoxy mortar grout and standard shear stud connectors to assure the horizontal shear transfer required for composite action. Epoxy mortar-grouted key joints are employed for the transfer of compressive normal forces between adjacent precast panels. Both connections are required to develop full composite action.

The construction method currently employed typically calls first for the removal of the deteriorated deck and existing shear connectors, leaving the top flanges of the I-beam stringers clean and bare. The modular precast panels are then laid on top of the I-beam floor system with or without the use of bearing pads or strips; the gap between the panels and the stringers is completely sealed and subsequently grouted with epoxy or polymer mortar. Adequate mechanical shear connectors are then welded to the top flange through molded openings in the concrete panels. Finally, the openings and the key joints between two adjacent panels are also grouted. After the grout has cured, the bond at the interface and the shear connectors, along with the continuity provided by the grouting of the key joints, forces the steel I-beams and the modular precast concrete panels to act as an integral unit in resisting structural loads.

The composite interaction between the steel I-beams and the precast panels is carried by the epoxy mortar bond unless there is a bond failure at the interface. In this case, the mechanical shear stud connectors would carry the horizontal shear forces for the necessary composite interaction.

These precast concrete decked bridges are being extensively subjected to repetitive highway loadings which may fatigue first the adhesive bond provided by the epoxy mortar and then the mechanical shear stud connectors. In the

presence of the adhesive bond, the shear connectors carry very little load because most of the shear transfer is performed by the epoxy mortar layer at the interface. Thus, the fatigue life of the total connection would be the sum of the fatigue life of the epoxy mortar bond plus that of the shear connectors. Therefore, in effect the adhesive bond tends to extend the fatigue life of the mechanical shear connectors.

The general objective of this investigation was to determine whether or not existing AASHTO fatigue design specifications are adequate for the composite connection between I-beams and precast concrete panels. The results of a test on a 1/3 scale model of a 60-ft long prototype bridge subjected to repetitive HS-20 loadings are reported.

Previous Tests on Precast Concrete Decking

Laboratory static tests to determine the adequacy of the shear connection between precast concrete panels and steel stringers have been conducted. First, a 20-ft long simply supported two-stringer model bridge was subjected to positive (sagging) bending moment by applying concentrated loads at the third points (3). The magnitude of the load was limited so that the elastic limit would not be exceeded because of planned subsequent experiments like fatigue, negative moment test and ultimate and punch-through tests. This positive moment test revealed that the interface epoxy mortar bond and the shear stud connectors, along with the grouted key joints, develop nearly 100% composite behavior. It also revealed that the relative slip between the precast slab and the stringers was negligible, despite the fact that during construction of the test specimen the epoxy mortar was deliberately applied to only 50% of the top flange area. It was also concluded that stiffness of the interface connection was almost entirely provided by the thin layer of epoxy mortar. There was no evidence of load being carried by the shear stud connectors (9).

The same specimen was subjected to negative (hogging) bending moments by anchoring the ends and applying upward concentrated loads at the midspan (5). It was reported that the structure behaved compositely at all times; however,

the tensile strengths of the key joints and of the concrete were not sufficient to maintain the full integrity of the precast deck. Failure occurred in the panels at the key joints, causing vertical cracks and reducing the composite sectional properties in a region of length approximately 18 times the slab thickness. No damage to the interface connection was observed.

Previous Research on Fatigue Strength of Shear Stud Connectors

The fatigue strength of shear connectors embedded in concrete and epoxy mortar may be different because of the difference in the elastic modulus of the embedment material. However, comparisons made by King, et al. (7), of tests on bare stud and push-out tests of concrete embedded studs revealed that the fatigue strength of stud connectors is about 2-1/2 times greater when the studs are not embedded. This comparison is made in Figure 1. It is concluded that the fatigue life of shear stud connectors is inversely dependent on the elastic modulus of the grouting material. Therefore, since values for the elastic modulus of epoxy mortar range from 500 to 5000 ksi, and values for concrete range from 3000 to 6000 ksi, it is expected that the fatigue strength of steel stud connectors embedded in epoxy mortar is greater than those embedded in concrete.

The aspect of fatigue strength of shear stud connectors in typical steel-concrete composite construction has been determined experimentally by means of beam and push-out tests by several investigators. Only the work that led to the current AASHTO Specifications on fatigue design of shear stud connectors is reviewed here.

Tests on seven composite beams with 3/4 in. diameter stud shear connectors are reported by Toprac (15). Each specimen consisted of a 36-ft long, W24X68 I-beam and a 6-in. thick, 6-ft wide slab. Any possible concrete bond to the I-beams was eliminated by oiling the top flange before casting. The repetitive loading tests showed that stud failure was progressive in nature and that dramatic increases in end slip and midspan deflection occurred only when most of the studs on one side had failed. Toprac concluded that the overall behavior was not sensitive to individual stud failure.

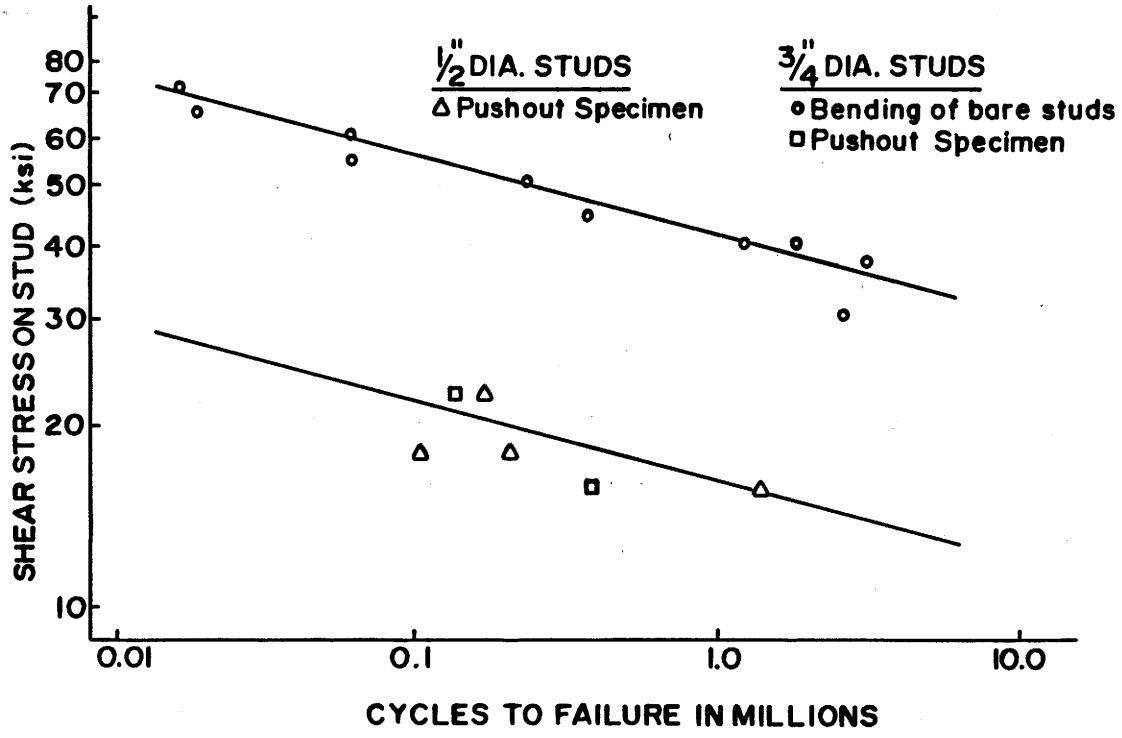

Figure 1. S-N Curves for Bare Studs and Push-out Tests (7).

Repetitive loading tests were also performed on twelve beams with 1/2 in. diameter shear studs by King, et al. (7). The typical beam specimen consisted of a W12X27 I-beam and a 4-in. thick, 4-ft wide concrete slab spanning 15 ft. The number and spacing of shear connectors was identical for all beam specimens; only the load range was varied. The concrete bond to the top flange was not neglected. The results are in general agreement with those reported by Toprac. However, valuable observations were also made about the concrete bond failure. The first decrease in composite interaction occurred as a result of the concrete bond failure, which was observed in the first 5,000 to 10,000 cycles of loading for all specimens. This failure started at the end of the member and progressed toward midspan. Thus, end shear connectors are the first to undergo an increase in stress due to the bond failure.

Fatigue tests on 44 push-out specimens reported by Slutter and Fisher (11) formed the basis of the current AASHTO Bridge Specifications (1) for fatigue design of shear stud connectors. Studs of 3/4 and 7/8 in. diameter were tested. The principal conclusion was that the stress range applied to the shear studs was the most important parameter affecting the fatigue life; the minimun stress level as well as the concrete strength were relatively unimportant. With stress reversals, the life of the studs was significantly longer for a given range of stress. The S-N curve resulting from the push-out tests is shown in Figure 2. Figure 3 shows a comparison of S-N curves between the push-out tests and the beam tests reported by Toprac and King, et al. It is observed that results from push-out tests yield a conservative result.

Description of Prototype Bridge and 1/3 Scaled Model

To establish a basis for design of the model, a typical design of a two-lane, 60-ft. nominal span bridge was selected from the Standard Drawings of Steel I-Beam Bridges of the Texas Highway Department (13). A typical cross section is shown in Figure 4-a. The stringers are old standard 36WF150 rolled sections, spaced at 8 ft center to center. One significant feature is that welded cover plates 3/4 in. thick, 10 in. wide, and 40 ft long were used top and bottom.

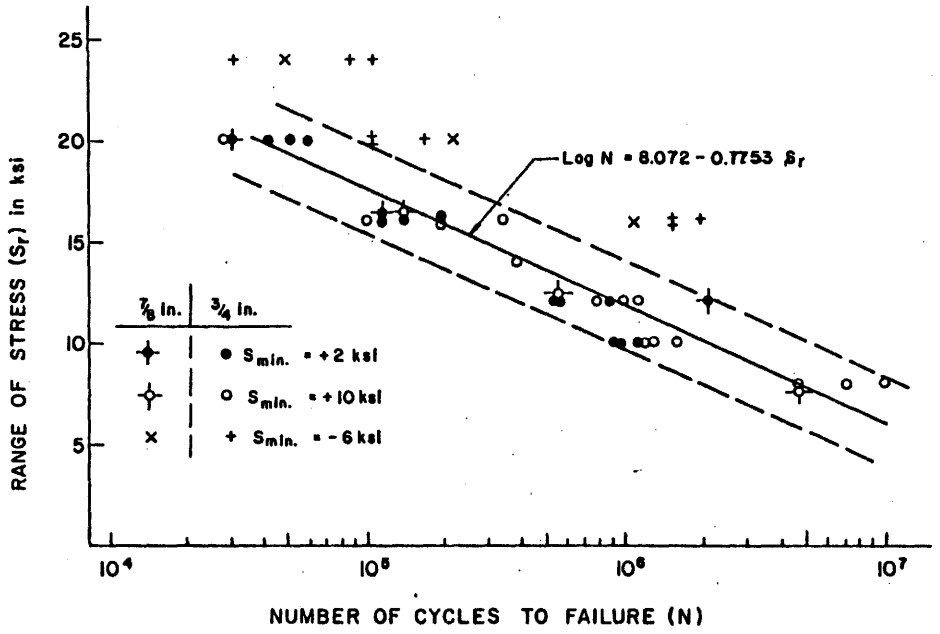

Figure 2. Push-out Test Results for 3/4 in. and 7/8 in. Diameter Studs (11).

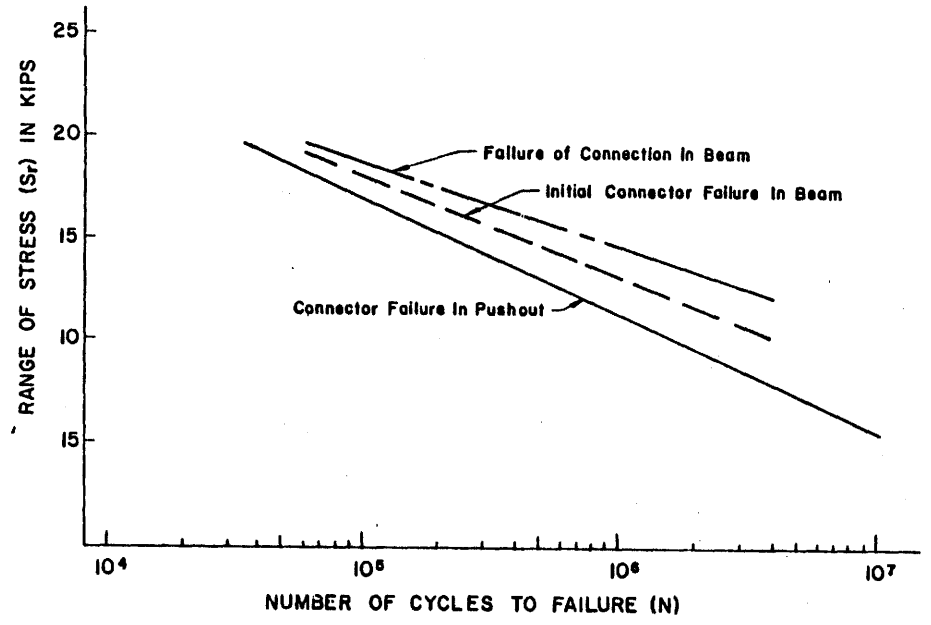

Figure 3. Comparison of Push-out Tests and Beam Fatigue Tests (11).

It was assumed that the existing deck of such a bridge would be replaced by a series of full-depth, 8 in.-thick precast panels typically 6 ft-long. A detail involving standard welded stud shear connectors and epoxy mortar would be used (4). The average nominal gap between the top of the stringer and the bottom of the precast panel would be 3/4 in. A side view of the prototype stringer and replacement panel is shown in Figure 4-b. It was further assumed that an isotropic reinforcement system consisting of same size bars, spaced equally both ways top and bottom, would be used for the precast slabs. Such reinforcement, for cast-in-place decks, is specified by the Ontario Bridge Design Code (8), and has been used experimentally by the New York State Department of Transportation (2).

Considering the facilities available, and upon review of the experience of models at other installations, a 1/3 scale was selected. Dead load and mass density effects were not included, considering that the composite action is engaged primarily to resist live loads only. This greatly simplified the design and loading scheme of the model. Necessary dimensional analyses were performed to scale the structural mechanics parameters in relation to live load only (9).

A 16 ft typical width of the prototype, including two interior stringers, was modeled. It was considered important to physically include cover plates in the model in order to simulate a realistic construction situation. A schematic layout of the model is shown in Figure 5. The value of the sectional property parameters of the prototype, an ideal 1/3 scale model, and the calculated values of the actual model design are shown in Table 1.

Model Stringer and Shear Connectors

The computed sectional properties of the stringers could ideally be obtained by welding plates cut to precise dimensions. However, a number of fabricators indicated that it would be difficult to mantain proper alignment. A compromise design was reached by using W 12x19 beam sections modified in the following manner: Cover plates, 3/16 in. thick, 2-3/4 in. wide and 13 ft-4 in. long were welded top and bottom, and both sides of top and bottom

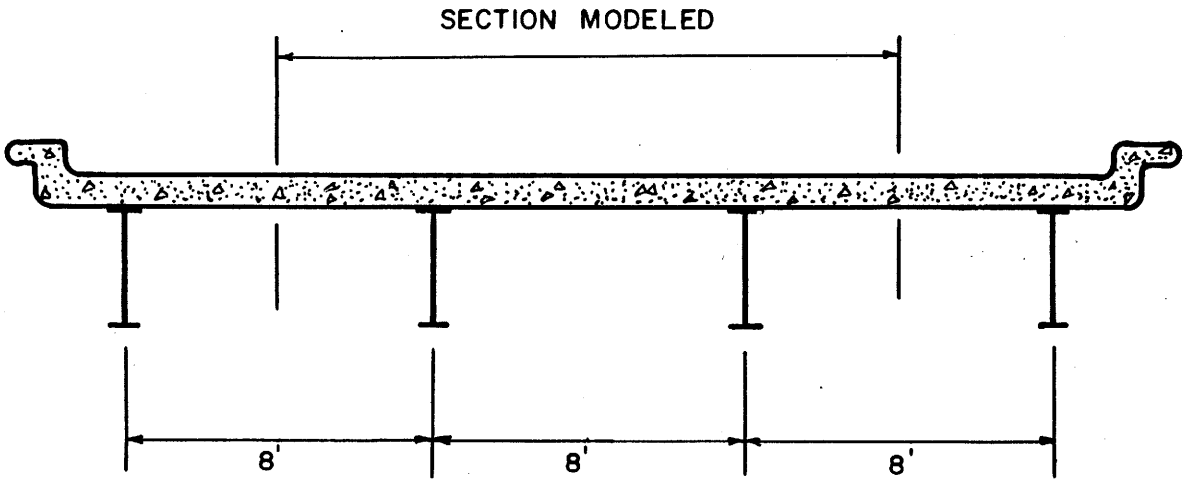

(a) CROSS SECTION

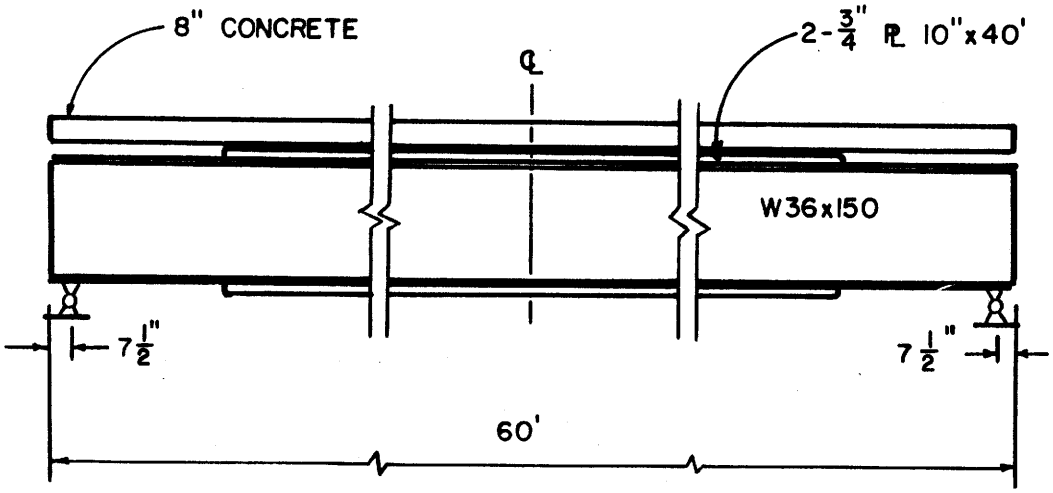

(b) SIDE VIEW

Figure 4. Schematic View of Prototype Bridge (13).

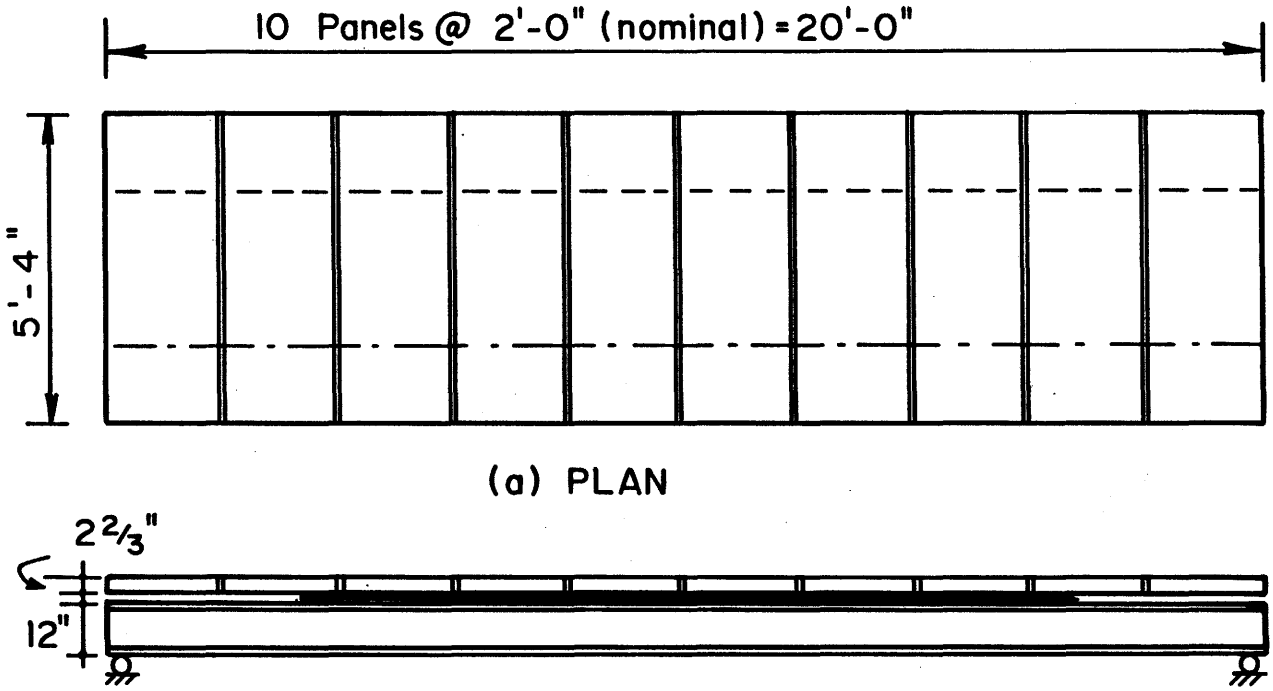

Figure 5. Layout of 1/3 Scale Model.

TABLE 1. Composite Sectional Properties of Prototype, a 1/3 Ideal Model, and the 1/3 Design Model (9).

	Composite Sectional Parameter	Prototype	1/3 Ideal Model	1/3 Design Model
MID SECTIONS	I, in $inches^4$	34370.	424.32	424.06
	Q, in $inches^3$	871.32	32.27	32.55
	S_{top}, in $inches^3$	2878.08	106.04	105.92
	S_{bot}, in $inches^3$	1029.1	38.11	37.87
	I/Q, in inches	39.45	13.15	13.03
END SECTIONS	I, in $inches^4$	25778.7	318.26	324.78
	Q, in $inches^3$	713.77	26.43	27.08
	S_{top}, in $inches^3$	2453.7	90.88	91.37
	S_{bot}, in $inches^3$	756.32	28.01	28.34
	I/Q, in inches	36.12	12.038	11.99

flanges at each end were coped by grinding away a 3/8 in. wide and 34-1/2 in. long strip from each edge. The design of the model stringers is shown in Figure 6.

In order to simulate realistic construction, available standard headed studs, 1/4 in. diameter, and 2-1/2 in. long were used. The shear studs were placed in pairs, with a lateral spacing of 1-3/4 in. and a longitudinal spacing of 6 in. center-to-center over the entire length of the model stringers.

Model Precast Concrete Panels and Reinforcing Steel

The overall dimensions of a typical, full depth, 1/3 scale precast concrete model panel is shown in Figure 7-a. Ten such identical panels were used in series to form the deck of the model span. The blocked-out holes were designed and positioned to fit over the headed studs which had been previously welded on the model stringers. Figure 7-b shows the details of the transverse joint between adjacent slabs.

Welded wire fabric, 3. x 3. - D3 x D3, was used as top and bottom reinforcement for the precast slab panels. This essentially eliminated all problems related to modeling the reinforcement. The mesh was equivalent to deformed 0.195 in. diameter bars spaced at 3.0 in. both ways. The steel area provided, with respect to the gross cross-sectional area of the slab, is 0.38%. This is less than the conventional steel requirement regarding transverse flexure, and it slightly exceeds the usual longitudinal distribution steel requirements of the AASHTO bridge specifications. The isotropic reinforcement provided, however, exceeds the requirements of the Specifications of the Ontario Highway Department and the practice of the New York State Department of Transportation.

Model Concrete Slab Casting

To model the concrete to the extent possible, nominal 3/8 in. maximum pea gravel, passed once through 1/4 in. sieve, was chosen as the coarse aggregate,

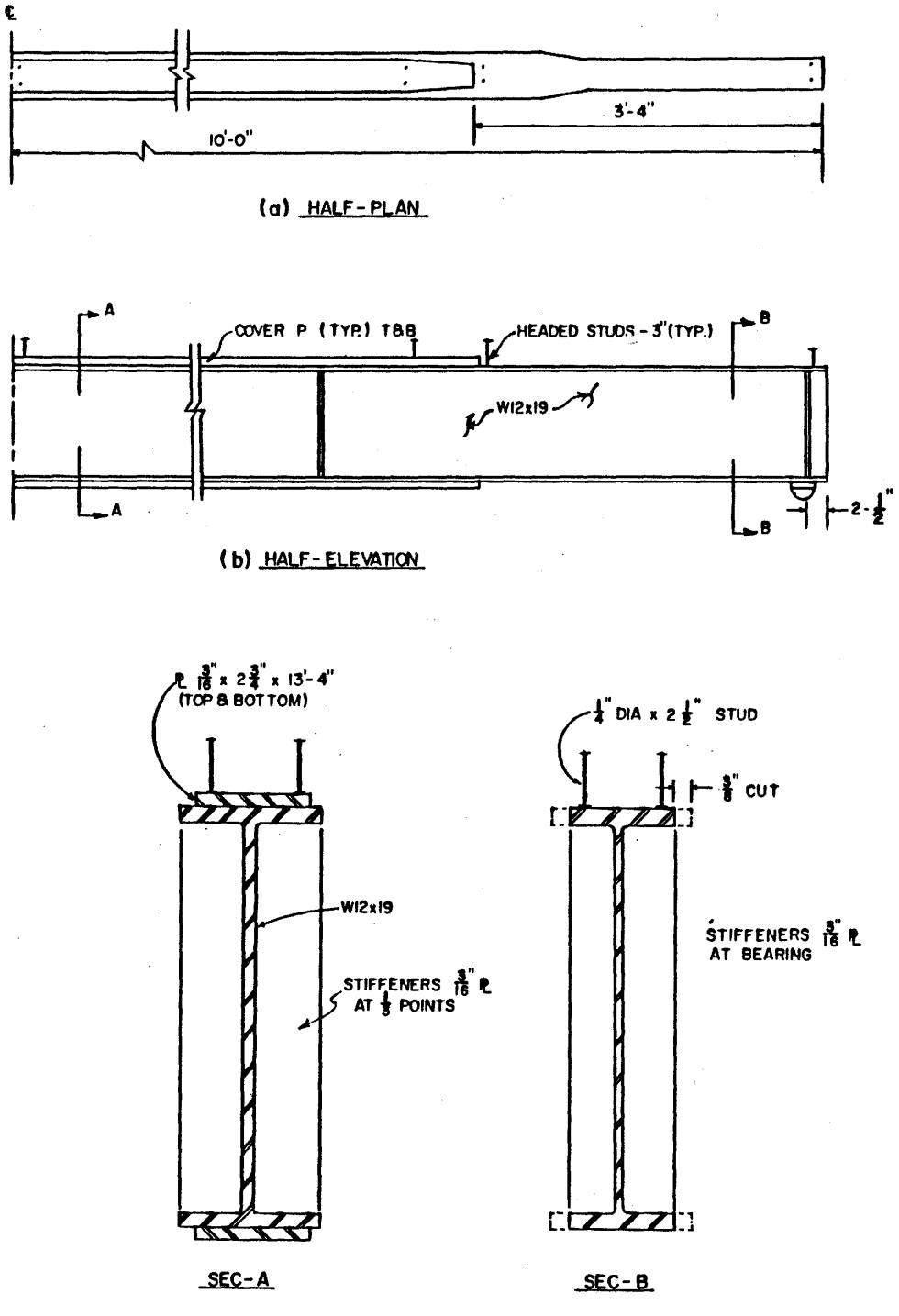

Figure 6. Details of Model Stringers.

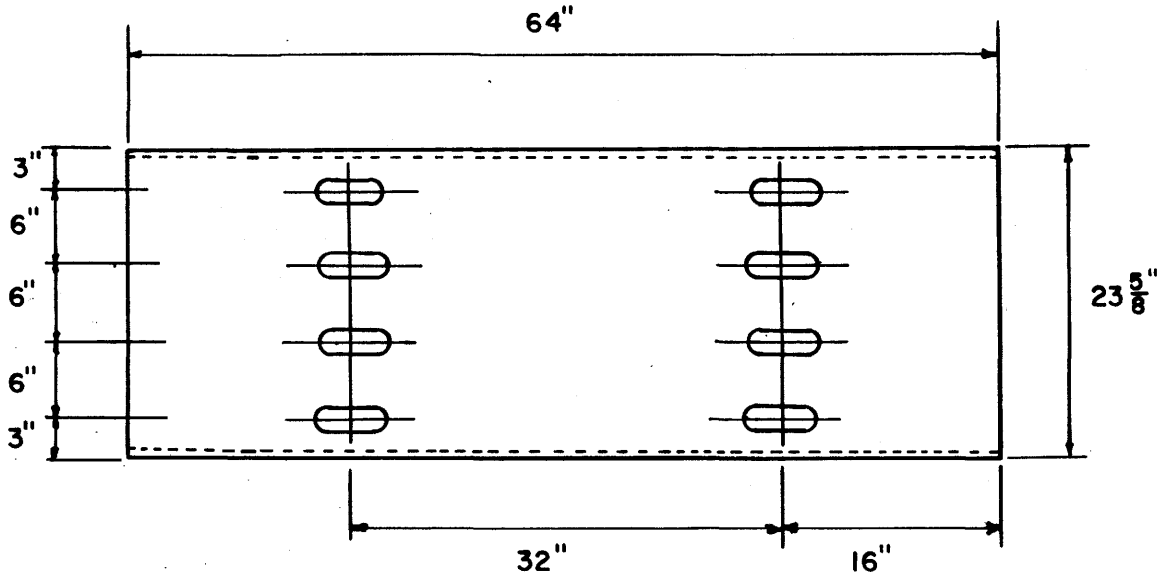

(a) PLAN

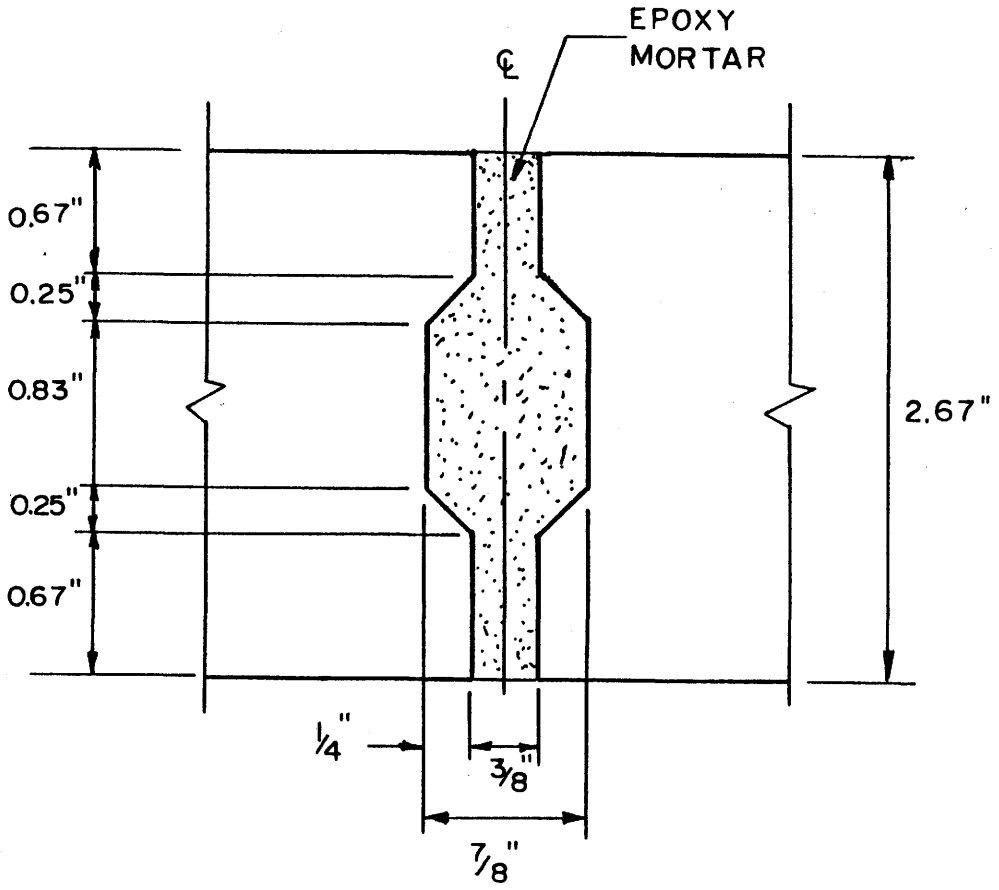

(b) SHEAR KEY

Figure 7. Details of Model Precast Panels.

and fine masonry sand was selected as the fine aggregate. The gradation of the coarse and fine aggregate, respectively, was nearly within the geometrically scaled down limits of AASHTO requirements. Because of the presence of a higher proportion of fines than in usual concrete, a larger amount of water was needed to obtain proper workability, and consequently, a relatively large cement factor of 9 bags per cubic yard was needed to obtain the necessary strength.

The panels were cured using wet burlap. Test cylinders of sizes 2 in. x 4 in. and 4 in. x 8 in. were also cast. All cylinders tested at over 6000 psi., in compression, at 28 days.

Epoxy Mortar

Texas Highway Department Standard Epoxy Binder B-102 was selected. It has customarily been used as a binder in a patching compound to repair existing concrete structures. It was not formally classified in accordance to the recent ASTM C-881 Specifications. However, it is similar to the ASTM Type III, Grade 1, Class C epoxy.

A compromise was made between using graded silica sand and common construction sand. Commercially available sandblasting sands, namely Texblast grades No. 2, No. 3 and No. 4, were considered. On the basis of sieve analyses, a 50-50 percent blend of Texblast No. 2 and No. 4 was selected. This blend meets the requirements of THD Grade No. 1 aggregate which is specified for mixing with B-102 epoxy compound (14).

The design of epoxy mortar mix was based on needed workability. Trial batches were made with sand to epoxy weight ratios of 2.75 to 3.50 at increments of 0.25.

A sand-to-epoxy weight ratio of 3 to 1 was selected to produce a trowellable mix which would be used to cast the pockets around the pairs of shear studs. A weight ratio of 2.75 to 1 was selected to produce a flowable mix which would be poured into the transverse keyways between adjacent slab panels.

Objectives of Study

The general objective of this investigation was to determine whether or not existing AASHTO fatigue design specifications are adequate for the composite connection between I-beams and precast concrete panels. This objective is accomplished by evaluating the overall performance of the 1/3 scale model bridge when two million load cycles of an equivalent AASHTO HS-20(44) truck are applied.

The performance is evaluated by measuring the following parameters throughout the test:

a) bridge deflections at the quarter points of the bridge,
b) flexural strains, to estimate the cross-sectional properties of the bridge model, and
c) relative slip displacements between the precast concrete modules and the model stringers at different locations.

Scope of the Study

This laboratory work is limited to a scale model test. A scale factor of 1/3 is used. Consequently, the dimension parameters are scaled by 1/3, the force quantities by 1/9 and stresses by unity. Dead load effects were not modeled; however, only live loads act on the composite sections if no shoring is used during construction.

This study is limited to the amount of obtainable information. Only 16 channels of information were collected, three for deflections, eight for strain gages to measure the flexural strains, and five for displacement transducers to measure slip displacements.

The HS-20 moving truck loads are applied as fixed concentrated loads distributed over each model stringer, placed to provide the design shear over a portion of the model structure.

CHAPTER II

ANALYTICAL WORK

General

The analytical work discussed in this chapter has a primary objective of providing simple theoretical solutions for verification of the experimental results to be obtained in the test. Static and dynamic analyses are performed to model the scaled bridge behavior assuming Euler beam theory. However, instead of following the procedure for determining the wheel load distribution on the I-beams outlined in the AASHTO specifications (1), a more rational procedure based on orthotropic plate theory is used.

To simulate HS-20 truck loads, it is considered that only repetitive vertical shear forces are likely to deteriorate or fatigue the shear stud and the epoxy mortar connection performing the horizontal shear force transfer, thus only the maximum live-load plus impact shear is used as criteria to determine the equivalent truck loads to be applied to the 1/3 scale model bridge.

This equivalent truck load is designed to be of the form of two fixed equal concentrated loads over each of the model stringers harmonically varying in time. Then, the Euler beam model that is used in the static and dynamic analyses is shown in Figure 8. Table 2 shows the main sectional parameters that are involved in the analyses.

The dynamic response of the structure is easily obtained in closed form solution using sine series approximations. Thus, the static results are also expressed in series form because dynamic amplification factors are to be obtained. Dynamic amplification factors are defined as the ratio of the maximum dynamic response to the static response.

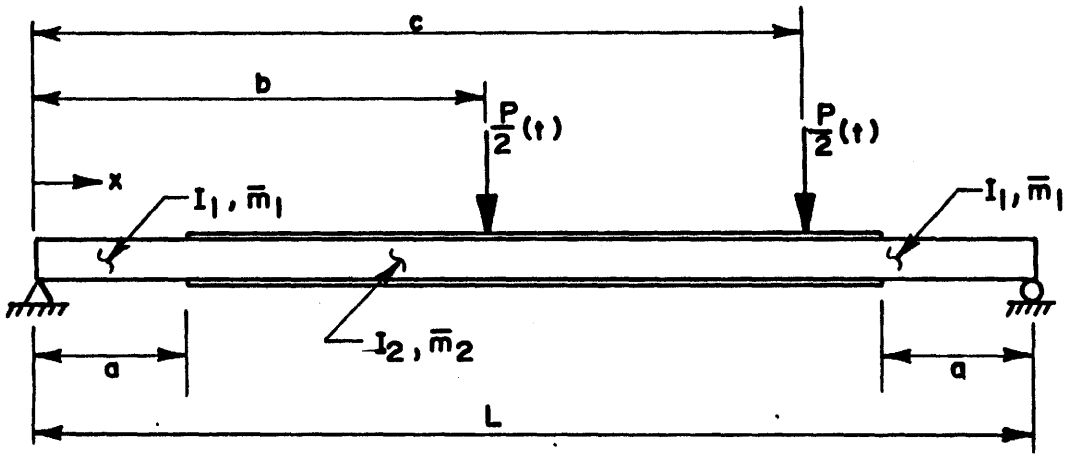

Figure 8. Euler Beam Model.

TABLE 2. Bridge Model Sectional Parameters.

Parameter	End Section	Middle Section
Moment of Inertia ($in.^4$)	$I_1 = 316.$	$I_2 = 424.$
Mass Moment of Inertia ($in.^4$)	$I_{m1} = 563.$	$I_{m2} = 411.$
Distributed Mass ($lb\text{-}sec/in.^2$)	$m_1 = .00244$	$m_2 = .02355$
Shear Area A_{s_2} ($in.^2$)	2.92	2.92

Wheel Load Distribution Factor

The wheel load distribution factor obtained for the 60-ft prototype bridge is based on orthotropic plate theory and the work performed by Sanders and Elleby (10). The maximum wheel load distribution factor is a function of the following principal variables:

α, the relative torsional stiffness parameter,

θ, the relative flexural stiffness parameter,

W, the actual width of the bridge structure and

N_w, the number of longitudinal lines of wheel load.

The flexural parameter θ and the torsional parameter α are computed using the following formulas:

$$\theta = \frac{W}{2L}\sqrt[4]{\frac{D_x}{D_y}} \tag{1}$$

and

$$\alpha = \frac{D_{xy} + D_{yx}}{2\sqrt{D_x D_y}} \tag{2}$$

where

L = span length

W = bridge width

D_{xy} = torsional stiffness in the longitudinal direction per unit width,

D_{yx} = torsional stiffness in the transverse direction per unit length,

D_x = flexural stiffness in the longitudinal direction per unit width, and

D_y = flexural stiffness in the transverse direction per unit length.

The calculations for the parameters θ and α for the prototype bridge are shown in Appendix B. The corresponding computed values are:

$$\theta = 0.74 \qquad \text{and} \qquad \alpha = 0.24$$

With the above values, the factor D is obtained from Table 3 to be used in computing the wheel load distribution factor LF, by the formula:

$$LF = \frac{S}{D} \tag{3}$$

where,

S = transverse stringer spacing

D = factor obtained from Table 3.

Therefore, after substituting all the values into Equation 3, a wheel load distribution factor of 1.33 is calculated. Notice that it is a different factor from the 1.45 suggested by the AASHTO Specification procedure.

Maximum Loads on Prototype Bridge

A static analysis is performed on the 60-ft prototype bridge to determine the maximum bending moment and vertical shear distributed over an interior stringer produced by an HS-20 AASHTO design truck. The analysis is shown in Appendix C.

The maximum live load plus impact bending moment is 681.2 k-ft and the maximum reaction and shear is 51.3 kips.

Static Analysis of 1/3 Scale Model

The Rayleigh-Ritz method is used to determine the static deflection and moment solutions. First, the deflection of the beam is approximated by a sine series function of the form:

$$w(x) = \sum_{n=1}^{\infty} w_n \sin\left(\frac{n \pi x}{L}\right) \tag{4}$$

The total strain energy due to bending is evaluated using the classical expression:

TABLE 3. Theoretical Values of D in L.F.= S/D (10).

		VALUE OF D FOR BRIDGE WIDTH, W, AND (N_w), NO. OF WHEEL LOADS											
θ	a	28 FT (4)	33 FT (4)	37 FT (4)	39 FT (6)	41 FT (6)	45 FT (6)	49 FT (6)	51 FT (8)	53 FT (8)	57 FT (8)	61 FT (8)	75 FT (10)
0.25	0.00	5.66	5.23	5.16	5.17	5.20	5.27	5.13	5.10	5.08	5.08	5.12	5.04
	0.04	5.97	5.78	5.82	5.87	5.88	5.72	5.68	5.68	5.70	5.76	5.65	5.63
	0.16	6.38	6.59	6.85	6.23	6.25	6.34	6.49	6.17	6.18	6.24	6.32	6.10
	0.36	6.60	7.12	7.55	6.33	6.46	6.73	7.01	6.24	6.34	6.54	6.75	6.16
	0.64	6.71	7.42	7.97	6.38	6.58	6.95	7.32	6.27[a]	6.43	6.71	6.99	6.18[a]
	1.00	6.78	7.61	8.25	6.40[a]	6.64	7.08	7.52	6.29[a]	6.48	6.81	7.14	6.19[a]
0.50	0.00	5.81	5.53	5.44	5.42	5.43	5.47	5.41	5.36	5.33	5.30	5.32	5.25
	0.04	5.89	5.70	5.63	5.63	5.64	5.67	5.57	5.53	5.51	5.50	5.53	5.45
	0.16	6.06[a]	6.07	6.10	6.09[a]	6.07	5.97	5.95	5.95	5.95	5.95	5.90	5.86
	0.36	6.17[a]	6.47	6.62	6.15[a]	6.24	6.29	6.36	6.03[a]	6.16	6.20	6.24	6.03[a]
	0.64	6.28[a]	6.79	7.08	6.20[a]	6.36	6.54	6.71	6.08[a]	6.26[a]	6.40	6.53	6.06[a]
	1.00	6.38[a]	7.05	7.45	6.25[a]	6.46	6.72	6.98	6.12[a]	6.31[a]	6.55	6.75	6.09[a]
0.75	0.00	5.13[a]	5.52[a]	5.86	5.58[a]	5.64[a]	5.73	5.74	5.49[a]	5.54[a]	5.66[a]	5.65	5.62
	0.04	5.21[a]	5.63[a]	5.92	5.63[a]	5.71[a]	5.83	5.86	5.54[a]	5.60[a]	5.73[a]	5.73	5.69[a]
	0.16	5.41[a]	5.89[a]	6.09	5.76[a]	5.86[a]	6.00	5.99	5.65[a]	5.73[a]	5.90[a]	5.96	5.77[a]
	0.36	5.62[a]	6.18[a]	6.33	5.88[a]	6.02[a]	6.15	6.17	5.76[a]	5.87[a]	6.09[a]	6.12	5.85[a]
	0.64	5.82[a]	6.43	6.61	5.99[a]	6.16[a]	6.30	6.39	5.86[a]	5.99[a]	6.23	6.29	5.92[a]
	1.00	5.98[a]	6.64	6.88	6.08[a]	6.27[a]	6.45	6.59	5.94[a]	6.09[a]	6.35	6.45	5.97[a]
1.00	0.00	4.64[a]	4.88[a]	5.15[a]	5.29[a]	5.29[a]	5.30[a]	5.37[a]	5.20[a]	5.20[a]	5.23[a]	5.29[a]	5.44[a]
	0.04	4.73[a]	4.98[a]	5.26[a]	5.35[a]	5.36[a]	5.40[a]	5.48[a]	5.25[a]	5.26[a]	5.31[a]	5.39[a]	5.48[a]
	0.16	4.93[a]	5.24[a]	5.56[a]	5.49[a]	5.54[a]	5.62[a]	5.74[a]	5.38[a]	5.42[a]	5.50[a]	5.61[a]	5.58[a]
	0.36	5.18[a]	5.56[a]	5.92[a]	5.66[a]	5.73[a]	5.88[a]	6.04[a]	5.52[a]	5.59[a]	5.73[a]	5.87[a]	5.68[a]
	0.64	5.41[a]	5.87[a]	6.27[a]	5.79[a]	5.91[a]	6.12[a]	6.21	5.65[a]	5.74[a]	5.93[a]	6.11[a]	5.77[a]
	1.00	5.61[a]	6.14[a]	6.54	5.91[a]	6.05[a]	6.29	6.36	5.76[a]	5.87[a]	6.10[a]	6.32[a]	5.85[a]
1.25	0.00	4.42[a]	4.58[a]	4.79[a]	4.91[a]	5.04[a]	5.15[a]	5.16[a]	5.06[a]	5.05[a]	5.06[a]	5.10[a]	5.28[a]
	0.04	4.49[a]	4.66[a]	4.88[a]	5.00[a]	5.13[a]	5.22[a]	5.24[a]	5.10[a]	5.10[a]	5.12[a]	5.17[a]	5.34[a]
	0.16	4.65[a]	4.86[a]	5.10[a]	5.24[a]	5.37[a]	5.40[a]	5.44[a]	5.21[a]	5.23[a]	5.28[a]	5.35[a]	5.45[a]
	0.36	4.86[a]	5.13[a]	5.41[a]	5.50[a]	5.54[a]	5.63[a]	5.70[a]	5.34[a]	5.39[a]	5.48[a]	5.57[a]	5.55[a]
	0.64	5.08[a]	5.42[a]	5.96[a]	5.64[a]	5.71[a]	5.85[a]	5.97[a]	5.47[a]	5.54[a]	5.67[a]	5.81[a]	5.64[a]
	1.00	5.29[a]	5.70[a]	6.06[a]	5.76[a]	5.86[a]	6.05[a]	6.20	5.59[a]	5.67[a]	5.85[a]	6.02[a]	5.73[a]

[a] Controlled by central loading; other values controlled by eccentric loading.

$$U_b = \frac{1}{2} \int_0^L EI(x) \{ w(x)'' \}^2 \, dx \tag{5}$$

Since the beam model has three distinct sections with different moments of inertia, Equation 5 becomes:

$$U_b = \frac{1}{2} E \left[2 I_1 \int_0^a \{ w(x)'' \}^2 dx + I_2 \int_a^{L-a} \{ w(x)'' \}^2 dx \right] \tag{6}$$

Differentiating Equation 4 twice, and substituting the results into Equation 6, the strain energy due to bending U_b, is found as:

$$U_b = \frac{w_n^2 \, n^4 \, \pi^2 \, E \, I_n}{4 \, L^3} \tag{7-a}$$

where,

$$I_n = I_2 - 2 (I_2 - I_1) \left\{ \frac{a}{L} - \frac{1}{2 \pi n} \sin\left(\frac{2n \pi a}{L} \right) \right\} \tag{7-b}$$

The total work done by the applied concentrated load is:

$$W = -\frac{P}{2} w_n \left\{ \sin\left(\frac{n \pi b}{L} \right) + \sin\left(\frac{n \pi c}{L} \right) \right\} \tag{8}$$

Therefore, the principle of total potential is used to determine the unknown coefficients. First, the following expression is utilized:

$$\Pi = U_b - W \tag{9}$$

Substituting Equations 7 and 8 into Equation 9 and then differentiating the results with respect to the deflection coefficient w_n and setting the results equal to zero, w_n is determined to be:

$$w_n = \frac{PL^3}{n^4 \, \pi^4 \, E \, I_n} \left\{ \sin\left(\frac{n \pi b}{L} \right) + \sin\left(\frac{n \pi c}{L} \right) \right\} \tag{10}$$

Equation 10 is now substituted into Equation 4. Thus, the sine series solution for the beam deflection is given by:

$$w(x) = \frac{P L^3}{E \pi^2} \sum_{n=1}^{\infty} \frac{\{\sin(\frac{n \pi b}{L}) + \sin(\frac{n \pi c}{L})\}}{n^4 I_n} \sin(\frac{n \pi x}{L}) \qquad (11)$$

A bending moment expression is easily obtained by employing the classical equation for an Euler beam:

$$M(x) = - EI\ w(x)'' \qquad (12)$$

Differentiating Equation 11 twice with respect to the variable x and substituting the results into Equation 12, the following sine series approximation is obtained for the bending moments:

$$M(x) = \frac{P L}{\pi^2} \sum_{n=1}^{\infty} \frac{1}{n^2} \{ \sin(\frac{n \pi b}{L}) + \sin(\frac{n \pi c}{L}) \} \sin(\frac{n \pi x}{L}) \qquad (13)$$

The static analysis is now concluded. The sine series solution for the static deflection and moment given by Equations 11 and 13 are later compared with the respective dynamic solution to determine dynamic amplification factors.

Dynamic Analysis

A dynamic analysis was performed on the beam model subjected to a harmonic loading as shown in Figure 8. The Rayleigh-Ritz method is employed. First it was assumed that the displacement at any location of the beam as a function of time is equal to a shape function $\phi_n(x)$ times the amplitude of motion $Y_n(t)$ in terms of the generalized coordinates. Thus, the general displacement function $w(x,t)$ can be expressed as:

$$w(x,t) = \phi_n(x)\ Y_n(t) \qquad (14)$$

Conventional expressions for the maximum strain energy and the maximum kinematic energy are obtained. By equating these two expressions, the natural vibration frequencies can be determined. The natural eigenfrequencies are given by (6):

$$\omega^2 = \frac{\int_0^L EI(x) \{ \phi(x)'' \}^2 dx}{\int_0^L m(x) \{ \phi(x) \}^2 dx} \qquad (15)$$

The above expression is valid for any Euler beam model. The specific expression for the eigenfrequencies for the bridge model is developed in the next section.

Determination of Model Eigenfrequencies

In order to determine the natural eigenfrequencies for the model bridge, a primary shape function is assigned to be an arbitrary sine wave function satisfying the assumed pin-roller support boundary conditions. Therefore, $\phi_n(x)$ is defined as follows:

$$\phi_n(x) = \sin\left(\frac{n \pi x}{L}\right) \qquad (16)$$

By substituting this expression and its second derivative into Equation 15 and then evaluating the integrals, a simple formula is obtained for the natural frequencies of the bridge model. This formula is given by:

$$\omega_n = n^2 \pi^2 \sqrt{\frac{E I_n}{L^4 m_n}} \qquad (17\text{-a})$$

where,

$$I_n = I_2 - 2 (I_2 - I_1) \left\{ \frac{a}{L} - \frac{1}{2 \pi n} \sin\left(\frac{2n \pi a}{L} \right) \right\} \qquad (17\text{-b})$$

$$m_n = m_2 - 2 (m_2 - m_1) \left\{ \frac{a}{L} - \frac{1}{2 \pi n} \sin\left(\frac{2n \pi a}{L} \right) \right\} \qquad (17\text{-c})$$

The terms I_n and m_n are the average transformed moment of inertia and the average distributed mass associated with the mode shape $\phi_n(x)$. Equation 17 does not include rotary inertia nor shear deformation effects. However, since the bridge model is composite, the rotary inertia and shear deformations may be significant to affect the the eigenfrequencies. Thus, a correction factor can be applied to Equation 17 to yield better results. This factor is given as follows (6):

$$CF = \frac{1}{1 + (\frac{n\pi}{L})^2 \{ (\frac{\rho I_{me}}{m_n}) + \frac{EI_n}{As\ G} \}} \qquad (18)$$

where

G = modulus of rigidity,

A_s = effective sectional area acting in shear,

ρ = mass density of steel, and

I_{me} = the average mass moment of inertia of the composite section transformed to equivalent steel mass.

Values for the eigenfrequencies can now be evaluated using Equations 17 and 18. Table 4 shows the eigenfrequencies for the first three bending modes for the bridge model. The first column shows the values obtained by evaluating Equation 17 with the parameters of Table 2. The next column was evaluated with Equation 18 and multiplying the results to the values of the first column. The third column was obtained by modeling the scaled bridge using finite elements and solved with the computer program STRUDL (12). Since the concrete panels and the steel stringers were modelled independently, some shear deformations and rotary inertia effects are included in the STRUDL results. Thus, the values obtained with STRUDL verify Equations 17 and 18.

It is observed that the values shown in the second and third columns of the previous table are very close and the error between them increases proportionally to the mode number. However, the loading frequency for the experiment is expected to be small compared to the fundamental frequency. Therefore, higher frequency vibration modes will not be excited by the harmonic loading. Thus, it is concluded that Equation 17 yields a good

TABLE 4. Eigenfrequencies for Model Bridge.

Mode Number	Eigenfrequency (rad/sec)		
	Euler Model (Eq. 17)	Corrected Euler Model (Eqs. 17 and 18)	STRUDL Model
1	128.4	120.9	125.4
2	507.0	408.8	462.3
3	1124.3	738.8	807.3

approximation to the natural eigenfrequencies of the bridge model when the correction factor for shear deformation and rotary inertia of Equation 18 is applied.

Dynamic Response to Harmonic Loading

General sine series solutions of the dynamic response of the scaled bridge when subjected to harmonic loading are obtained. First, the harmonic loading function simulating the equivalent HS-20 truck load cycles is assumed to be of the following form:

$$P(x,t) = \frac{P}{4} \{ 1 + \sin(\bar{\omega} t) \} \tag{19}$$

Second, the following undamped, uncoupled flexural equation of motion is used (6):

$$\ddot{Y}_n(t) + \omega_n^2 Y_n(t) = \frac{P_n(t)}{M_n} \tag{20}$$

where

M_n = the generalized mass of the beam model associated with the n^{th} mode shape function,

P_n = the generalized load associated with the n^{th} mode shape function,

ω_n = the eigenfrequency of the n^{th} mode shape and

Y_n = the modal response of the n^{th} mode.

The generalized mass and the generalized load can be found by evaluating the integrals of the following two expressions, respectively:

$$M_n = \int_0^L \phi_n(x)\, m(x)\, dx \tag{21}$$

and

$$P_n = \int_0^L \phi_n(x)\, P(x,t)\, dx \tag{22}$$

Substituting the mode shape function of Equation 16 into Equation 21 and integrating over the length according to Figure 8, the generalized mass of the beam model becomes:

$$M_n = \frac{m_n L}{2} \tag{23}$$

In order to evaluate the integral of Equation 22, it is noted that the harmonic load of Equation 19 is applied at two different locations, b and c, measured from the left support. Thus Equation 22 becomes:

$$P_n(t) = P(x,t) \{ \phi_n(x=b) + \phi_n(x=c) \} \tag{24}$$

Substituting Equation 19 into the previous expressions and evaluating the mode shape function at b and c, the generalized load gives:

$$P_n = \frac{P}{4} (1 + \sin \bar{\omega} t) \{ \sin (\frac{n \pi b}{L}) + \sin (\frac{n \pi c}{L}) \} \tag{25}$$

Now, the second order differential expression of Equation 20 can be solved by substituting Equations 23 and 25. Therefore, the general solution for the modal response is given by:

$$Y_n(t) = A \sin \omega_n t + B \cos \omega_n t + \frac{P C_n \sin \bar{\omega} t}{4 M_n (\omega_n^2 - \bar{\omega}^2)} + \frac{P C_n}{4 \omega_n^2 M_n} \qquad (26\text{-a})$$

$$C_n = \sin\left(\frac{n \pi b}{L} \right) + \sin\left(\frac{n \pi c}{L} \right) \qquad (26\text{-b})$$

where A and B are constants that are obtained by applying the following initial boundary conditions:

$$Y_n(t=0) = \frac{P C_n}{2 \omega_n^2 M_n} \quad \text{and} \quad Y_n(t=0) = 0 \qquad (27)$$

When the above initial conditions are substituted in to Equation 26, the constants A and B are solved to be as follows:

$$A = - \frac{P C_n \bar{\omega}}{4 M_n \omega_n (\omega_n^2 - \bar{\omega}^2)} \qquad (28\text{-a})$$

$$B = 0 \qquad (28\text{-b})$$

Substituting the constants of Equations 28-a and 28-b into Equation 26, a general solution is obtained for the modal response $Y_n(t)$:

$$Y_n(t) = \frac{P C_n}{4 \omega_n^2 M_n} \left\{ 1 + \frac{1}{1-\beta^2} \sin \bar{\omega} t - \frac{\beta}{1-\beta^2} \sin \omega_n t \right\} \qquad (29)$$

where

β = the ratio of the loading frequency to the natural eigenfrequencies.

The displacement as a function of x and time can be found by using Equation 14. Substituting the modal shape function $\phi_n(x)$ of Equation 16 and the modal response $Y_n(t)$ of Equation 29 into Equation 14, an approximation function is found for the displacement:

$$w(x,t) = \sum_{n=1}^{\infty} \frac{P\,C_n}{4\,\omega_n^2\,M_n} \left\{ 1 + \frac{1}{1-\beta^2}\sin \bar{\omega}\,t - \frac{\beta}{1-\beta^2}\sin \omega_n t \right\} \sin\left(\frac{n\pi x}{L}\right) \qquad (30)$$

Substituting the expressions for the eigenfrequencies and the generalized modal mass, Equation 30 now becomes:

$$w(x,t) = \frac{P\,L^3}{2\,\pi^4\,E} \sum_{n=1}^{\infty} \frac{C_n}{n^4\,I_n} \left\{ 1 + \frac{1}{1-\beta^2} \sin \bar{\omega}\,t - \frac{\beta}{1-\beta^2}\sin \omega_n t \right\} \sin\left(\frac{n\pi x}{L}\right) \qquad (31)$$

Equation 31 is now the basic expression from which dynamic moments and dynamic amplification factors can be calculated. This is performed in the next section.

Dynamic Amplification Factors

The dynamic response solutions obtained in the previous section are compared to the static solution. However, the dynamic response solutions need to be simplified and expressed in terms of the maximum response amplitudes.

The transient part of Equation 31 is neglected because it is much smaller than the steady state solution. This is also supported by the fact that the transient term quickly damps out. Thus, the maximum displacement response is:

$$w(x)_{max} = \frac{P\,L^3}{\pi^4\,E} \sum_{n=1}^{\infty} \frac{C_n}{n^4\,I_n} \left\{ \frac{1}{1-\beta^2} \right\} \sin\left(\frac{n\pi x}{L}\right) \qquad (32)$$

Subsequently, the maximum moment response is obtained by using the Euler beam Equation 12, and the maximum moment becomes:

$$M(x)_{max} = \frac{P\,L}{\pi^2} \sum_{n=1}^{\infty} \frac{C_n}{n^2} \left\{ \frac{1}{1-\beta^2} \right\} \sin\left(\frac{n\pi x}{L}\right) \qquad (33)$$

Then the dynamic amplification factors are obtained by dividing the maximum dynamic response solution to the static solution. These factors are obtained for deflection and bending moment as functions of the variable x.

The deflection amplification factor is obtained by dividing Equation 32 by Equation 11. After cancelling terms and simplifying, the dynamic amplification factor for deflection D_w, becomes:

$$D_w(x) = \frac{\sum_{n=1}^{\infty} \frac{C_n}{n^4 I_n} \sin\left(\frac{n\pi x}{L}\right) \left\{\frac{1}{1-\beta^2}\right\}}{\sum_{n=1}^{\infty} \frac{C_n}{n^4 I_n} \sin\left(\frac{n\pi x}{L}\right)} \tag{34}$$

Similarly, the dynamic moment amplification factors are obtained by dividing Equation 33 to Equation 13. And after cancelling terms, the dynamic moment amplification factor D_m, becomes:

$$D_m(x) = \frac{\sum_{n=1}^{\infty} \frac{C_n}{n^2} \sin\left(\frac{n\pi x}{L}\right) \left\{\frac{1}{1-\beta^2}\right\}}{\sum_{n=1}^{\infty} \frac{C_n}{n^2} \sin\left(\frac{n\pi x}{L}\right)} \tag{35}$$

It was found the these amplification factors are function of x as shown in Figure 9.

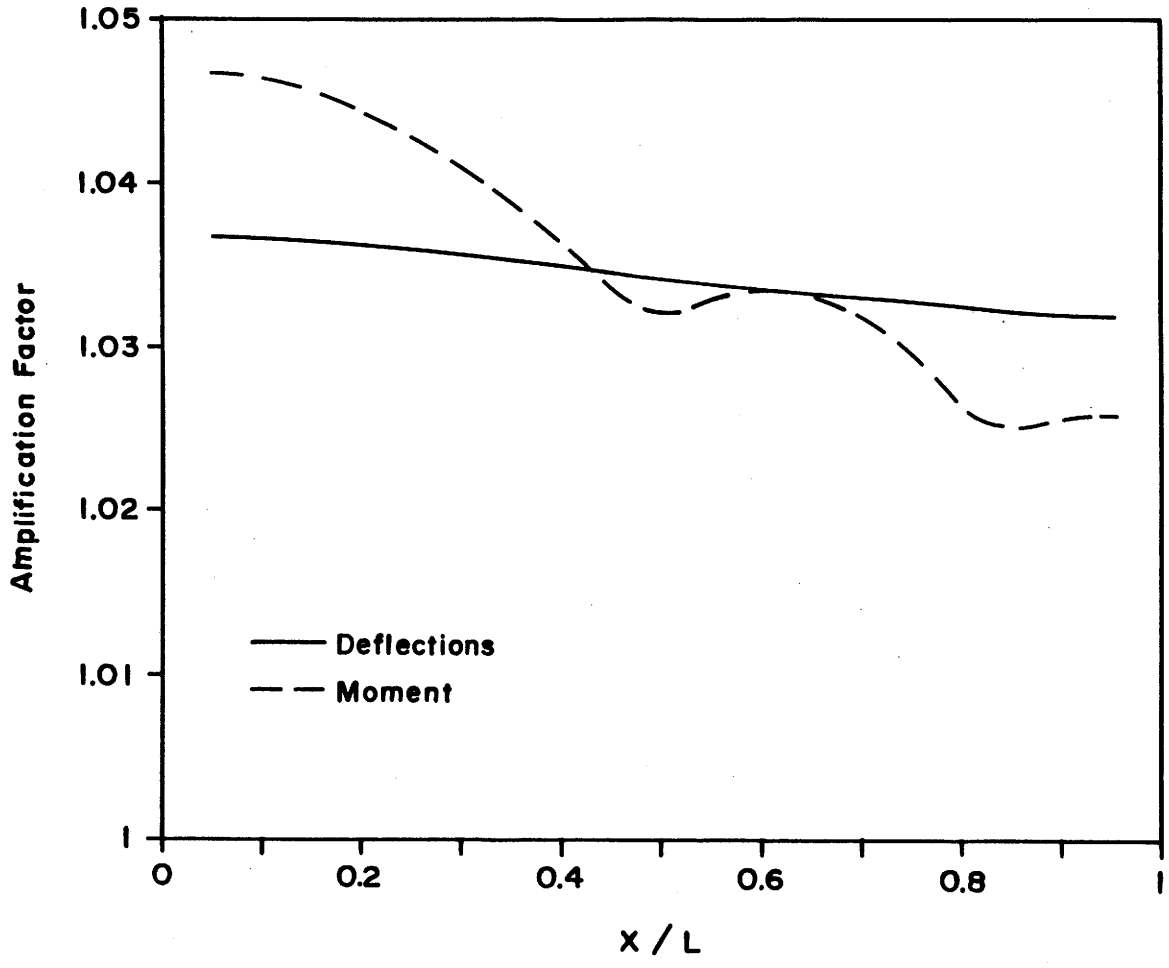

Figure 9. Dynamic Amplification Factors.

CHAPTER III

EXPERIMENTAL WORK

General

Descriptions of the test set-up, the loading system, the instrumentation and the test procedures are presented in this section. The set-up of the model bridge was such that the maximum equivalent HS-20 shear would be applied at only one end portion of the model. Thus, the loading was not symmetrical about the midspan. The loads were applied with two identical 55-kip actuators controlled by a voltage signal generator.

Strain gages and deflection transducers were used to measure flexural strains, vertical deflections and slip displacements. A computerized data acquisition system was employed to manipulate and store the acquired data on floppy disks.

Description of Test Set-up

The model bridge was set up inside the Texas A&M University Structures Laboratory. The set-up was designed to achieve the loading conditions shown in Figure 10. The centroid of the two equal loads was located at 36 in. from the midspan toward the west end of the model bridge. The model was placed on top of a support system which was bolted to a reaction floor. Each end of the model bridge was resting directly upon a W16x26 steel section; however, the supports were transversely braced to avoid unwanted vibrations during the dynamic loading. Additionally, a W6x24 reference beam was welded between the supports to provide a fixed reference line for measuring deflections.

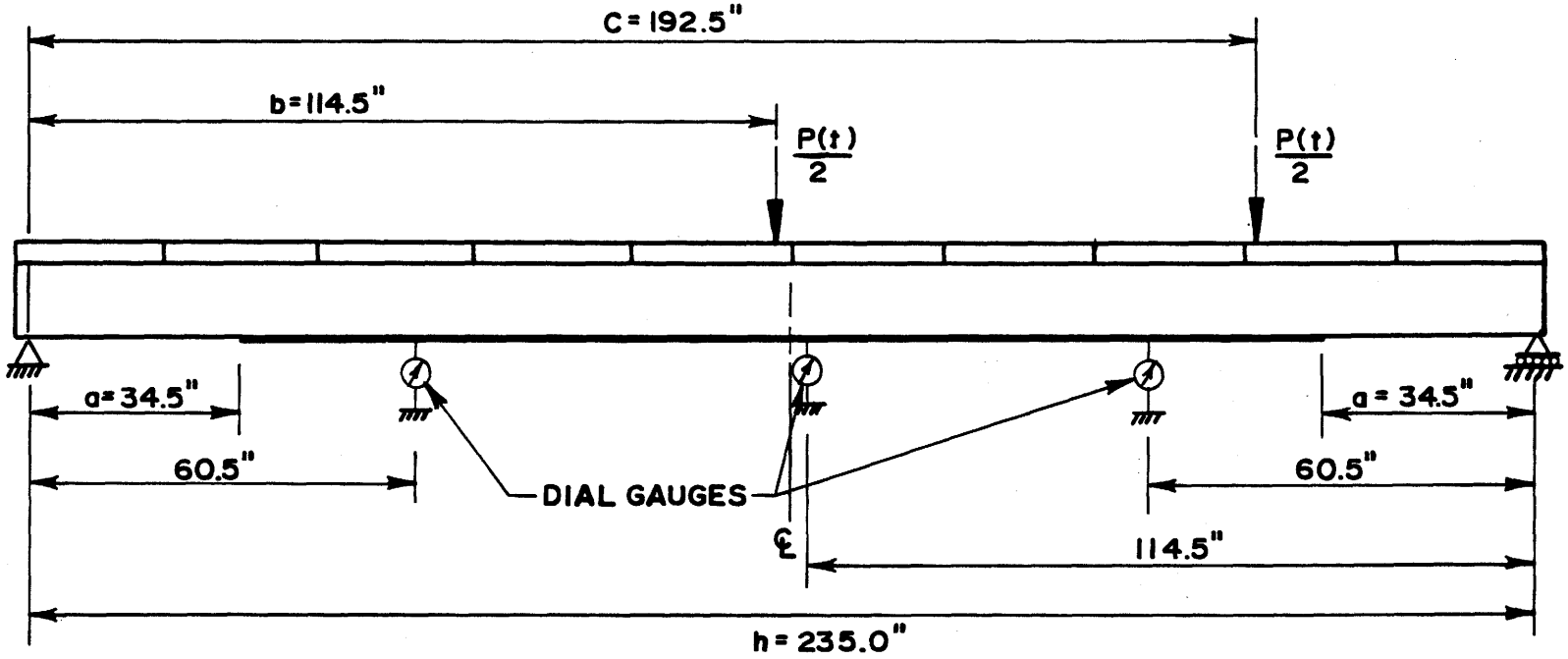

Figure 10. Loading of Model Bridge.

Description of the Loading System

The loading system consisted of two identical MTS brand 55-kip hydraulic actuators, a reaction frame, and a voltage signal generator to control the desired sinusoidal loading. Careful adjustments were required to accomplish equal and in-phase loadings by the two actuators. Additionally, a spread beam was bolted to each of the actuators to distribute the load to two points per model stringer.

The reaction frame consisted of two W14x61 columns, each 14 ft tall and spaced 9 ft center-to-center, and a W14x135 cross beam spanning between the two columns. The frame was bolted to the reaction floor and placed transversely across the model bridge at a station 36 in. from the midspan.

The actuators were attached to the bottom flange of the frame cross beam. Each actuator included a linear variable displacement transducer (LVDT), a load cell and a servo-valve which controlled the internal pressure of the actuators.

Instrumentation

The instrumentation consisted of strain gages, strain-gage type displacement transducers and the load cells and LVDT's incorporated in the hydraulic actuators. The strain gages were used to measure flexural strains at two different cross sections of the north model stringer. The displacement transducers were employed to measure the model deflections and the relative slip displacements between the modular panels and the steel stringers.

Eight resistance strain gages were bonded to the steel surface of the model stringers to measure flexural strains for determination of dynamic section properties at the two sections. The displacement transducers used for measuring deflection were installed under the north beam of the model bridge for measurements at the quarter points between the supports. Five displace ment transducers were used for measuring slip displacement; four were

installed on the north model stringer to obtain a slip displacement profile, and the other was employed as a back-up point in the south model stringer.

The load cell and LVDT signals from each actuator were also monitored and recorded. Thus, twenty channels of information were monitored throughout the experiment. Figure 11 graphically illustrates the first sixteen instrumented locations. Slip displacement measurements were performed at locations 1 to 5. At locations 6, 7, and 8 the deflections between the bottom flange and the reference beam were measured. Locations 9 through 12 and 13 through 16 were used to measure flexural strains at cross section 1 and cross section 2, respectively. Channels 17 and 18 were employed to monitor the load and stroke displacement of the actuator acting on the north beam. Channels 19 and 20 were employed to monitor the load and stroke of the south actuator. The description and location of the instrumentation is summarized in Table 5.

The data was collected by a computerized system consisting of a PDP 11/23 Digital Computer in conjuction with an MTS data acquisition system. Figure 12 shows the computerized data acquisition system.

Figure 13 shows the overall test set-up, the loading frame, and the 55-kip actuators.

Test Procedures

Two million cycles of equivalent HS-20 truck load were applied to the bridge model. To speed up the test and still minimize dynamic effects, the load cycles were applied at a frequency of 3.5 hz. Approximately eight days were required to complete the test. However, since the deterioration was expected to be logarithmic, the procedure of recording data at cycles 1, 10, 100, 1000, etc., was adopted.

The general test procedures were the following:

1. The load cells of the actuators were electronically calibrated.
2. The excitation load signals were adjusted to avoid out-of-phase frequencies between the two actuators.

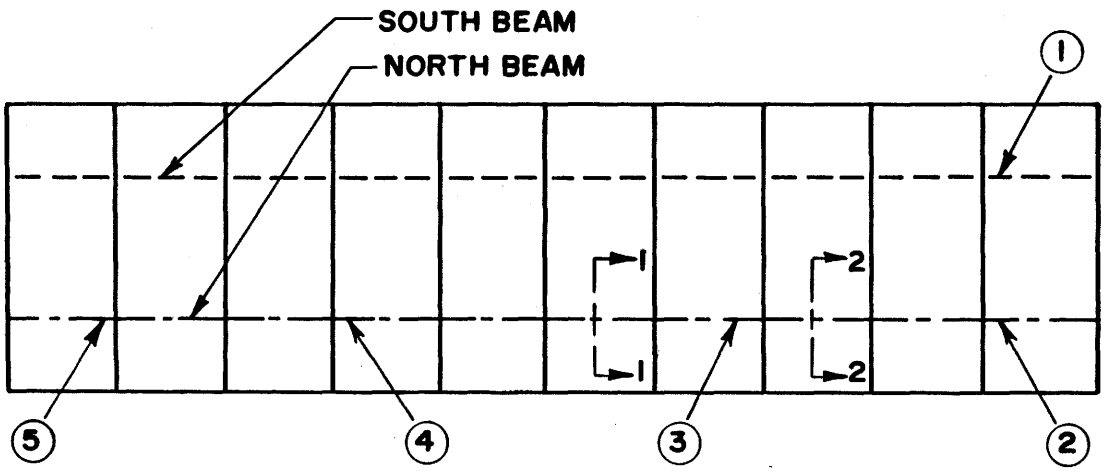

(a) SLIP DISPLACEMENT

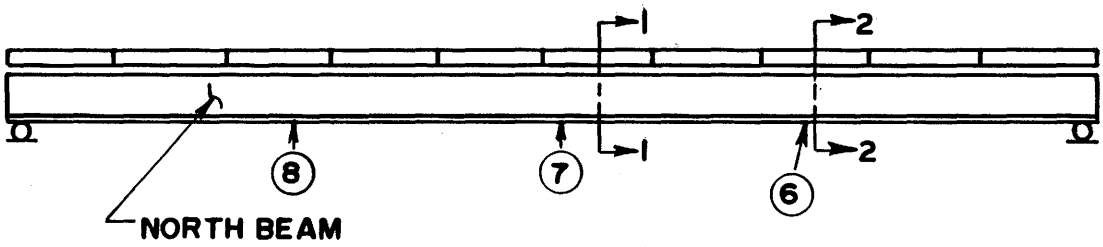

(b) DEFLECTION

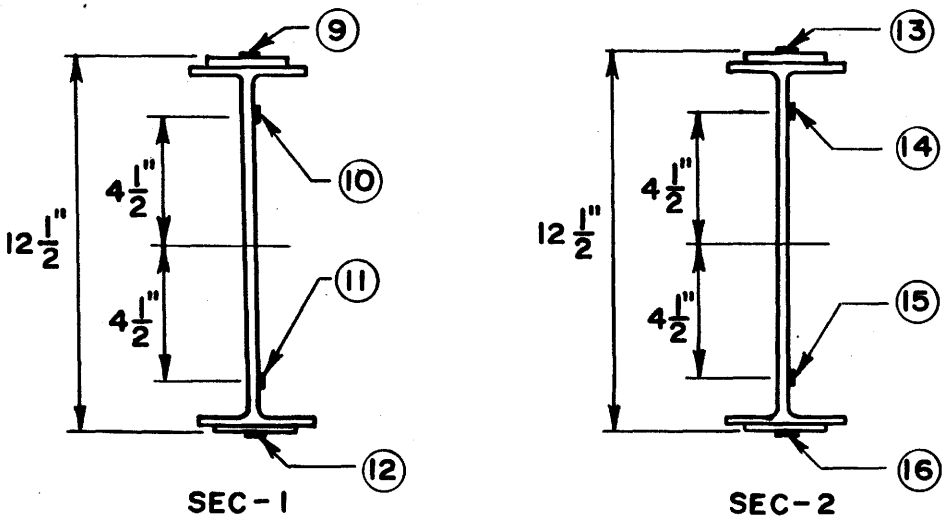

(c) STRAIN GAUGES

Figure 11. Instrumented Locations of Model Bridge.

TABLE 5. Description and location of instrumentation.

Location	Type*	Purpose	Beam	x(in.)	y(in.)
1	DT	Slip	South	217.0	12.5
2	DT	Slip	North	217.0	12.5
3	DT	Slip	North	161.0	12.5
4	DT	Slip	North	74.5	12.5
5	DT	Slip	North	18.0	12.5
6	DT	Def.	North	174.5	0.0
7	DT	Def.	North	120.5	0.0
8	DT	Def.	North	60.5	0.0
9	SG	Strain	North	129.5	12.5
10	SG	Strain	North	129.5	10.75
11	SG	Strain	North	129.5	1.75
12	SG	Strain	North	129.5	0.0
13	SG	Strain	North	177.5	12.5
14	SG	Strain	North	177.5	10.75
15	SG	Strain	North	177.5	1.75
16	SG	Strain	North	177.5	0.0
17	LC	Load	North	153.5	-
18	LVDT	Stroke	North	153.5	-
19	LC	Load	South	153.5	-
20	LVDT	Stroke	South	153.5	-

* DT = Displacement Transducer
SG = Strain Gage
LC = Load Cell
LVDT = Linear Variable Displacement Transducer

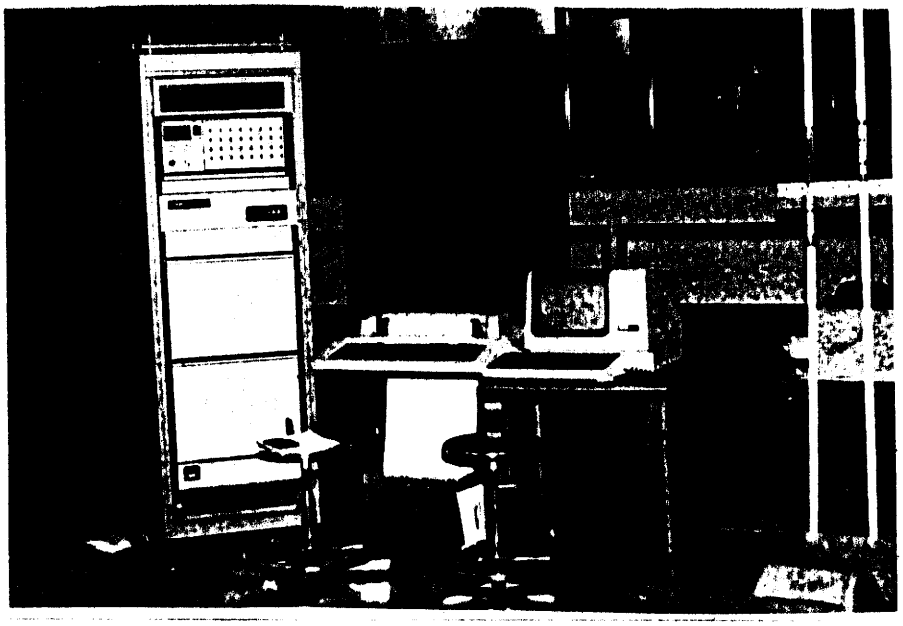

Figure 12. Computerized Data Acquisition System.

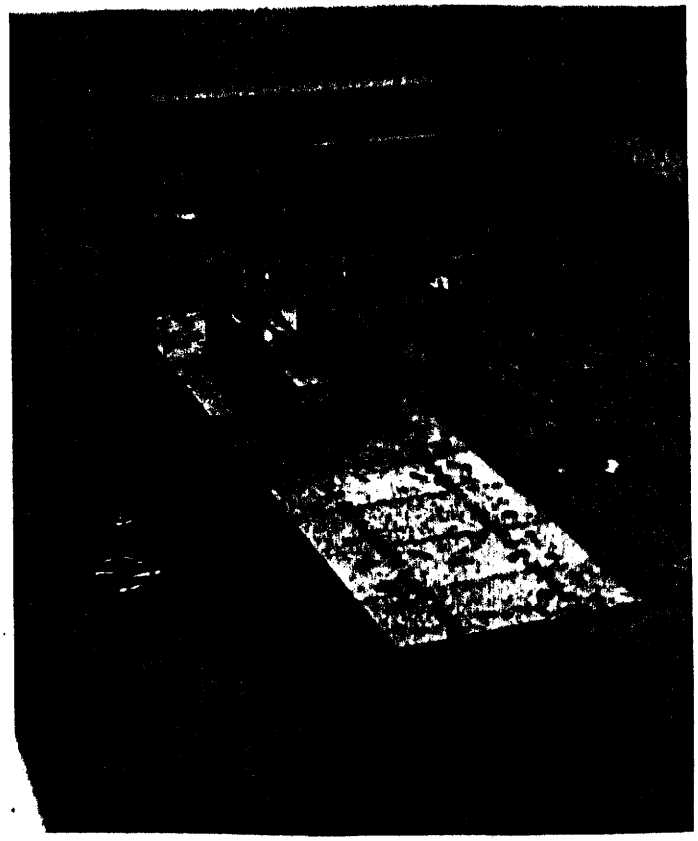

Figure 13. Test Set-up.

3. Each of the channels of the data acquisition system was set to read zero as the initial reading.
4. The excitation load signal generator was activated, causing each of the actuators to apply a sinusoidal dynamic load.
5. A computer program was executed to count for the number of load cycles and to store and process the required data as necessary. When the logarithm of the cycle number was an integer, the program activated the data acquisition system which continuously recorded the voltage readings of all 20 channels for a time lapse of .75 sec at a sampling rate of 0.01 sec. Then this data was written on to a floppy disk for future processing.

The system experienced a malfunction and randomly stopped the test. Fortunately no significant data was lost. The system was reactivated and steps 4 and 5 were repeated as required.

CHAPTER IV

TEST RESULTS

General

A total of two million cycles of equivalent HS-20 truck loads was applied throughout the test. During this test, data was collected and recorded during 826 time windows, each lasting 0.75 sec. The example results presented in this section were those recorded from one time window only. Similar results were recorded from the other time windows and provided the bases for subsequent analyses. The results are presented in four groups: load, deflections, flexural strains and slip displacements.

Cyclic Load

Channels 17 and 19 recorded the excitation load signals of the actuators reacting on the model bridge. Before the test started, careful attention was given to the two actuators because the two loads were required to be equal in magnitude and to act in-phase. This was accomplished by adjusting the excitation signals while observing the difference between the loads of the two actuators on an oscilloscope.

The load was applied at a 3.5 Hz frequency oscillating between 1700 and 9900 lbs, so a load range of approximately 8200 lbs was applied during each of the two million cycles. Figures 14 and 15 show the loads for actuators 1 and 2 as they were recorded during the time window commencing at the tenth load cycle of the experiment. It can be observed that the two actuators were acting in phase.

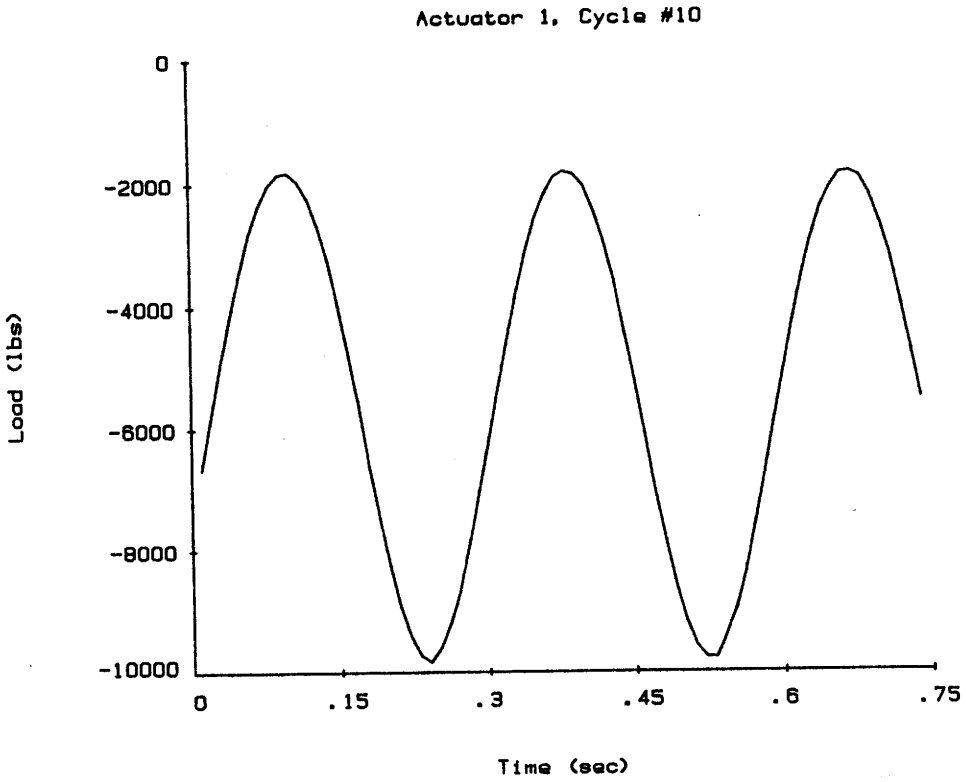

Figure 14. Load Signal as Recorded at Actuator 1.

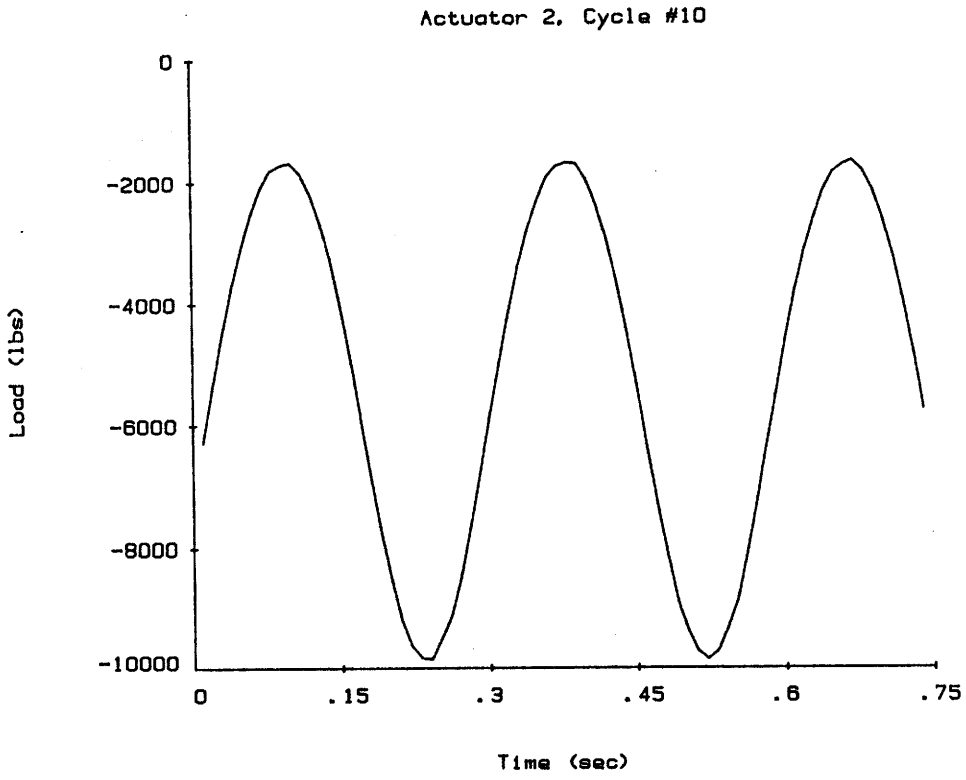

Figure 15. Load Signal as Recorded at Actuator 2.

Deflections

The deflections at the inside quarter points of the north stringer of the model bridge were recorded using strain gage type displacement transducers on channels 6, 7 and 8. Channel 6 recorded the deflection at the quarter point in the high shear side; channel 7 at the midspan and channel 8 at the quarter point in the low shear side. The deflections as recorded during the time window of the tenth cycle of the experiment are illustrated in Figures 16 through 18. Note that the polarity of the transducer recording the midspan deflection was inadvertently reversed. However, it is observed that the deflections were also acting in-phase with the load signal.

Flexural Strains

Uniaxial strain gages bonded to the north stringer of the bridge model were used to investigate the flexural properties of two cross sections. Strain gages bonded at locations 9 through 12 were employed to investigate cross section 1 and at locations 13 through 16 to investigate cross section 2. Due to the nature of the loading, cross section 1 was subjected to higher bending moment than cross section 2.

Figures 19 through 22 show the flexural strains at locations 9 through 12, respectively, as they were recorded during the tenth load cycle of the experiment. It is observed that the strains at locations 9 and 10 are oscillating around positive values or in compression, and that the strains of location 11 and 12 are oscillating around negative values or in tension. Therefore, it is concluded that the effective neutral axis of cross section 1 is between location 10 and 11. Notice that the electronic noise effects are greater at locations with smaller strain amplitudes.

Similarly, Figures 23 through 26 show the flexural strains at locations 13 through 16 as they were recorded. Note that location 13 is the only one with positive oscillations. Thus, in contrast to cross section 1, the neutral axis of cross section 2 is between locations 13 and 14.

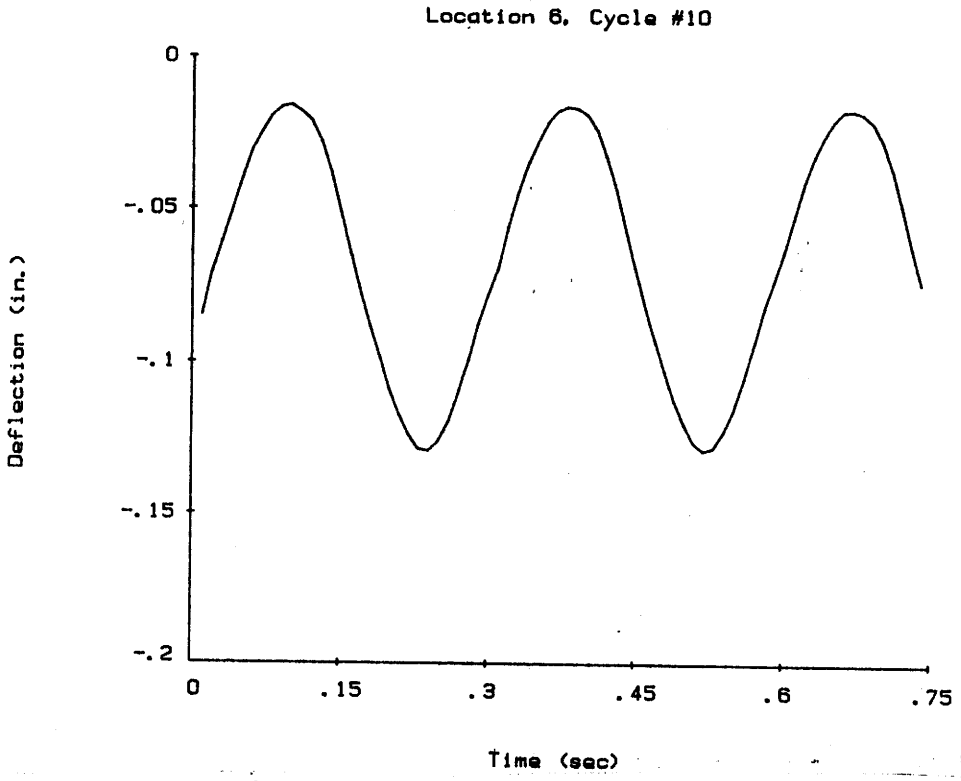

Figure 16. Deflection Response Signal at High Shear Side.

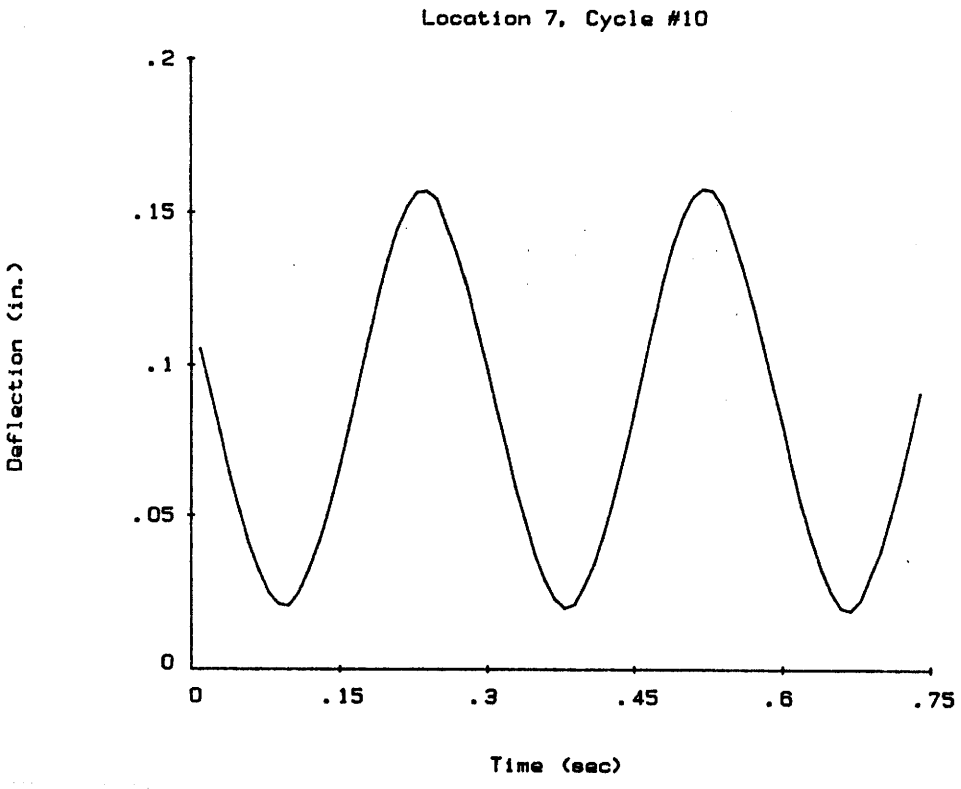

Figure 17. Deflection Response Signal at Midspan.

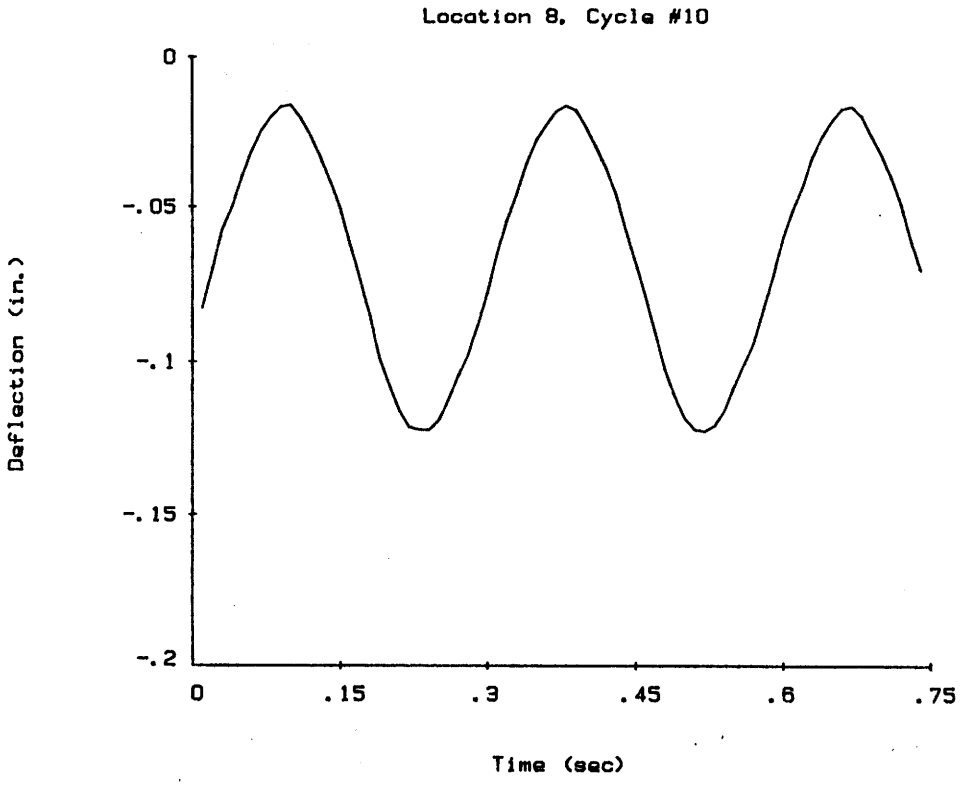

Figure 18. Deflection Response Signal at Low Shear Side.

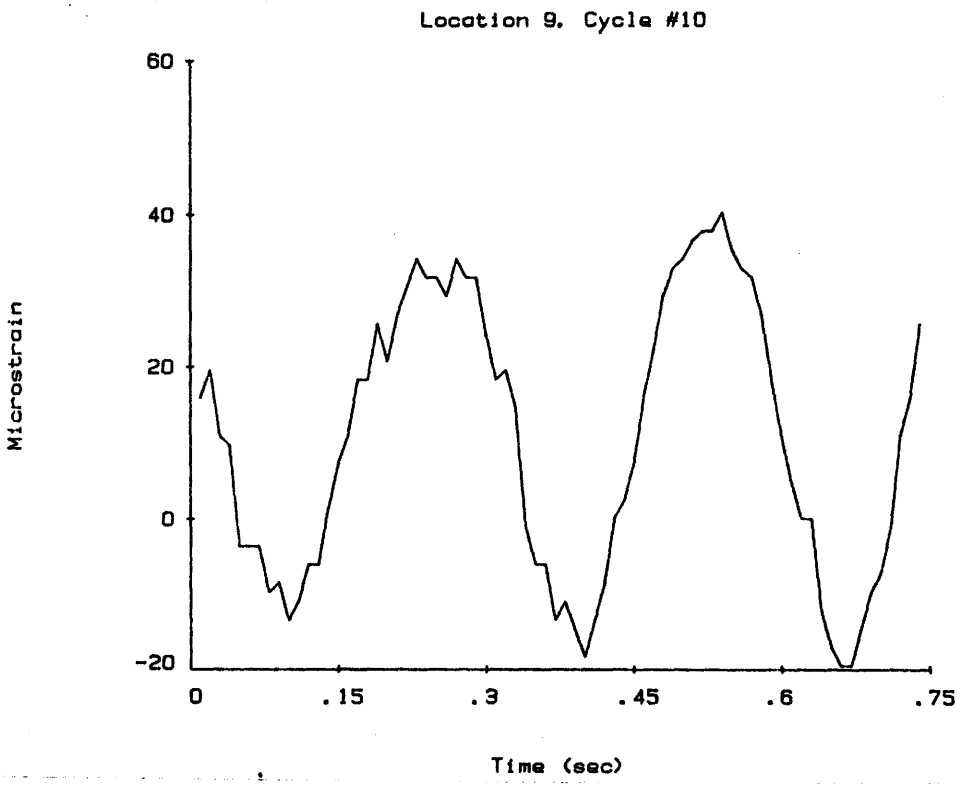

Figure 19. Strain Response Signal, Top Flange of Cross Section 1.

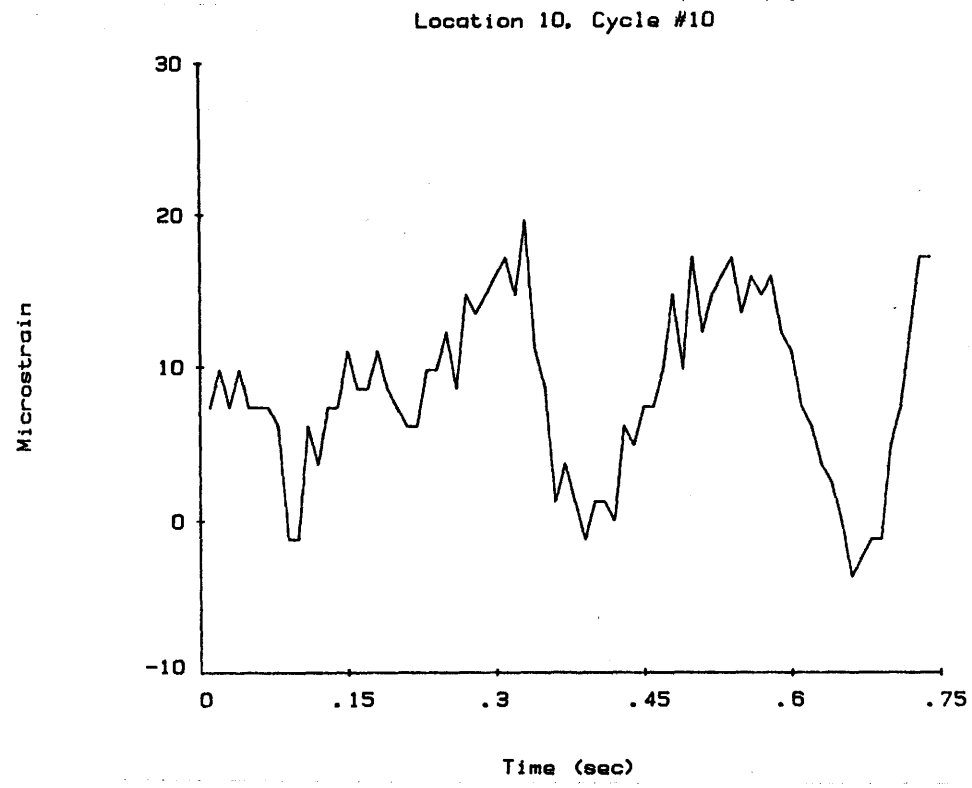

Figure 20. Strain Response Signal, Top Web of Cross Section 1.

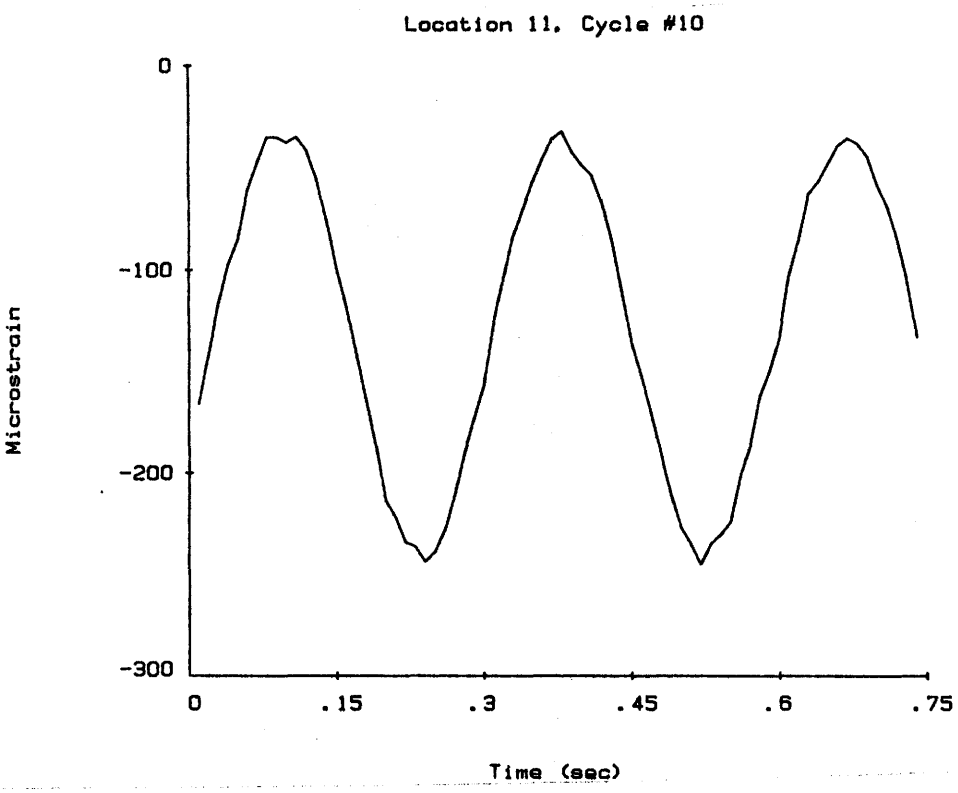

Figure 21. Strain Response Signal, Bottom Web of Cross Section 1.

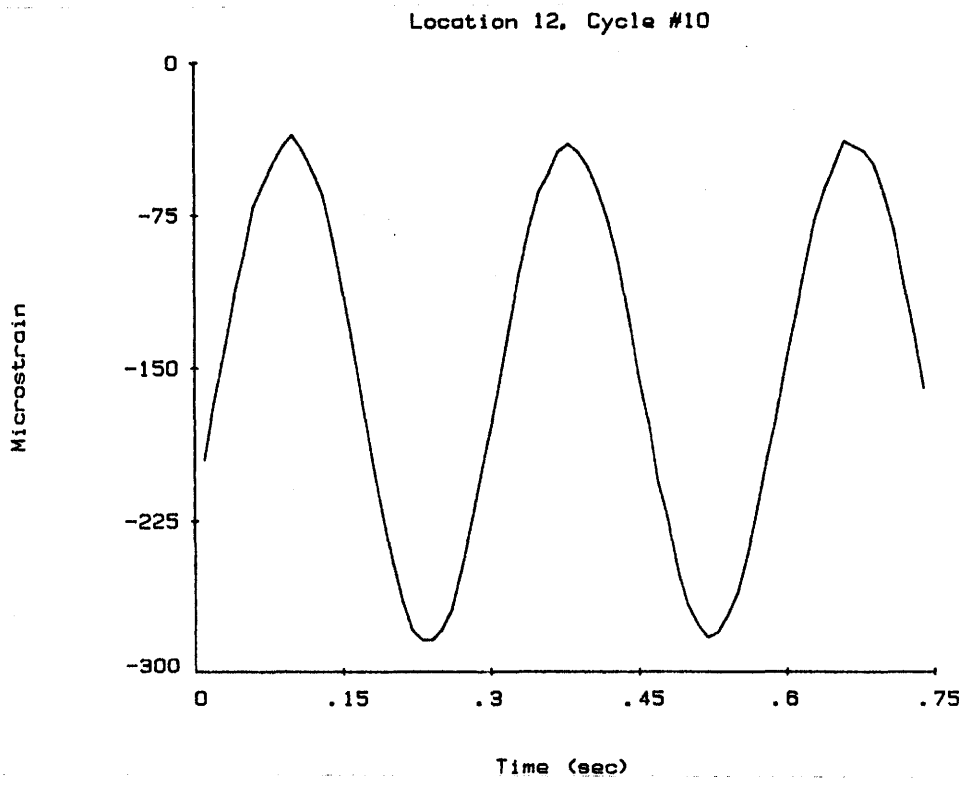

Figure 22. Strain Response Signal, Bottom Flange of Cross Section 1.

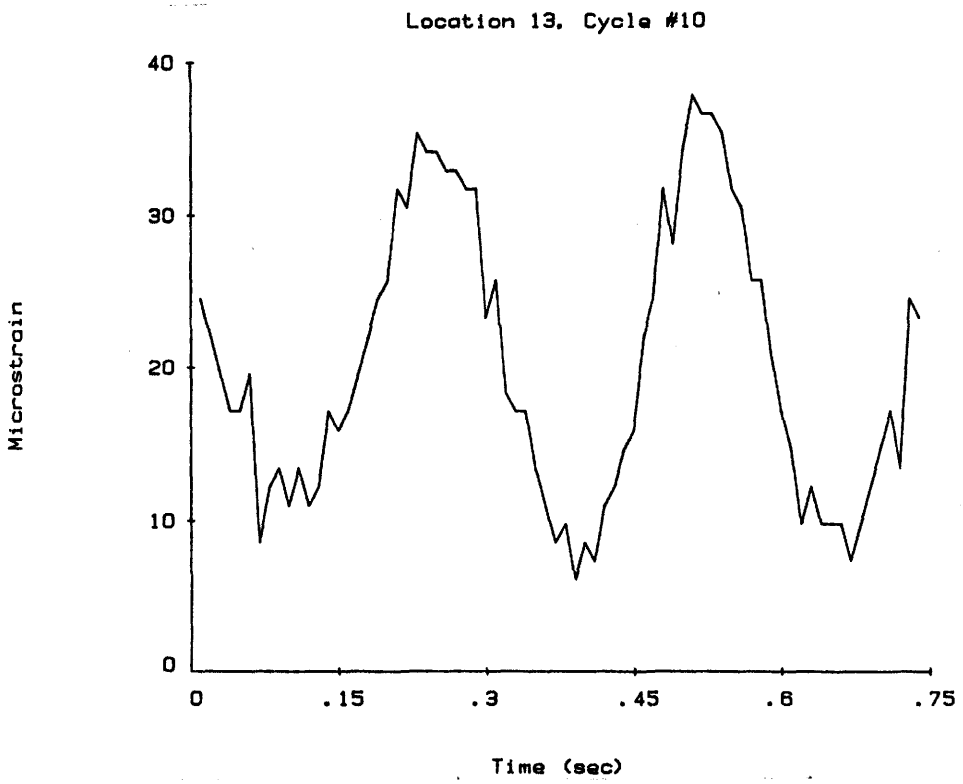

Figure 23. Strain Response Signal, Top Flange of Cross Section 2.

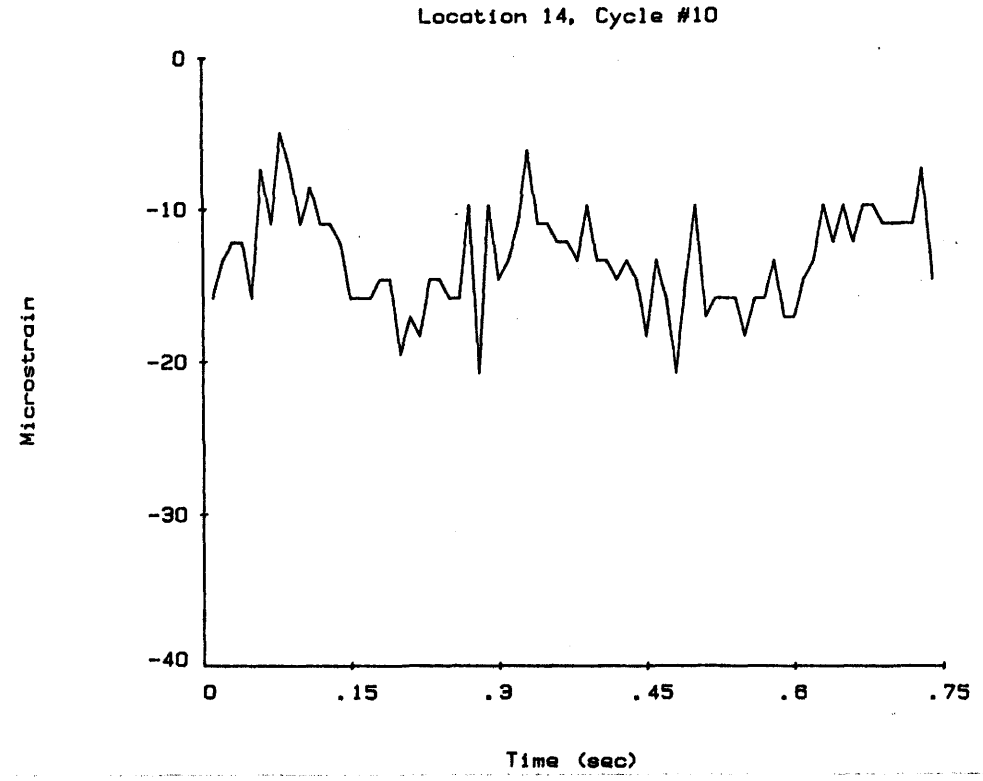

Figure 24. Strain Response Signal, Top Web of Cross Section 2.

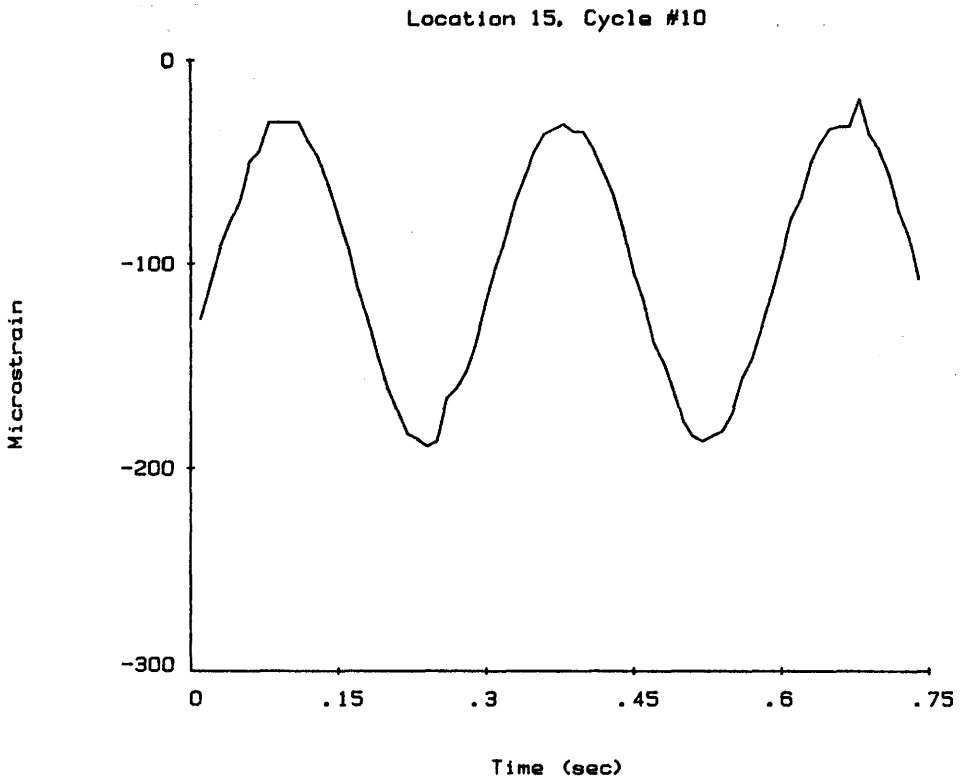

Figure 25. Strain Response Signal, Bottom Web of Cross Section 2.

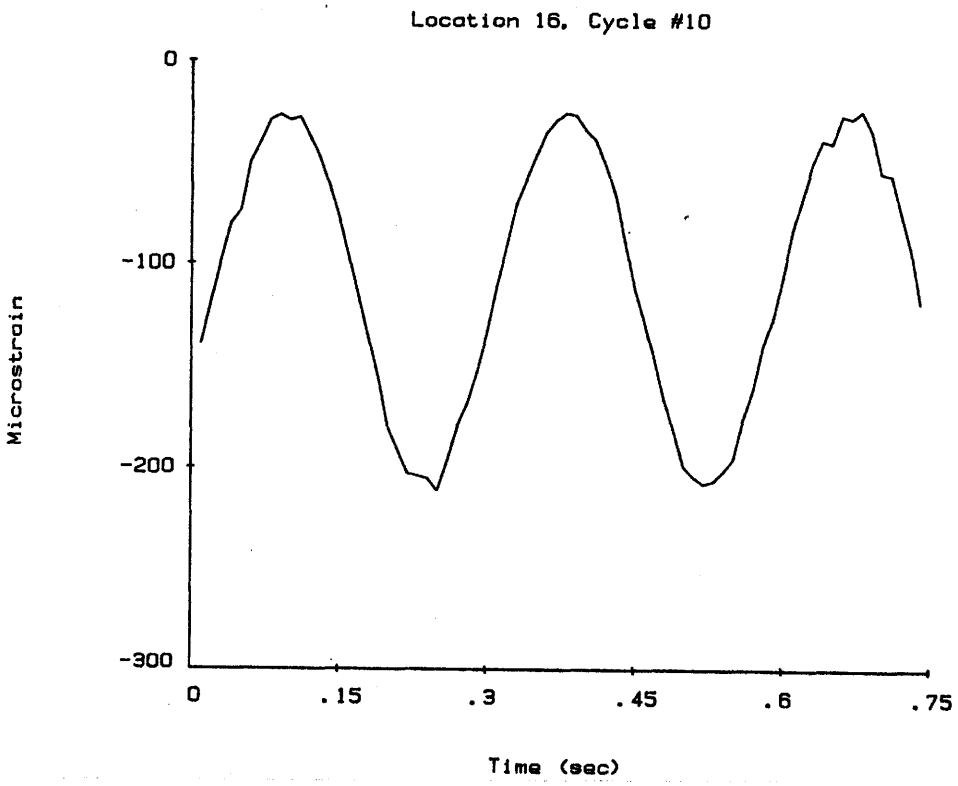

Figure 26. Strain Response Signal, Bottom Flange of Cross Section 2.

Slip Displacement

Slip displacement transducers between the concrete slab and the top flange of the steel beams were mounted at the interface at five different locations in the model bridge. These measurements are inversely proportional to the stiffness of the epoxy mortar interface connections. Thus, if there is any deterioration of this connection, the amplitude of the slip displacement should increase. These measurements are the only ones which could directly detect or provide information about deterioration at the interface and the pocket connections.

Figures 27 through 31 show the slip displacement measurements recorded at locations 1 through 5 during the tenth cycle of the experiment for a time span of 0.3 seconds. Since the slip displacements were very small, their magnitude was of the same order as the electronic noise of the acquisition system. Consequently, these measurements were severely affected by the electronic noise, and the best steady state representation of these data is obtained by fitting a least square sine wave curve of the form:

$$g(t) = A + B \sin \bar{\omega}t + C \cos \bar{\omega}t \qquad (36)$$

where, A, B and C are constants to be determined through the least square method, and $\bar{\omega}$ is the loading frequency of 3.5 Hz. Figures 27 through 31 also show the results of the corresponding fitted sine wave. Generally, a good fit was obtained for the data collected at locations 1 and 2 because the amplitude of the slip displacements were greater at these locations than at the other three.

Summary

The results shown in this section are those of the 16 channels of instrumentation and the two load excitation signals corresponding to the two

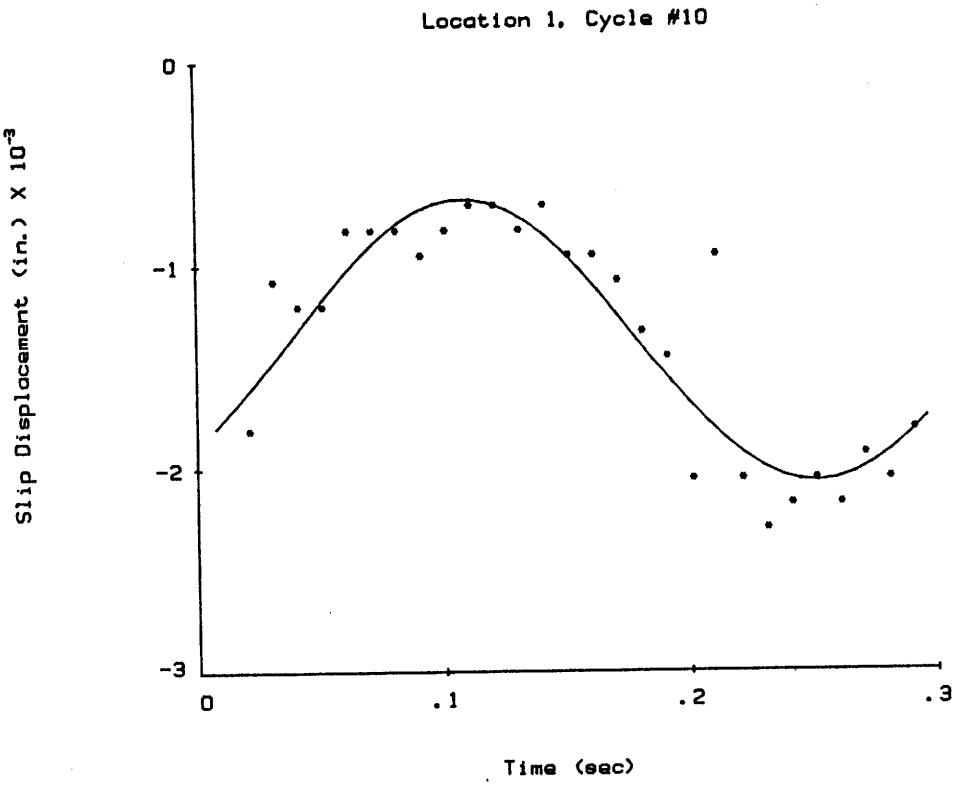

Figure 27. Slip Displacement Response Signal, Location 1.

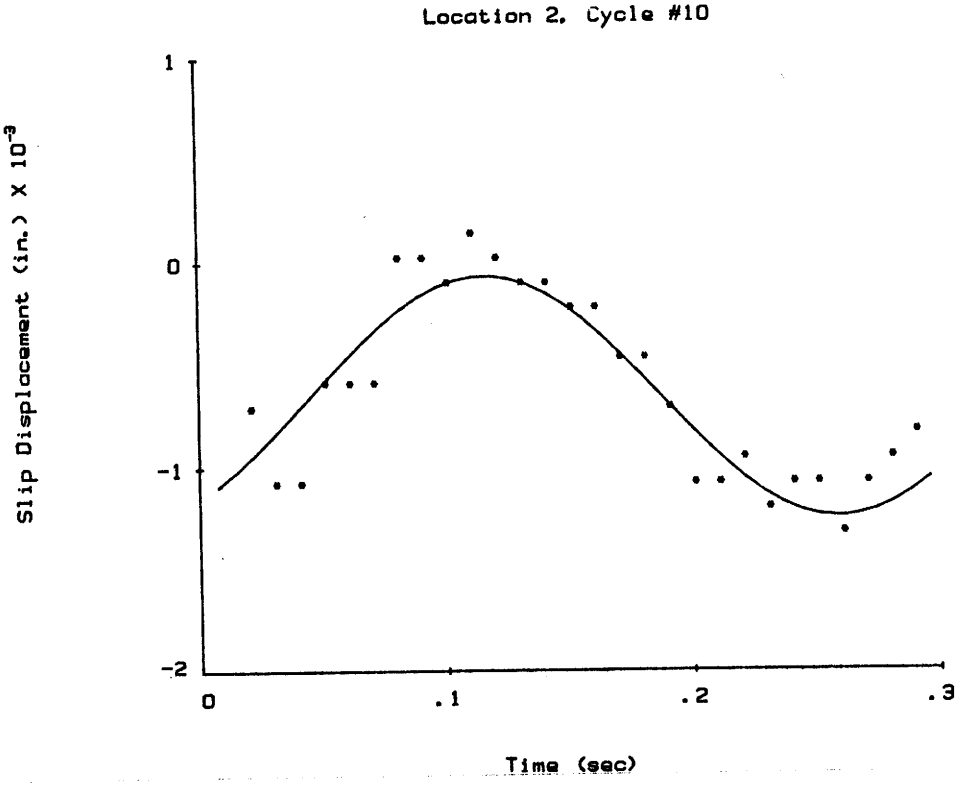

Figure 28. Slip Displacement Response Signal, Location 2.

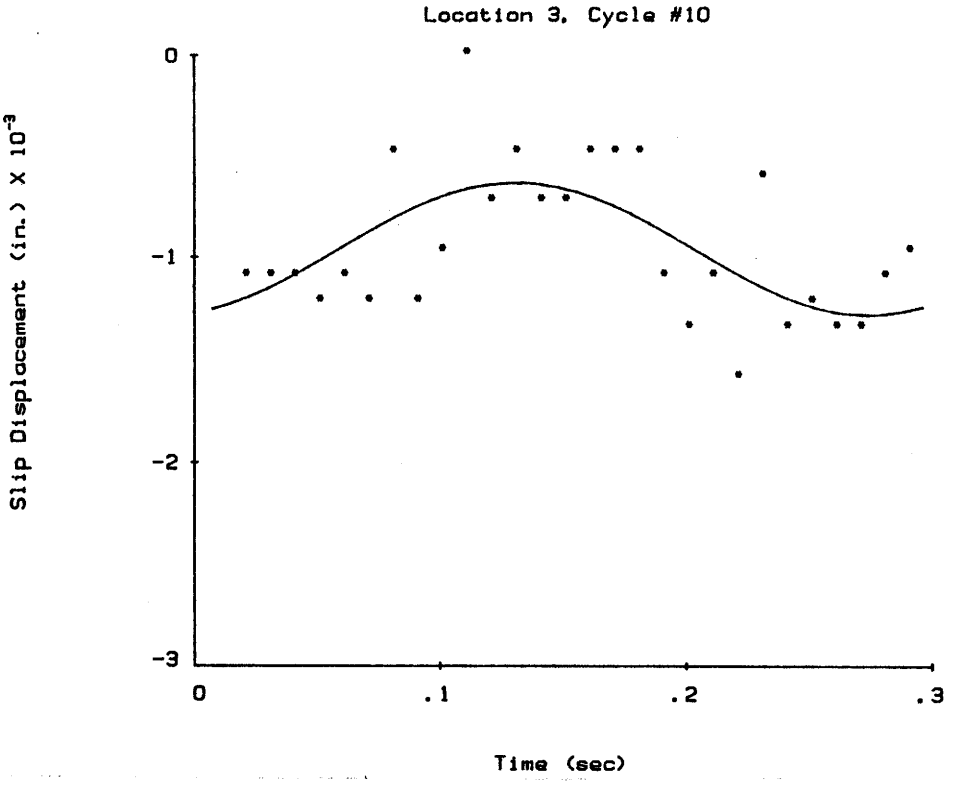

Figure 29. Slip Displacement Response Signal, Location 3.

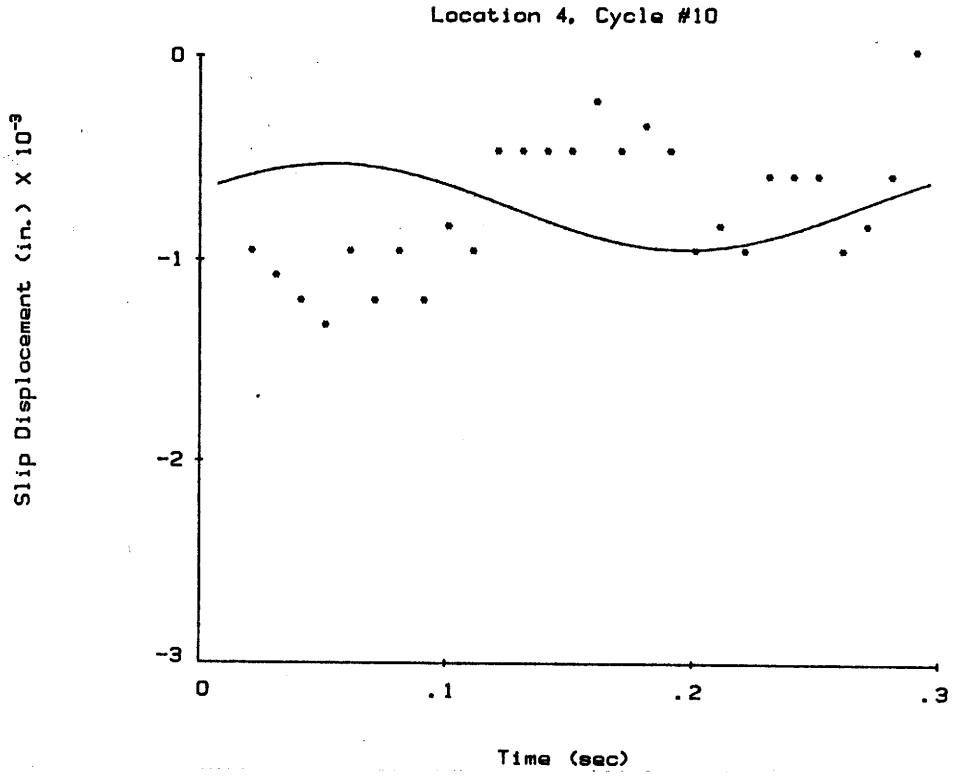

Figure 30. Slip Displacement Response Signal, Location 4.

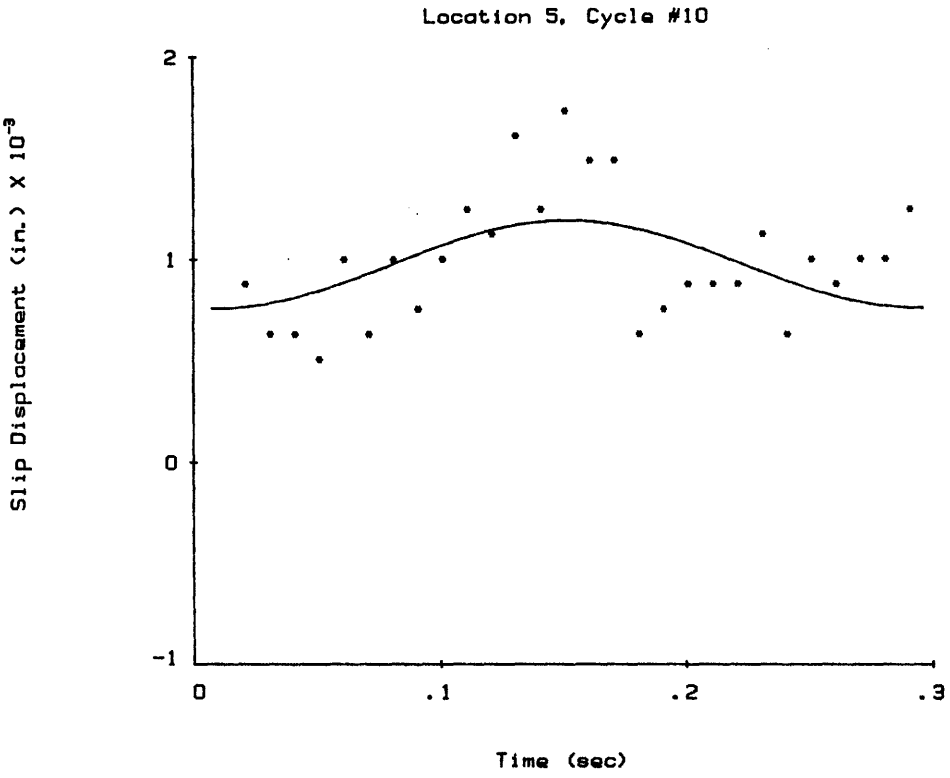

Figure 31. Slip Displacement Response Signal, Location 5.

actuators collected during the time window commencing at the tenth cycle of the experiment. Similar data was collected for the other 825 time windows that were monitored.

To evaluate the deterioration produced by the repetitive loads, the amplitude of the dynamic response signals were obtained for every monitored cycle. Then, to observe if there were changes in the overall stiffness of the bridge model, the amplitude of the deflection response was graphed against the log of the cycle number. Similarly, to study the changes in the cross sectional properties, the dynamic strain amplitude response of the four gages were combined to generate average moment of inertia, section modulus and neutral axis location for the corresponding cross section. Then these sectional parameters were graphed against the log cycle number. Similarly, increases in the dynamic slip displacement response would indicate losses of stiffness at the interface connections.

CHAPTER V

ANALYSIS OF TEST RESULTS

General

The data acquired during the repetitive loading test were reduced and analyzed to find if there were deteriorations of the overall stiffness, sectional properties or the panel-stringer connections. The reduction of the test data consisted of obtaining the average amplitude of the excitation (load) signal and the response signals (strains, deflections and slip displacements) for every time window that was continuously monitored. Then the average deflection responses were graphed against the log of the cycle number to investigate changes in the overall stiffness of the bridge model. To investigate changes in the cross-sectional properties of the instrumented sections, the corresponding strain amplitude responses were used to compute moment of inertia, section modulus, and neutral axis location. Then these sectional parameters were graphed against the log cycle number. The slip displacement amplitude responses were also obtained and graphed against the log cycle number to make inferences about changes in the stiffness of the panel-stringer connections.

After completing the data reduction, a statistical test was performed to establish confidence on the inferences about changes in the properties of the bridge model. The statistical test was accomplished by performing a linear regression between the amplitude of the parameters involved and the log cycle number. This regression fits the amplitude response with a straight line when it is correlated with the log cycle number. The resulting linear regression function yields a constant or an initial value and a slope component which predicts the rate of change of the properties of the parameters involved per change in the log cycle number of applied equivalent HS-20 truck loads. Therefore, the inferences are made on the slope of the regression line. Statistical evidence is sought that the slope of the regression line is other than zero.

Least Square Sine Wave Approximation

The total amplitude response of load, deflection, strain and slip displacement signals were obtained by performing a least square sine wave approximation for every time window that was recorded. Since the load or excitation signal is a sine wave function, it is assumed that the response signals are also sine wave functions with predominant oscillation frequencies of 3.5 Hz, the same as the excitation frequency. That is, the gathered data was approximated to a steady state response neglecting amplitudes of motion produced by vibrations at higher frequencies. Then the load, deflection, strain and slip displacement data are approximated to a function of the form:

$$g(t) = A + B \sin \bar{\omega} t + C \cos \bar{\omega} t \tag{37}$$

where

A,B,C = unknown regression coefficients,

$\bar{\omega}$ = excitation frequency of 3.5 Hz.

The actual error between the approximation function and the measured data points can be defined as follows:

$$E = \{ A + B \sin \bar{\omega} t_i + C \cos \bar{\omega} t_i - f(t_i) \}^2 \tag{38}$$

where

n = number of measured data points and

$f(t_i)$ = value of gathered data at time t_i.

The parameters that can be varied to minimize the error are the regression coefficients. Then three equations are obtained by setting:

$$\frac{\partial \bar{E}}{\partial A} = 0 \quad ; \quad \frac{\partial \bar{E}}{\partial B} = 0 \quad ; \text{ and } \quad \frac{\partial \bar{E}}{\partial C} = 0 \tag{39}$$

Inserting the expression for the error $\bar{E}$, into the above equation, and collecting terms, the equations, expressed in matrix form, become:

$$\begin{bmatrix} n & \Sigma \sin \bar{\omega} t_i & \Sigma \cos \bar{\omega} t_i \\ \Sigma \sin \bar{\omega} t_i & \Sigma \sin^2 \bar{\omega} t_i & \Sigma \sin \bar{\omega} t_i \cos \bar{\omega} t_i \\ \Sigma \cos \bar{\omega} t_i & \Sigma \sin \bar{\omega} t_i \cos \bar{\omega} t_i & \Sigma \cos^2 \bar{\omega} t_i \end{bmatrix} \begin{Bmatrix} A \\ B \\ C \end{Bmatrix} = \begin{Bmatrix} \Sigma f(t_i) \\ \Sigma f(t_i) \sin \bar{\omega} t_i \\ \Sigma f(t_i) \cos \bar{\omega} t_i \end{Bmatrix} \quad (40)$$

Then the regression coefficients A,B and C are obtained by solving the above system of equations. The amplitude of the sine wave function, $\bar{a}$, and the phase angle, t_o, are simply obtained by the following expressions:

$$\bar{a} = 2\sqrt{B^2 + C^2} \quad (41\text{-a})$$

$$t_o = \tan^{-1}\left(\frac{B}{C}\right) \quad (41\text{-b})$$

Now, writing Equation 37 in the form of the loading function given in Equation 19, it is obtained that the approximation function can also be written as follows:

$$g(t) = A + \frac{\bar{a}}{2} \sin\{\bar{\omega}(t-t_o)\} \quad (42)$$

where

A = static component of the approximation function,

$\bar{a}$ = total wave amplitude of the approximation function,

t_o = phase angle and

$\bar{\omega}$ = loading frequency of 3.5 Hz.

Amplitude of Load Signal

The least square sine wave approximation method was employed to determine the total load amplitude of the excitation signal applied to the bridge model for every recorded load cycle. The load amplitude or the range was obtained for every one of the 876 cycles recorded, and was utilized to unitize the total amplitude of deflection and slip displacements by dividing these response amplitudes by the load or excitation signal amplitudes.

Unitized Deflection Amplitude

The total deflection amplitudes measured at the inside quarter points of the north stringer of the bridge model were determined using the least square sine approximation method. The approximation was performed employing sets of 74 continuous deflection readings, or a time span of .73 sec. The system of equations given by expression 40 was set up and the regression constants A, B and C were solved. Then the average total amplitude of deflections was calculated using Equation 41-a.

This procedure was repeated for every recorded load cycle. Then the calculated deflection amplitudes were unitized by dividing them by the load amplitude also obtained by the least square sine wave approximation.

The unitized deflections of the inside quarter points of the north stringer of the bridge model were graphed against the log of the cycle number. Figures 32 through 34 show the unitized deflection amplitude at the high shear side, midspan and low shear side, respectively, graphed against the log of the cycle number. It is observed that there are slight increases in the deflection amplitudes; however, those increases are small compared to the total deflection amplitude.

Cross-Sectional Properties

The cross-sectional properties were investigated for two different cross sections of the north beam of the model bridge. Cross section 1 is located at

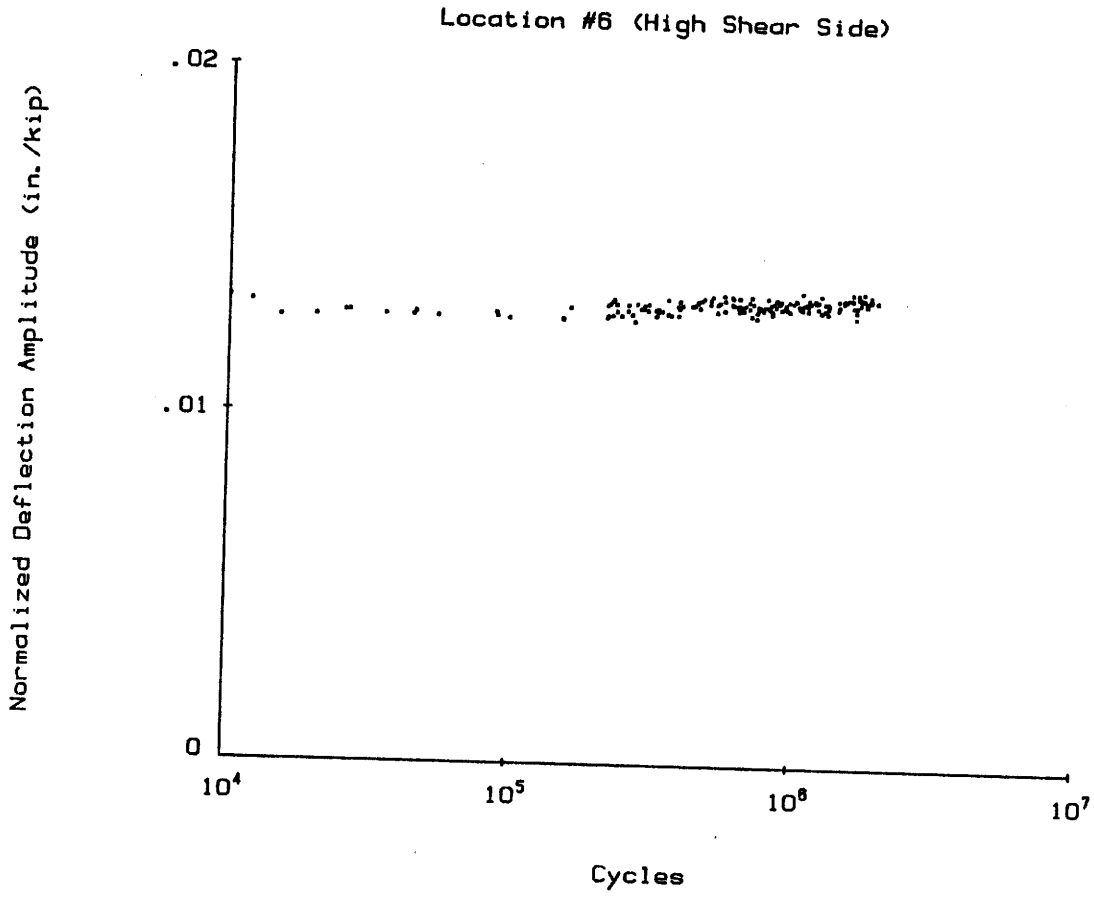

Figure 32. Unitized Deflection Amplitude, High Shear Side.

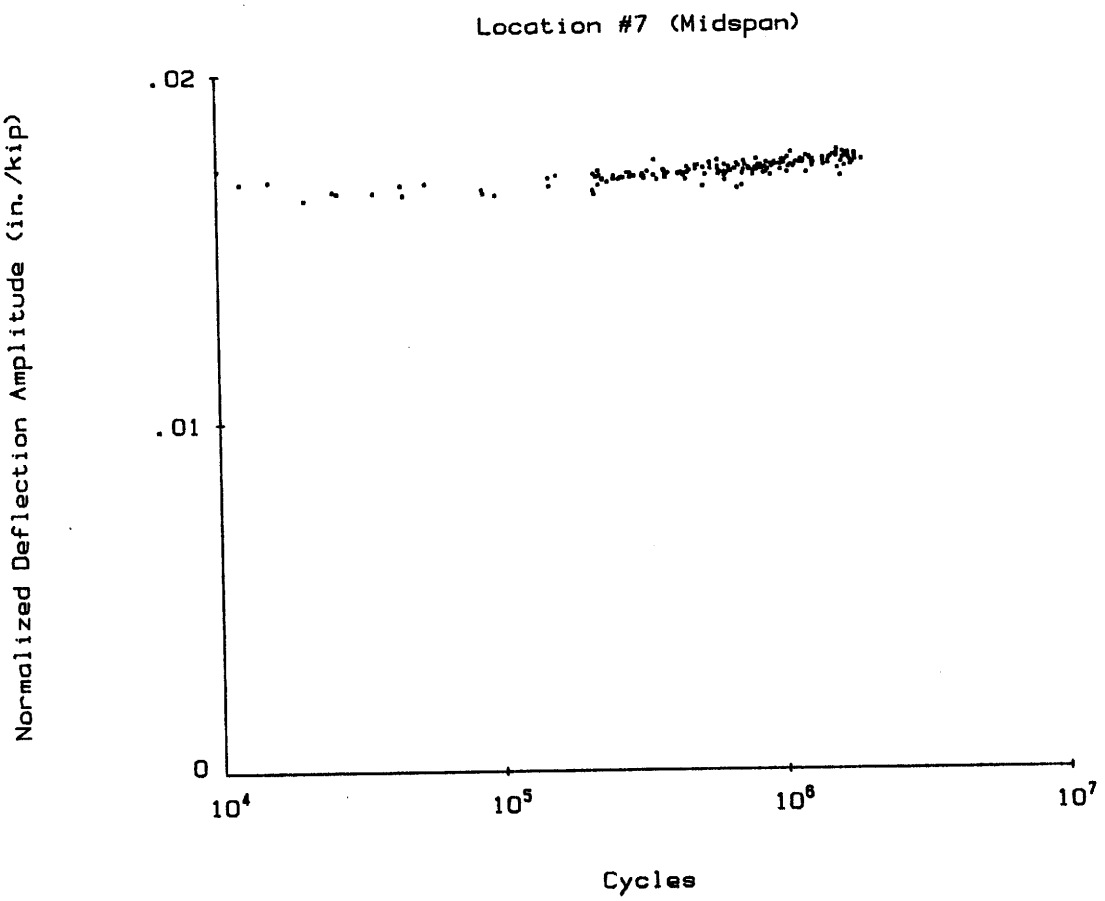

Figure 33. Unitized Deflection Amplitude, Midspan.

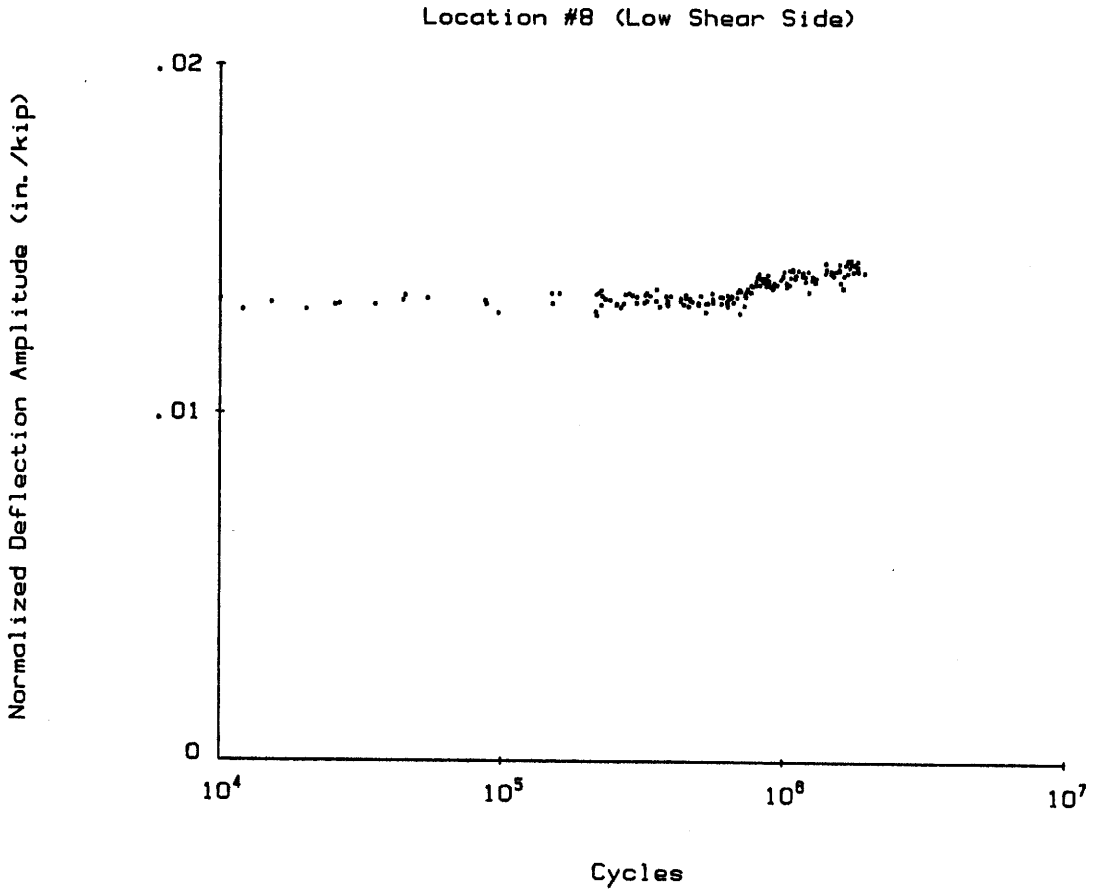

Figure 34. Unitized Deflection Amplitude, Low Shear Side.

10 ft 9.5 in. from the east roller support, and cross section 2 is located at 14 ft 9-1/2 in. from the same support. Four strain gages were used for each cross section. From the data gathered by the strain gages, the sectional properties were obtained using the following approach:

1. The total strain amplitude recorded at locations 9 through 12 and 13 through 16 associated with cross section 1 and 2, respectively, are determined using the least square approximation method.
2. A straight line least square fit is performed on the total strain amplitude obtained in the first step versus the vertical position of the respective gage, as illustrated in Figure 35. The strain amplitude profile is approximated as a straight line of the form:

$$\varepsilon(y) = \varepsilon_o + \phi y \tag{43}$$

where

ε_o = strain at extreme bottom fibers,

ϕ = rate of change between the strain profile and the y-axis or curvature of cross section.

3. The neutral axis location is obtained by setting Equation 43 to zero and solving for the variable y. This yields:

$$\bar{y} = -\frac{\varepsilon_o}{\phi} \tag{44}$$

4. The moment of inertia I is obtained by solving the following formula:

$$I = \frac{\Delta P \; Mf \; \bar{y}}{E \; \varepsilon_o} \tag{45}$$

where

ΔP = load amplitude during a load cycle,

Mf = moment factor for the corresponding cross section,

$\bar{y}$ = neutral axis location of the corresponding cross section during the k^{th} load cycle,

E = modulus of elasticity, taken as 29,000 ksi, and

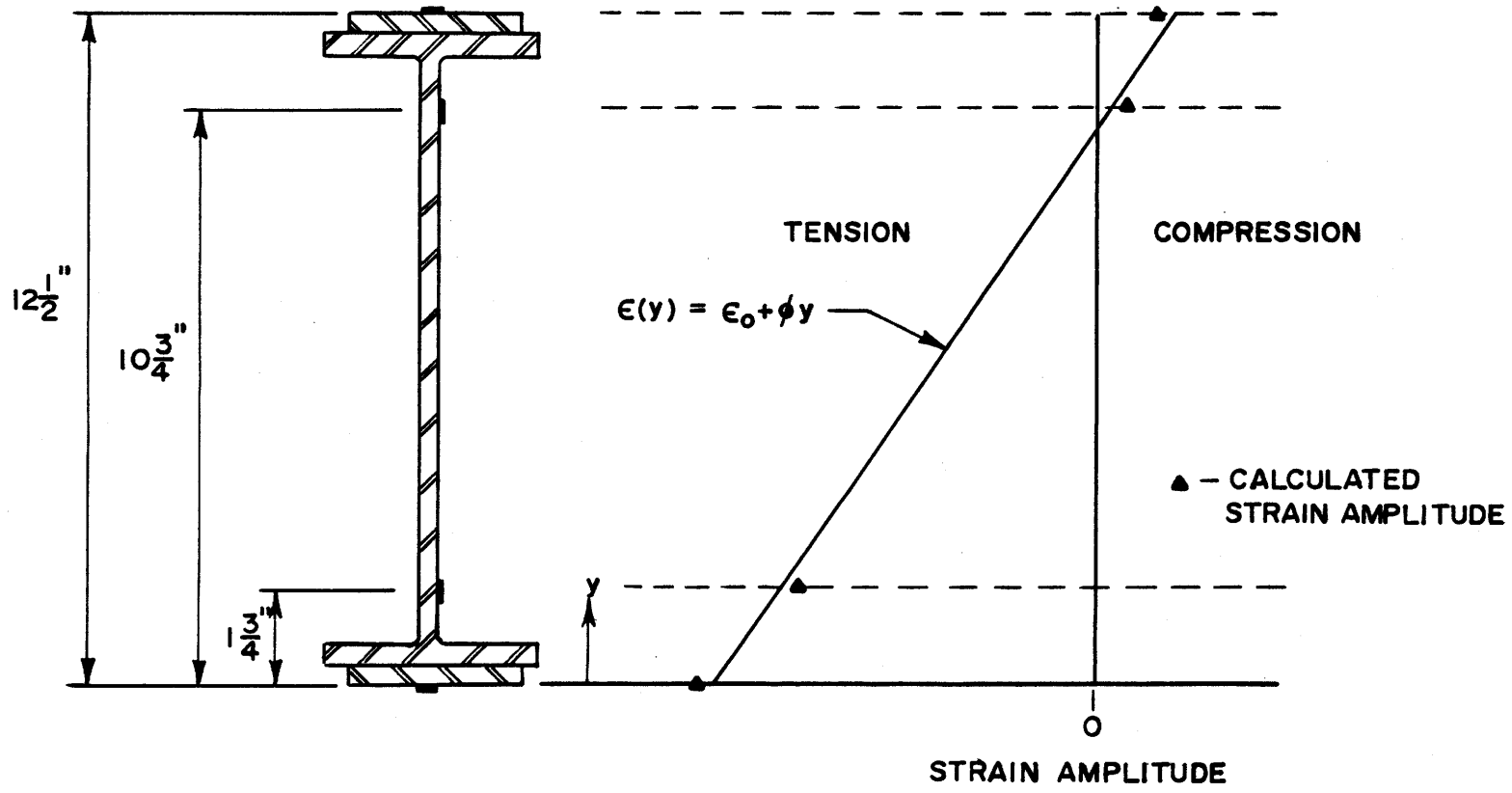

Figure 35. Approximation to Strain Amplitude Profile.

ε_o = strain at the extreme bottom fibers resulted from the straight line fit.

By performing the previously described procedure, the sectional properties are investigated from the measured strains.

Cross Section 1

The results of the bending properties of cross section 1 are presented here. First, the least square aproximation was performed on the strain gathered at locations 9, 10, 11 and 12. Then, the total average strain amplitudes were used to calculate the corresponding properties. Figure 36 shows the location of the neutral axis during the load cycles that were monitored. It is observed that no significant drop of the neutral axis occurred throughout the experiment. The average distance from the bottom fibers to the neutral axis is about 10.25 in.

Figure 37 shows the moment of inertia graphed against the log cycle number. By visual inspection, no significant increase or decrease is detected. The average moment of inertia at this location is about 450 in^4.

Similarly, Figure 38 illustrates the section modulus graphed versus the log cycle number. The same conclusions can be drawn: there were no significant changes. The average section modulus of cross section 1 is about 44 in^3.

Cross Section 2

The results of the investigation for the properties of cross section 2 are presented here. Section 2 is located at 14 ft 9.5 in. from the east roller support of the north stringer. The least square sine wave approximation was performed to obtain the total strain amplitude recorded at locations 13 through 16 for each monitored load cycle. Then the amplitudes were used to compute the sectional properties following the steps previously described.

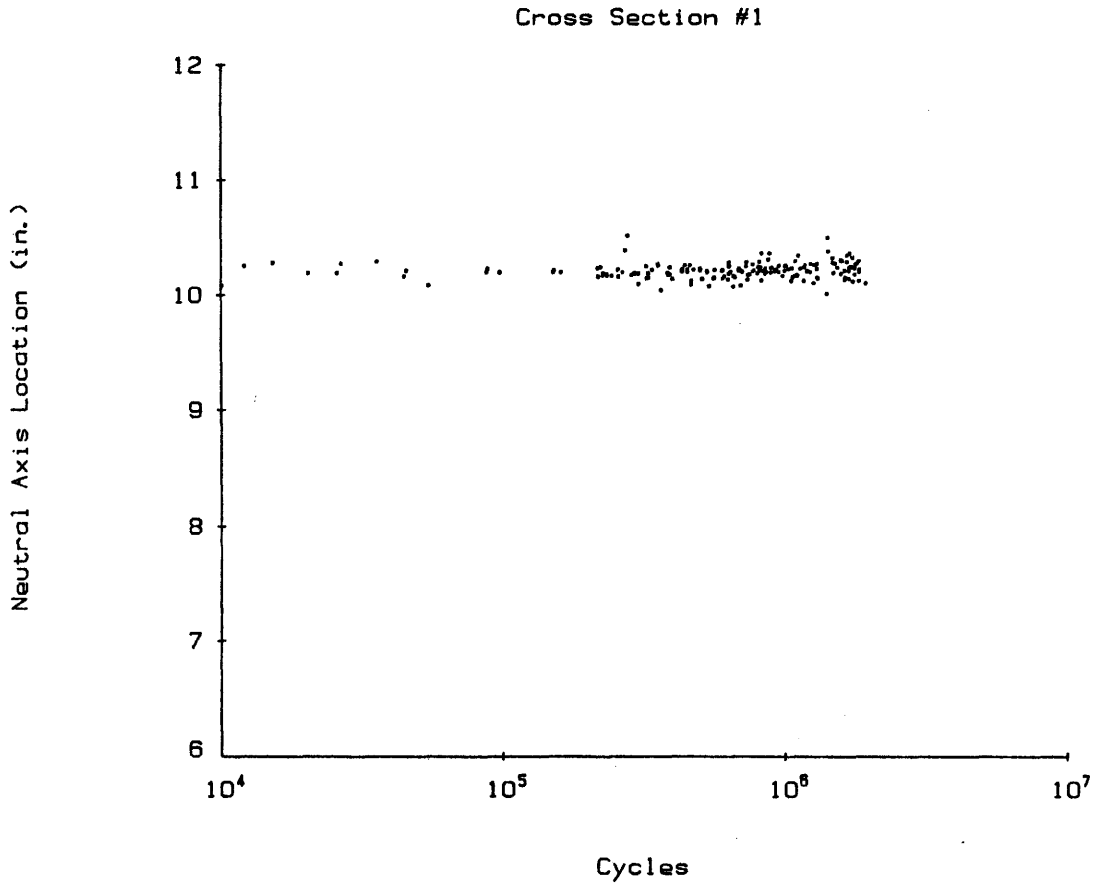

Figure 36. Neutral Axis Location, Cross Section 1.

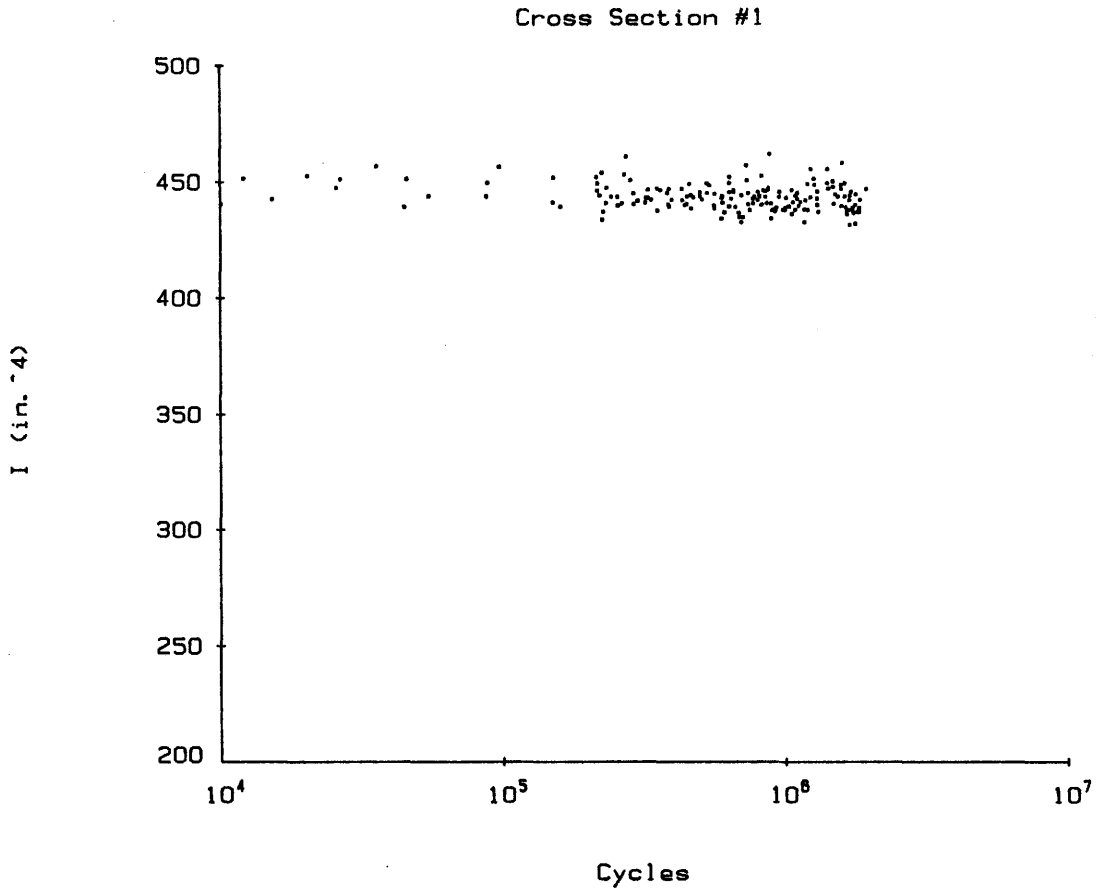

Figure 37. Moment of Inertia, Cross Section 1.

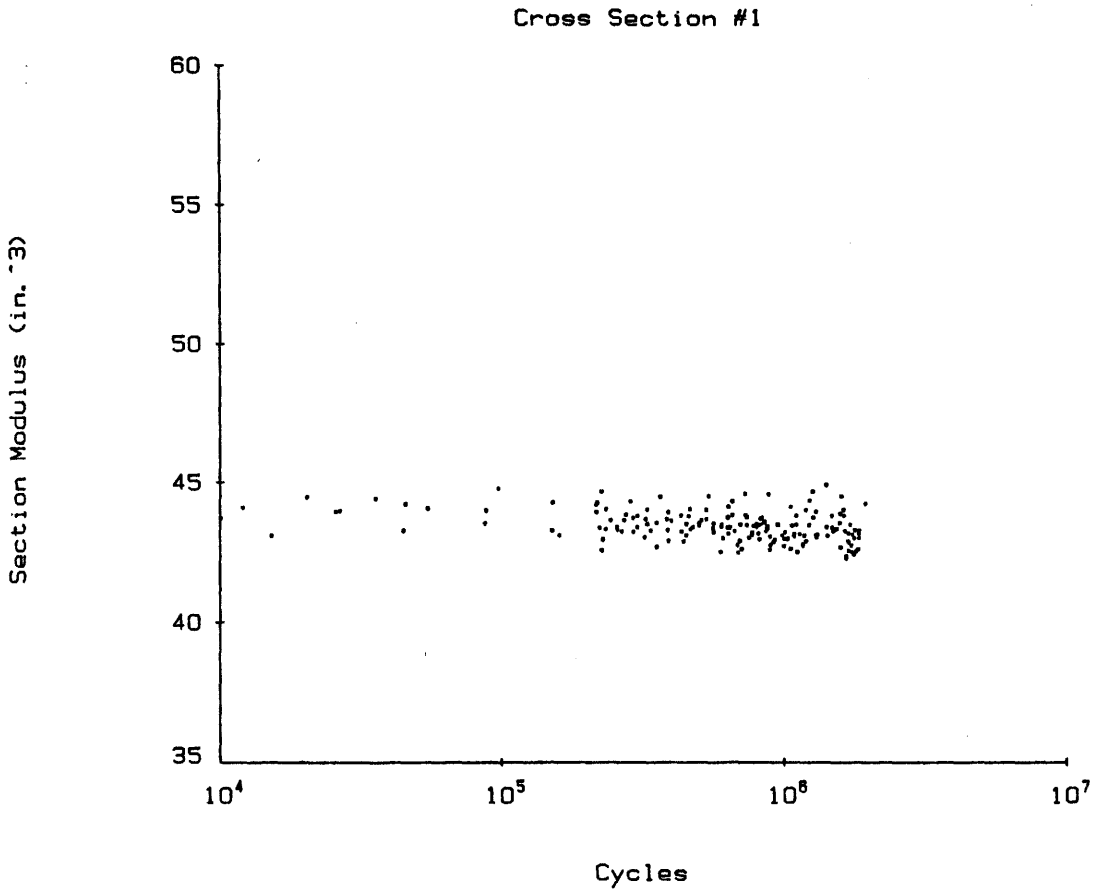

Figure 38. Section Modulus, Cross Section 1.

Figure 39 shows the location of the neutral axis calculated for section 2. It is observed that there is no significant change in the neutral axis location; however, the average location is 10.8 in. from the extreme bottom fibers, higher than that of cross section 1.

Figure 40 shows the moment of inertia calculated using Equation 45 for every recorded load cycle. The average value is about 500 in^4 and it is higher than that obtained by cross section 1. However, there is also no significant loss of inertia in the section.

Figure 41 shows the section modulus of cross section 2 graphed against the log cycle number. From a visual inspection, there is no evidence of losses in section modulus.

Slip Displacements

The total slip displacement amplitudes recorded at location 1 through 5 were also obtained using the least square sine wave approximation method. The same procedure used for analyzing the deflection amplitude was employed in this section. The slip displacement amplitude was obtained and then divided by the load excitation amplitude. Figure 42 through 46 shows the unitized slip displacement amplitude for locations 1 through 5. The following observations can be made from these figures:

1. The unitized slip displacement amplitude was very scattered for all locations. This was probably caused by the electronic noise which significantly affected small amplitude readings.
2. Locations 1 and 2 experienced the highest slip displacement amplitude because these locations are in the high shear side.
3. The slip displacement amplitude was negligible at the other three locations.
4. Since the slip displacement amplitude was small at all times and did not increase with load cycles, it can be concluded that there was no damage induced at the interface connection by the repetitive loading.

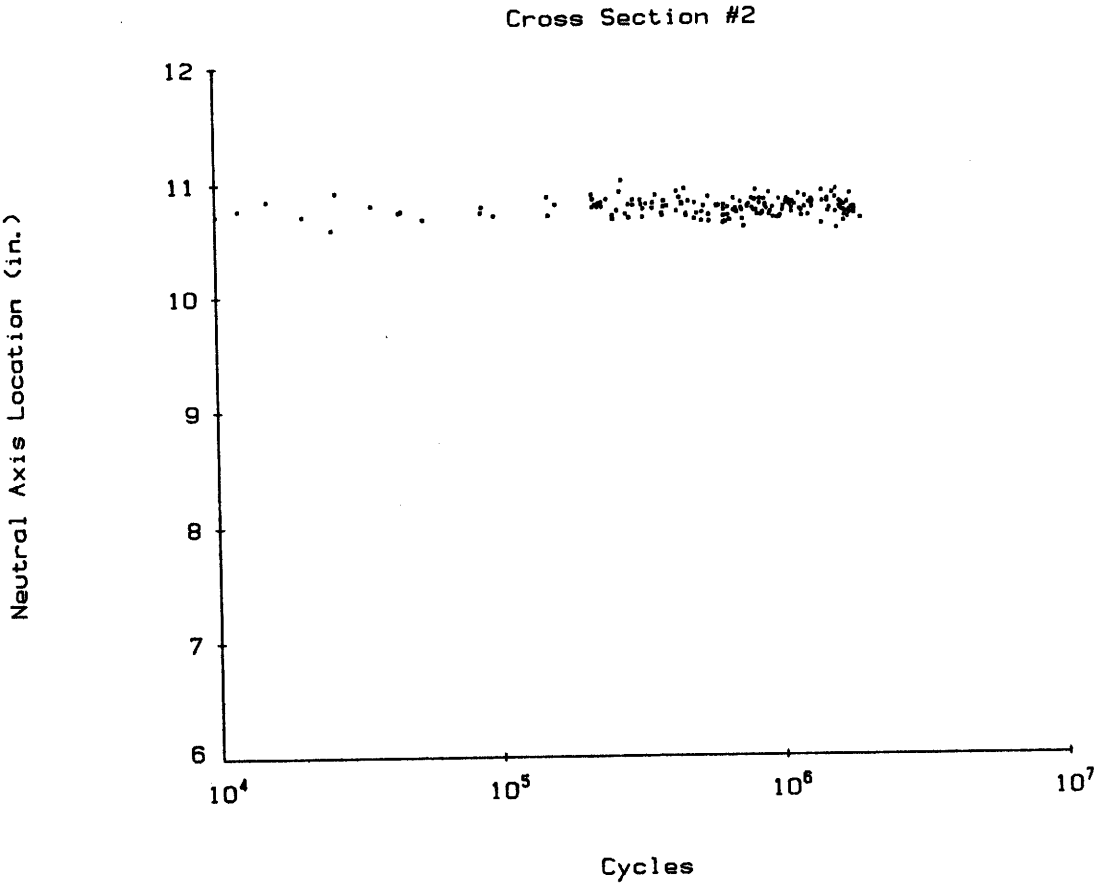

Figure 39. Neutral Axis Location, Cross Section 2.

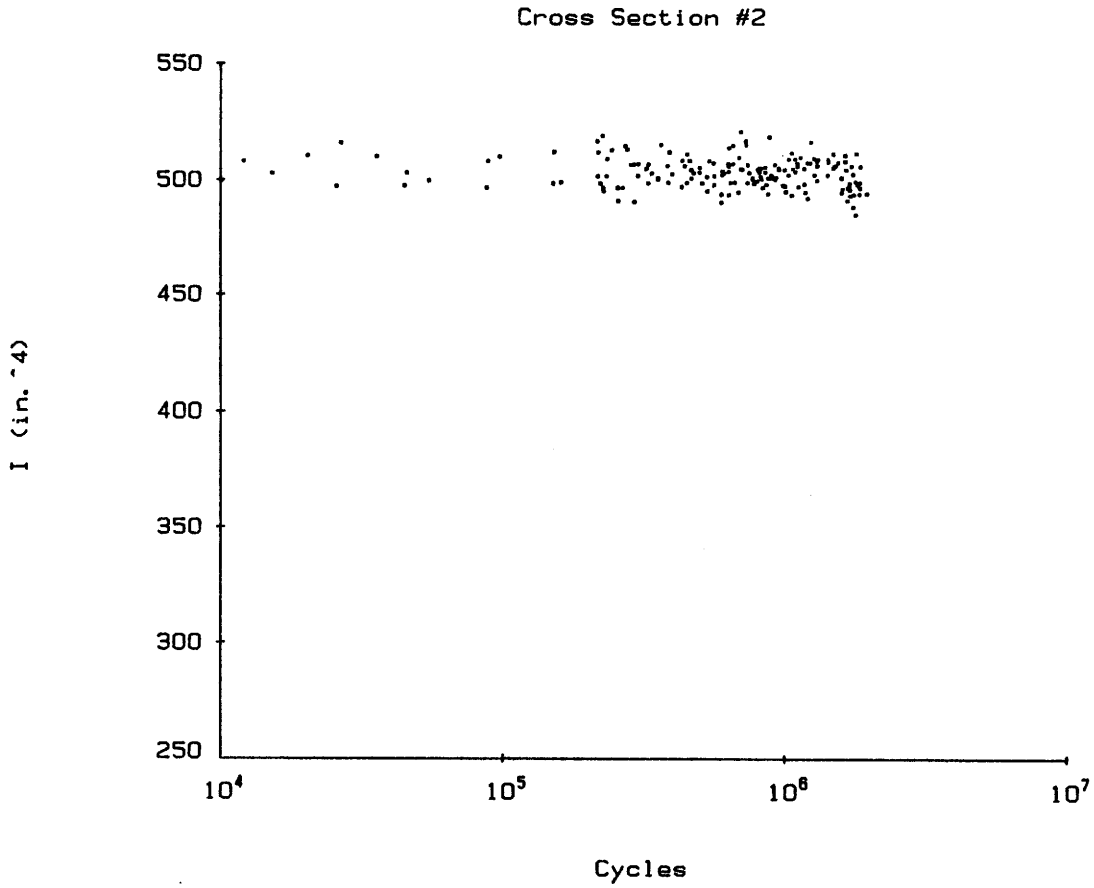

Figure 40. Moment of Inertia, Cross Section 2.

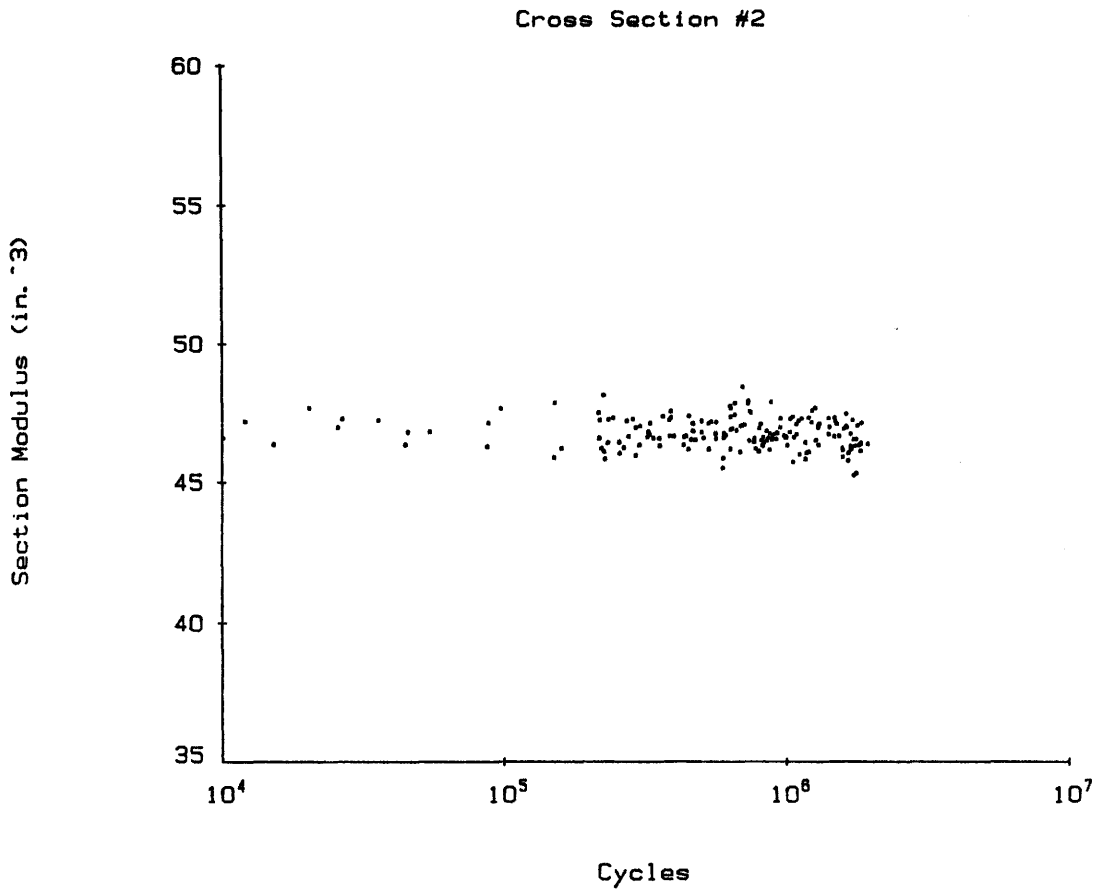

Figure 41. Section Modulus, Cross Section 2.

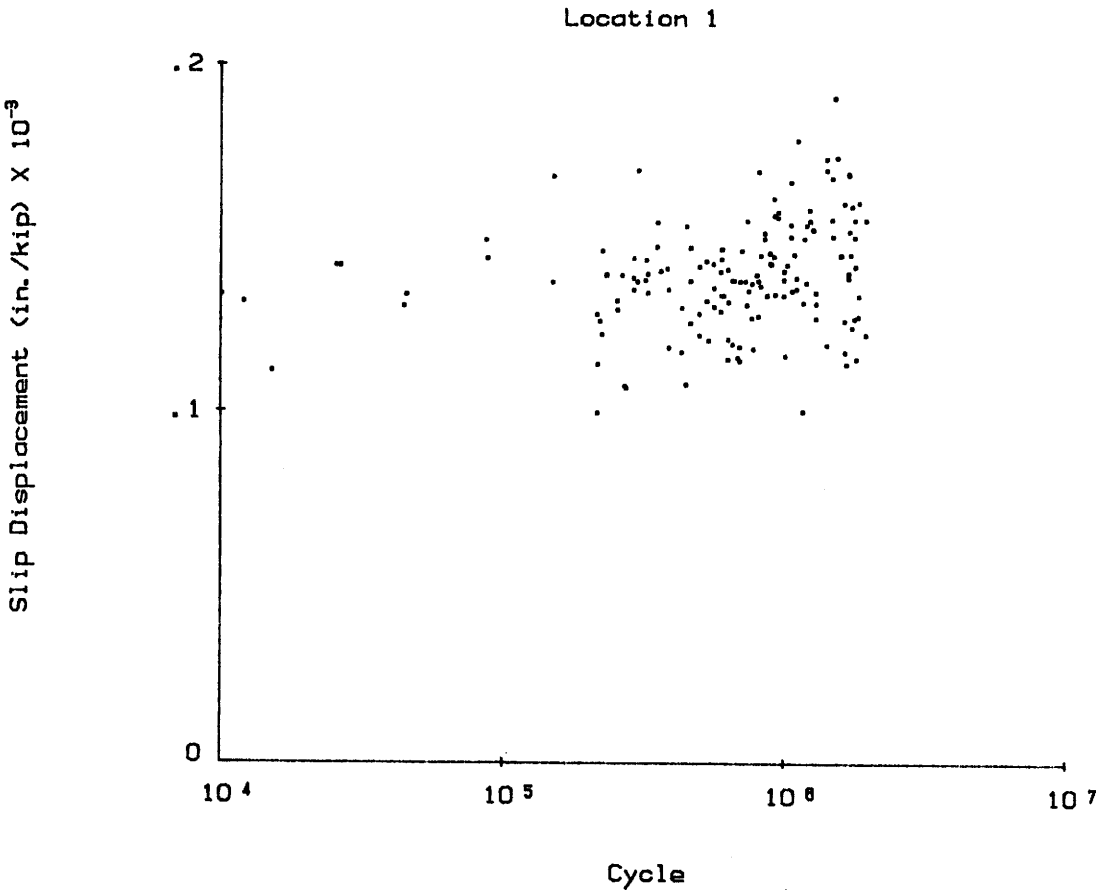

Figure 42. Unitized Slip Displacement Amplitude, Location 1.

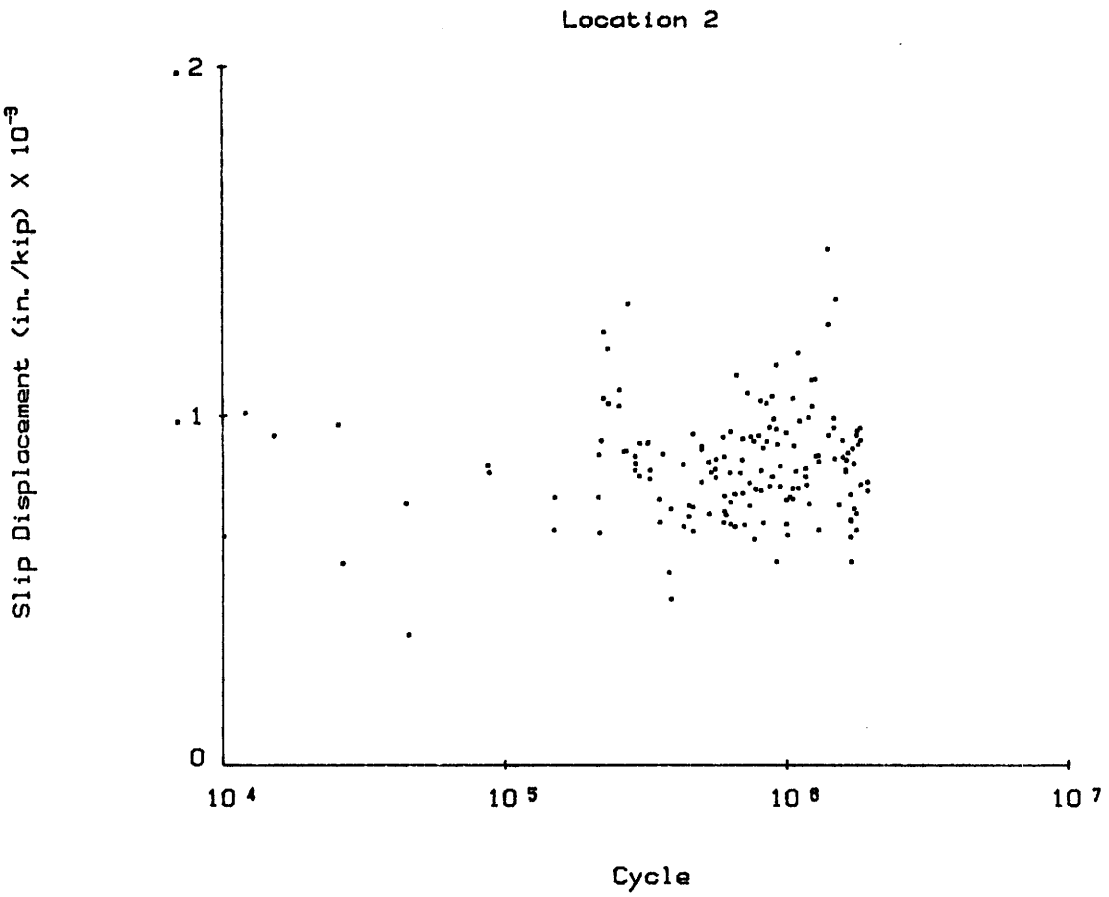

Figure 43. Unitized Slip Displacement Amplitude, Location 2.

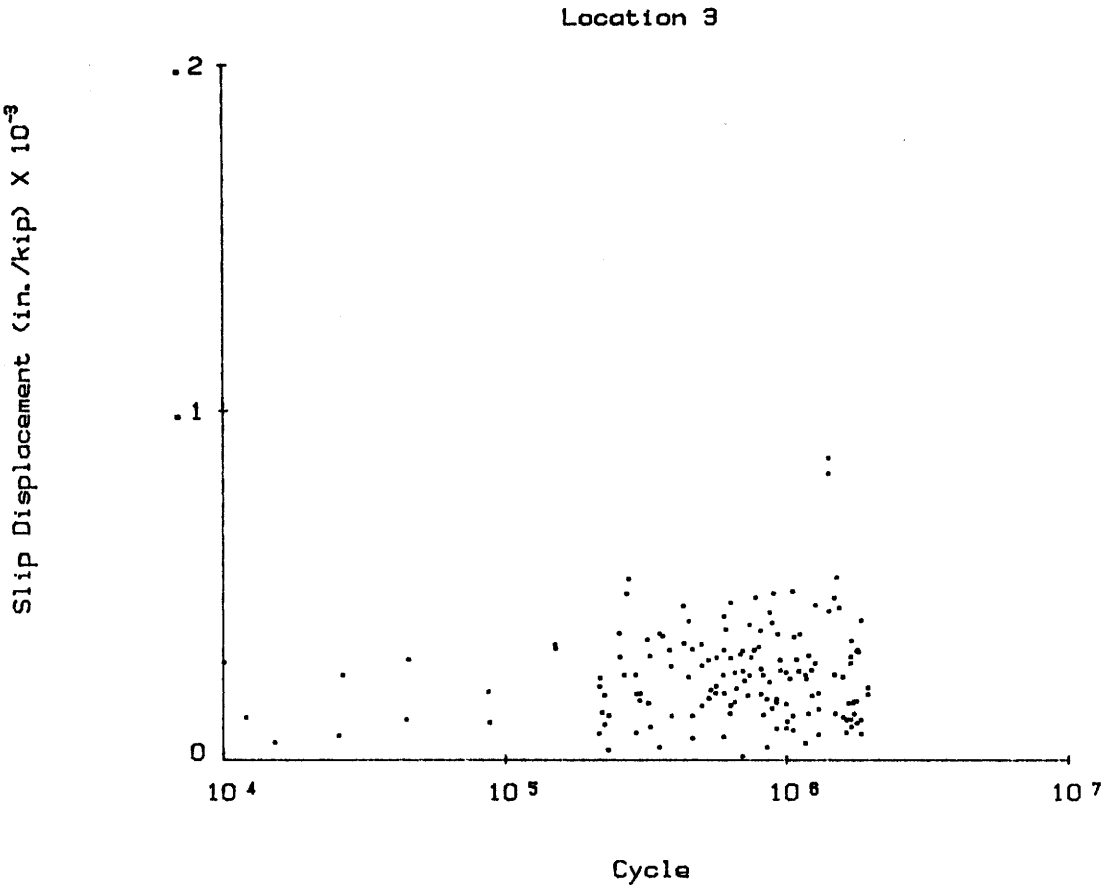

Figure 44. Unitized Slip Displacement Amplitude, Location 3.

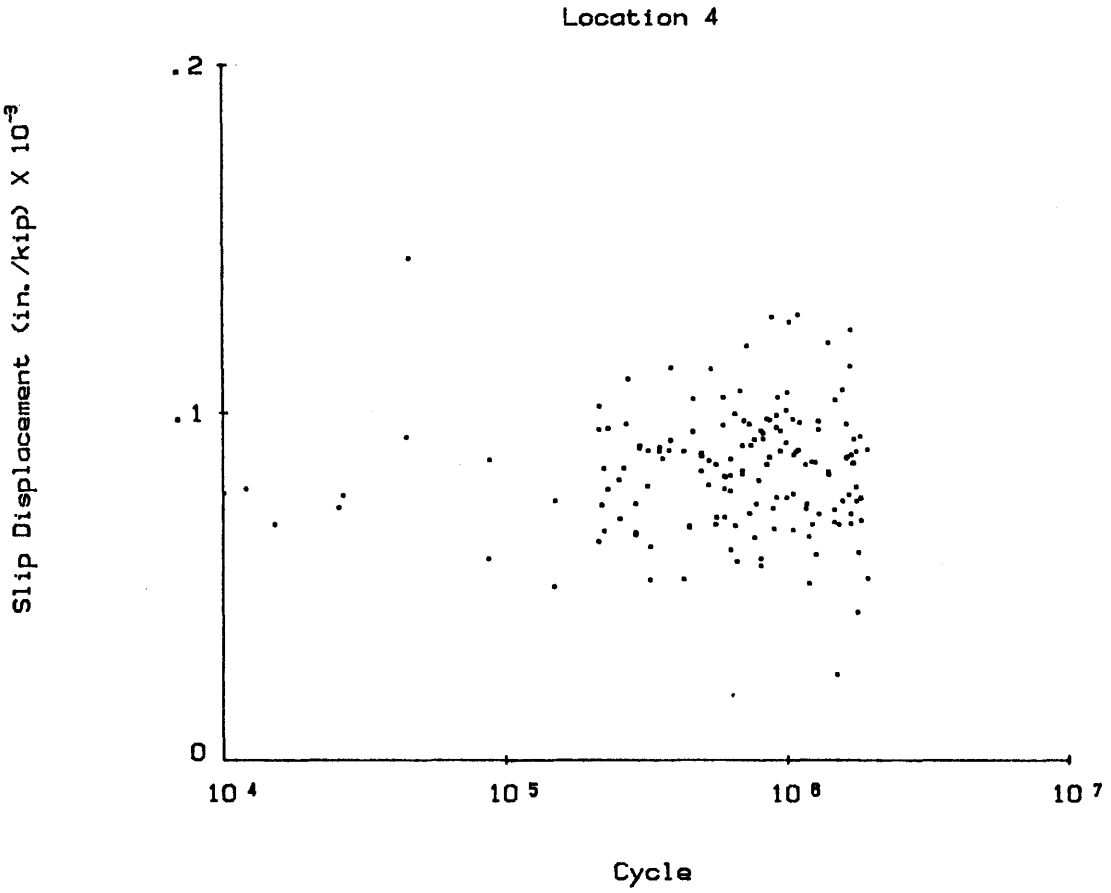

Figure 45. Unitized Slip Displacement Amplitude, Location 4.

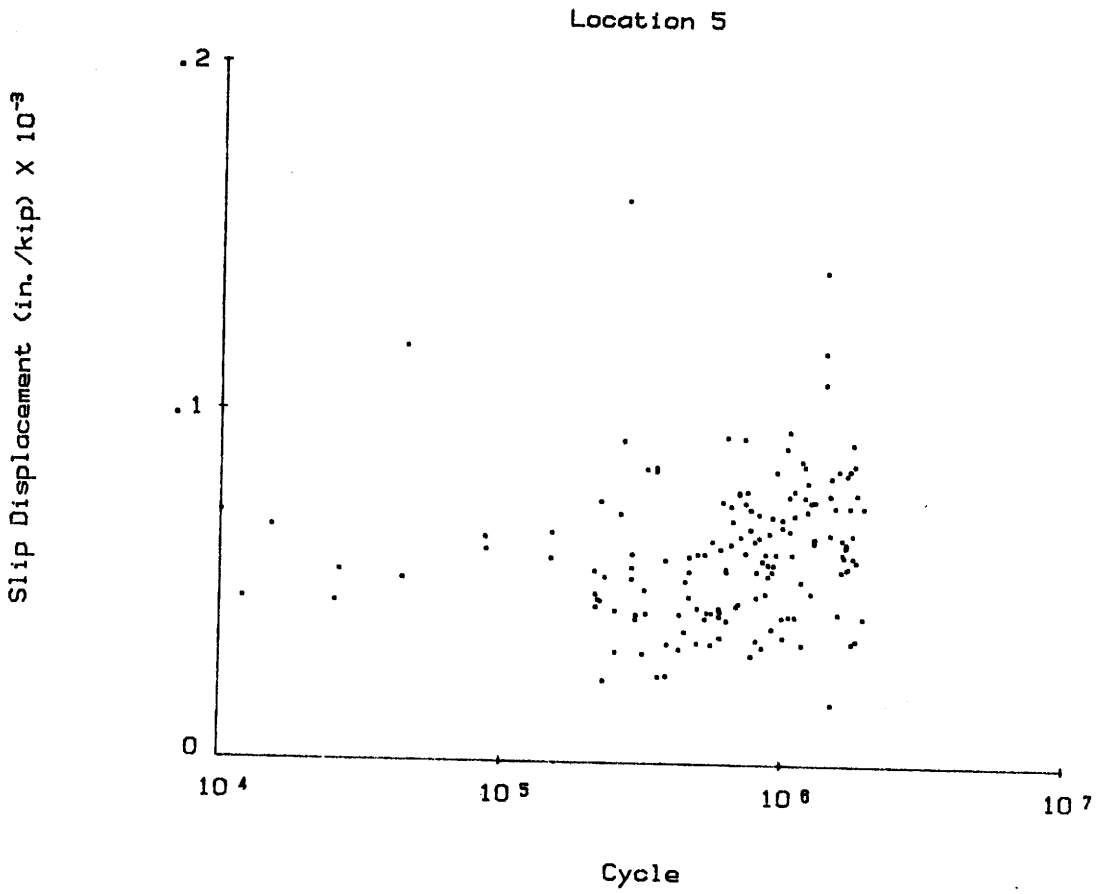

Figure 46. Unitized Slip Displacement Amplitude, Location 5.

Hypothesis Testing of Model Bridge Properties

A statistical test was performed on the processed data to search for statistical evidence of any deterioration during the two million loads cycles applied to the model bridge. This was performed for deflections, for the section properties of cross sections 1 and 2 and for the slip displacements of the high shear side. However, in order to draw conclusions, the following statistical assumptions must be made first:

- the statistical model relation between the parameters involved and the log of the cycle number is linear,
- the errors are statistically independent,
- constant variance, and
- the parameters are assumed normally distributed with means laying on a straight line.

After stating the above assumptions, the following procedure was used to search for statistical evidence of deterioration:

1. The deflections, neutral axis, section modulus, moment of inertia and slip displacement were assumed to map linearly in a logarithmic space of the cycle number, N. Then the following regression equation was employed:

$$f(N) = \hat{\beta}_0 + \hat{\beta}_1 \log(N) \qquad (46)$$

where

$\hat{\beta}_0$ = the intercept when N = 1 and

$\hat{\beta}_1$ = the slope of the linear regression equation, or the rate of change of the parameters per unit change of log(N).

2. After obtaining the linear regression coefficients, inferences about changes in the parameter are made by testing the null hypothesis:

$$H_0: \beta_1 = 0$$

consequently,the alternate hypothesis:

$$H_a: |\beta_1| > 0$$

The null hypothesis, when it is true, means that there is no statistical evidence that there were changes in the corresponding parameter involved. Alternately, H_a means that there is sufficient evidence of changes in the parameter.

3. The statistical test is made using Student t-distribution and, thus, using the formulas:

$$\bar{t} = \frac{S_x \hat{\beta}_1}{\sigma} \qquad (47\text{-a})$$

$$S_x = \Sigma(\log N)^2 - n\,(\Sigma \log N)^2 \qquad (47\text{-b})$$

$$\sigma = \sqrt{\frac{\Sigma(f(N_i) - \hat{\beta}_o - \hat{\beta}_1 \log N_i)^2}{n - 2}} \qquad (47\text{-c})$$

The value calculated for t enables one to determine if the null hypothesis can be accepted or rejected using basic probability theory.

4. An arbitrary criteria is established in order to reject or accept the null hypothesis. This criteria is based upon probability theory and the null hypothesis is rejected if:

$$P\,[\,|\beta_1| > 0\,] > .95$$

Thus, if the probability that the magnitude of the slope of the linear regression line is other than zero is greater than 0.95, then the null hypothesis testing would be rejected and one would accept the result that there were changes in the parameter.

Statistical Test on Deflection Amplitude

The statistical test described in the previous section is performed to the unitized deflection amplitudes calculated for the inside quarter points of the north stringer of the bridge model. The results of the linear regression coefficients and the statistical test are shown in Table 6. It is observed that there is statistical evidence that the unitized deflection amplitude increased during the two million load cycles and, therefore, that there were changes in the overall stiffness of the bridge model. However, the magnitude of the changes needs to be determined to establish the significance of the loss of stiffness. This is done by comparing the initial and final amplitude after the two million load cycles were applied. The initial values are taken to be those at N=10,000 cycles because most of the supporting data is between this number and $2X10^6$ cycles. Table 7 shows the initial and final values of the deflection amplitude and the percent change. It is concluded that the percent change is very small, thus, negligible.

Statistical Test on Section Properties

The statistical test procedure was repeated to investigate changes in the sectional properties of cross sections 1 and 2 of the north stringer of the model bridge. Therefore, the hypothesis test was performed on the neutral axis location, section modulus and the moment of inertia. The results of the regression analysis and the statistical test are shown in Table 8. It is observed that there is statistical evidence that the moment of inertia at cross section 1 decreased as a function of the number of cycles. Note that cross section 1 is located at the vicinity of tensile concrete cracks around the midspan. In contrast, there is no statistical evidence that cross section 2 suffered any inertia loss. However, the total loss of inertia of section 1, over the two million cycles, amounts to only 2.2 % of the initial inertia. Therefore, it is concluded that there were no significant losses in the moment of inertia of the bridge model.

TABLE 6. Linear Regression and Statistical Test Results for Deflection Amplitudes.

Location	$\hat{\beta}_o$ (in./kip)	$\hat{\beta}_1$ (in./kip)	$\bar{t}$	$P[\lvert\beta_1\rvert>0]$
6, High Shear Side	0.0126	0.00020	5.26	1.00
7, Midspan	0.0156	0.00028	11.47	1.00
8, Low Shear Side	0.0113	0.00039	10.15	1.00

TABLE 7. Percent Change in Deflection Amplitude

Location	δ_i (in./kip)	δ_f (in./kip)	Percent Change
6, High Shear Side	0.0134	0.0139	3.7
7, Midspan	0.0167	0.0174	4.1
8, Low Shear Side	0.0129	0.0138	7.3

TABLE 8. Linear Regression and Statistical Test Results for Sectional Parameters of Cross Sections 1 and 2.

Section	Parameter	$\hat{\beta}_0$	$\hat{\beta}_1$	$\bar{t}$	$P[\lvert\beta_1\rvert > 0]$
1	y (in.)	10.25	-0.0078	-0.85	0.61
1	S (in^3)	44.10	-1.239	-1.92	0.94
1	I (in^4)	451.99	-1.589	-2.40	0.98
2	y (in.)	10.94	-0.031	-3.35	1.00
2	S (in^3)	46.36	+0.065	+0.95	0.66
2	I (in^4)	506.99	-0.709	-0.90	0.63

Statistical Test on Slip Displacement

The statistical test was performed for the slip displacement amplitude recorded at the inside of the high shear region corresponding to Locations 1 and 2. No conclusive slip displacement data were obtained at the other three locations. The results of the linear regression and the statistical test are shown in Table 9. It is concluded that there is no statistical evidence of changes in the interface connection modulus.

Summary of Analysis

A summary of the analysis of test results is presented in this section. Two million cycles of scaled equivalent HS-20 truck loads were applied to the model bridge. By analyzing the response amplitude of deflections, strains and

slip displacements, from the start through the two million cycles, it was deduced that there were no significant changes in the properties of the model bridge.

The deflections recorded at the quarter points experienced some increase; however, it was not larger than 7.3 percent. From the strain amplitudes, flexural properties were obtained at two different cross sections. Only cross section 1 was proved to have lost some inertia during the experiment, but the total loss was less than 2.2 % of the initial moment of inertia, thus negligible. The other instrumented section did not experience any change.

Similarly, from the slip displacement amplitudes, it was concluded that there was no significant damage at the interface connections.

TABLE 9. Linear Regression and Statistical Test for Slip Displacements.

Location	$\hat{\beta}_0$ (in./kip)	$\hat{\beta}_1$ (in./kip)	$\bar{t}$	$P[\lvert\beta_1\rvert>0]$
1	8.8×10^{-5}	8.6×10^{-6}	1.94	0.92
2	6.4×10^{-5}	$3.8\times10_{-6}$	1.26	0.94

CHAPTER VI

DISCUSSION OF TEST RESULTS AND CONCLUSIONS

General

Two million cycles of scaled, equivalent AASHTO HS-20 truck loads were applied to the 1/3 model bridge. The test set-up was arranged to produce more deterioration due to shear forces than due to bending moments. Thus, deteriorations of the interface connections, consisting of epoxy mortar bond and steel stud connectors, were by design more likely to occur. Since the rigidity of the interface connections is primarily provided by the epoxy mortar bond, there was concern that normal traffic loading would tend to fatigue the epoxy mortar bond and thus produce losses of moment of inertia.

By monitoring changes in deflections, slip displacements and section properties, the overall performance of the 1/3 scale model bridge was evaluated.

Discussion of Test Results

From the amplitude of deflections, slip displacements and section properties, there was no strong evidence of significant deterioration or damage in the scaled model bridge structure. However, statistical evidence was pursued by means of linear regressions and hypothesis testing analyses. The statistical analyses showed that only the deflections consistently increased. This apparently means that some losses in the overall inertia occurred during the test. However, no changes were deduced from the obtained slip displacements and calculated flexural properties. Thus, it is possible that the electronic calibration of the strain gage type displacement transducers measuring deflections drifted during the time period it took to complete the experiment, producing an apparent change in the deflection amplitude of the model.

The slip displacements were not very conclusive because of the electronic noise, but it is noted that all slip displacements were very small because of the rigidity provided by the epoxy mortar bond at the interface. If the bond had failed, drastic changes in the slip displacements would have occurred because the horizontal shear forces would have directly acted on the steel stud connectors, which have a much lower rigidity. Since no drastic slippages were observed, it is concluded that the interface connection consisting of the epoxy mortar and steel stud connectors performs well under repetitive loading.

Conclusions

After the two million cycles of equivalent HS-20 AASHTO truck loads were applied to the 1/3 scale model bridge with full-depth precast concrete panels, the following significant conclusions may be extrapolated to a prototype bridge:

1. The epoxy mortar and steel stud connections perform satisfactorily to hold together precast concrete panels and steel I-beam stringers.
2. Losses of rigidity of the interface connections do not occur under normal traffic conditions. There were no drastic slippages or changes on the slip displacements at the interface between the precast panels and steel I-beams of the model bridge.
3. Repetitive highway loadings do not significantly affect the overall stiffness of the bridge structure. The amplitude of deflections of the model bridge did not significantly increase during the two million load cycles.
4. Since the connections are holding together, no losses of the composite flexural properties of the bridge structure are expected.

As a major conclusion, it can be stated that the interface connections using epoxy mortar and shear stud connectors for holding the precast concrete panels are fatigue-resistant. The bond area is so large that the level of shear stresses at the interface is small so that fatigue is not a problem.

Recommendations

It is recommended that existing AASHTO Bridge Specifications for the fatigue design of shear stud connectors be used for the design of the stud connectors employed in the pocket connections with epoxy mortar grout. Even though the existing fatigue design considerations were established only for concrete embedment, the specifications prove to be conservative because the interface epoxy mortar bond prolongs the fatigue life of the shear connectors and the elastic modulus of the epoxy mortar is typically lower than that of concrete.

REFERENCES

1. American Association of State Highways and Transportation Officials, "AASHTO Standard Specification for Highway Bridges," 12th Ed., 1977.

2. Beal, David A., "Strength of Concrete Bridge Decks," Research Report 89, Engineering Research and Development Bureau, New York State Department of Transportation, July 1981.

3. Biswas, M., Osegueda, R. A. and Noel, J. S., "Scale Model Tests for Full Depth Precast Concrete Panel Decked Composite Bridge Span," Transportation Research Record No. 950, Transportation Research Board, Volume 1, pp. 163173, Washington, D. C., 1984.

4. Biswas, M., et al., "Bridge Replacement with Precast Concrete Panels," Special Report 148, Transportation Research Board, Washington, D.C., 1974, pp 136-148.

5. Bonilla, F. E., "Composite Action of Precast Panel Bridge Decks in Negative Moment Regions," Thesis presented to Texas A&M University, College Station, Texas, in partial fulfillment of the requirements for the degree of Master of Science, August 1985.

6. Clough, R. W. and Penzien, J, Dynamics of Structures, McGraw-Hill Publishers, New York, 1975.

7. King, D. C., Slutter, R. G. and Driscoll, G. C., "Fatigue Strength of 1/2-Inch Diameter Stud Shear Connectors," Highway Research Record No. 103, 1965, pp 78-106.

8. Ontario Ministry of Transportation and Communications, "Ontario Bridge Design Code," Section 7, Ontario, Canada, 1978.

9. Osegueda, R. A., "Rapid Bridge Deck Replacement," Thesis presented to Texas A&M University, College Station, Texas, in partial fulfillment of the requirements for the degree of Master of Science, December 1983.

10. Sanders, W. W. and Elleby, N. A., "Distribution of Wheel Loads on Highway Bridges." National Cooperative Highway Research Program No. 83, 1970.

11. Slutter, R. G.and Fisher, J. W., "Fatigue Strength of Shear Connectors." Highway Research Record No. 147, pp. 65-88, 1966.

12. STRUDL User Manual, McDonnel Douglas Automation Company, St. Louis, 1984.

13. Texas Highway Department, "Drawing and Details for I-Beam Bridges." Nov. 1960, Revised 1962, Austin, Texas.

14. Texas Highway Department, "Instructions for the Use of Texas Highway Department Epoxy Binder B-102," Report of the Materials and Test Division, Austin, Texas.

15. Toprac, A. A., "Fatigue Strength of 3/4-Inch Stud Shear Connectors." Highway Research Record No. 103, pp. 53-77, 1965.

A P P E N D I X A

NOTATION

a = distance from one stringer support to point at which moment of inertia changes

$\bar{a}$ = total amplitude of sinusoidal response signal

A = regression coefficient

A_s = effective cross sectional area acting in shear

b = distance from one stringer support to the concentrated load P

B = regression coefficient

c = distance from one stringer support to the concentrated load P

C = regression coefficient

CF = shear deformation and rotary inertia correction factors for eigenfrequencies

D = distribution factor for use in LF = S/D

D_m = dynamic amplification factor for moments

D_w = dynamic amplification factor for deflections

D_x = flexural stiffness in the longitudinal direction per unit width

D_{xy} = torsional stiffness in the longitudinal direction per unit width

D_y = flexural stiffness in the transverse direction per unit length

D_{yx} = torsional stiffness in the transverse direction per unit length

E = modulus of elasticity

G = modulus of rigidity

I = moment of inertia

I_n = average transformed moment of inertia

I_{me} = average mass moment of inertia

I_1 = transformed moment of inertia of end sections

I_2 = transformed moment of inertia of the middle section

L = span length

LF = lateral wheel load distribution factor

m_n = average distributed mass per unit width

m_1 = distributed mass per unit width at end sections

m_2 = distributed mass per unit width at middle section

M = bending moment

M_n = generalized modal mass

Mf = moment factor for a given cross section

N = cycle number

P = concentrated load

P_n = generalized modal load

S = lateral stringer spacing

t = time variable

$\bar{t}$ = value for use in the "t" distribution

t_o = phase angle

U_b = strain energy due to bending

w = deflection variable

w_n = deflection fourier coefficient

W = width of bridge

$\bar{W}$ = total work done by externally applied loads

x = horizontal coordinate

y = vertical coordinate

Y_n = generalized modal coordinates

$\bar{y}$ = neutral axis location

α = torsional parameter

β = ratio of loading frequency to natural frequency

$\hat{\beta}_o$ = regression coefficient, intercept

$\hat{\beta}_1$ = regression coefficient, slope

δ = deflection

ΔP = load range

ε = strain

ε_o = strain at extreme bottom fibers

θ = flexural parameter

Π = total potential energy

ρ = mass density

σ = standard deviation

ϕ = curvature

ϕ_n = mode shape function

ω = fundamental frequency

ω_n = natural frequency associated with the n^{th} mode shape

$\bar{\omega}$ = loading frequency, 3.5 Hz

A P P E N D I X B

FLEXURAL AND TORSIONAL PARAMETERS

Given the 60-ft prototype bridge shown in Figure 4, the flexural and torsional parameters θ and α are computed according to Sanders and Elleby (10). The flexural parameter is calculated by the use of Equation 1:

$$\theta = \frac{W}{2L}\sqrt[4]{\frac{D_x}{D_y}}$$

The flexural stiffness in the longitudinal direction are given by the transformed section properties of the bridge. Thus, the average effective moment of inertia given in Equation 7-b is employed along with the property values shown in Table 1. Therefore,

$$I_n = I_2 - 2\,(I_2 - I_1)\,\left\{\frac{a}{L} - \frac{1}{2\pi n}\sin\left(\frac{2n\pi a}{L}\right)\right\}$$

$$= 35700 \text{ in.}^4 - 2(3570-25780) \text{ in.}^4 \left\{ 1/6 - \sin(\pi/3)/2 \right\}$$

$$I = 35128 \text{ in}^4 \text{ per stringer}$$

Now, the flexural stiffness is distributed over the width of the bridge. Thus, D_x becomes:

$$D_x = \frac{29000 \text{ ksi} \times 35{,}128 \text{ in.}^4}{8 \text{ ft} \times (12 \text{ in./ft})} = 1.0612 \times 10^7 \text{ k-in}^2/\text{in.}$$

The flexural stiffness in the transverse direction is simply given by:

$$D_y = E_c\, I_c / W = 176761.9 \text{ k-in}^2/\text{in.}$$

When plugging in the values of the flexural stiffnesses into

Equation 1, the following flexural parameter is obtained:

$$\theta = 0.74$$

The torsional parameter is calculated using the torsional sectional properties of the bridge. First, the J is obtained for the longitudinal direction (no beams):

$$J = \frac{1}{3} \Sigma\, a\, b^3$$

where,

a = the longest slab dimension

b = the shortest slab dimension

Then, D_{xy} becomes:

$$D_{xy} = G_c\, J$$

$$D_{xy} = (1883.\ \text{ksi}) \times (8\ \text{in.})^3 \times (60\ \text{ft} \times 12\ \text{in./ft}) = 321{,}384.\ \text{k-in}^2/\text{in}$$

The torsional stiffnes in the transverse direction will be D_{xy} plus the contributions from the torsional stiffness of the I-beams. Then,

$$J = \{(35.84\text{in.}) \times (.625\text{in.})^3 + 2(11.972\text{in.}) \times (.940\text{in.})^3 \} / 3$$

$$J = 9.55\ \text{in}^4/\ \text{beam}$$

Then,

$$D_{yx} = D_{xy} + 4\ (G\ J\ /\ W\ )$$

where W is the width of the bridge.

$$D_{yx} = 321,384. + 4x(11700 \text{ ksi})x9.55 \text{ in}^4 / (32x12 \text{ in.})$$

$$D_{yx} = 322,638. \text{ k-in}^2/\text{in}$$

Now, using the values obtained for the flexural and torsional stiffnesses in Equation 2, the torsional parameter is computed as:

$$\alpha = 0.24$$

A P P E N D I X C

MAXIMUM HS20-44 LOADS

The maximum moment and shear produced by a HS20-44 design truck load plus impact on the 60-ft prototype bridge are computed according to the AASHTO Bridge Specifications.(1) Table C-1 shows the maximum shears and moments for two wheel lines for an HS20-44 truck loading. From this table the following values are obtained:

M = 806.5 k-ft per 2 lines
V = 60.8 k per 2 lines

Thus, applying the lateral load distribution factor calculated in Chapter II, to one line of wheel loads, it is obtained:

$$M_{LL} = 1.33 \left(\frac{806.5}{2} \text{ k-ft}\right) = 536.3 \text{ k-ft}$$

$$V_{LL} = 1.33 \left(\frac{60.8}{2} \text{ kip}\right) = 40.43 \text{ kip}$$

And now, multiplying the above results by the impact factor of I=0.27, and adding the the results to the live load shear and moment, the maximum design shear and moment for the prototype bridge are:

$$M_{LL+I} = (1 + 0.27)(\ 536.3 \text{ k-ft}) = 681.2 \text{ k-ft}$$

$$V_{LL+I} = (1 + 0.27)(\ 40.43 \text{ kip}) = 51.35 \text{ kip}$$

TABLE C-1. Maximum Moments and Shears for HS20-44 Loading (1).

Spans in feet ; moments in thousands of foot-pounds ; shears and reactions in thousands of pounds.

These values are subject to specification reduction for loading of multiple lanes.

Impact not included.

Span	Moment	End Shear and end reaction (a)	Span	Moment	End shear and end reaction (a)
1	8.0	32.0(b)	42	485.3(b)	56.0(b)
2	16.0	32.0(b)	44	520.9(b)	56.7(b)
3	24.0	32.0(b)	46	556.5(b)	57.3(b)
4	32.0	32.0(b)	48	592.1(b)	58.0(b)
5	40.0	32.0(b)	50	627.9(b)	58.5(b)
6	48.0	32.0(b)	52	663.6(b)	59.1(b)
7	56.0	32.0(b)	54	699.3(b)	59.6(b)
8	64.0	32.0(b)	56	735.1(b)	60.0(b)
9	72.0	32.0(b)	58	770.8(b)	60.4(b)
10	80.0	32.0(b)	60	806.5(b)	60.8(b)
11	88.0	32.0(b)	62	842.4(b)	61.2(b)
12	96.0	32.0(b)	64	878.1(b)	61.5(b)
13	104.0	32.0(b)	66	914.0(b)	61.9(b)
14	112.0	32.0(b)	68	949.7(b)	62.1(b)
15	120.0	34.1(b)	70	985.6(b)	62.4(b)
16	128.0	36.0(b)	75	1,075.1(b)	63.1(b)
17	136.0	37.7(b)	80	1,164.9(b)	63.6(b)
18	144.0	39.1(b)	85	1,254.7(b)	64.1(b)
19	152.0	40.4(b)	90	1,344.4(b)	64.5(b)
20	160.0	41.6(b)	95	1,434.1(b)	64.9(b)
21	168.0	42.7(b)	100	1,524.0(b)	65.3(b)
22	176.0	43.6(b)	110	1,703.6(b)	65.9(b)
23	184.0	44.5(b)	120	1,883.3(b)	66.4(b)
24	192.7	45.3(b)	130	2,063.1(b)	67.6
25	207.4	46.1(b)	140	2,242.8(b)	70.8
26	222.2	46.8(b)	150	2,475.1	74.0
27	237.0	47.4(b)	160	2,768.0	77.2
28	252.0	48.0(b)	170	3,077.1	80.4
29	267.0	48.8(b)	180	3,402.1	83.6
30	282.1	49.6(b)	190	3,743.1	86.8
31	297.3	50.3(b)	200	4,100.0	90.0
32	312.5	51.0(b)	220	4,862.0	96.4
33	327.8	51.6(b)	240	5,688.0	102.8
34	343.5	52.2(b)	260	6,578.0	109.2
35	361.2	52.8(b)	280	7,532.0	115.6
36	378.9	53.3(b)	300	8,550.0	122.0
37	396.6	53.8(b)			
38	414.3	54.3(b)			
39	432.1	54.8(b)			
40	449.8	55.2(b)			

(a) Concentrated load is considered placed at the support. Loads used are those stipulated for shear.

(b) Maximum value determined by Standard Truck Loading. Otherwise the Standard Lane Loading governs.